UNIVERSITY OF CAMBRIDGE

Use of a Purple Non-Sulphur Bacterium, *Rhodopseudomonas palustris*, as a Biocatalyst for Hydrogen Production from Glycerol

Ning Xiao

Department of Chemical Engineering and Biotechnology
University of Cambridge

This dissertation is submitted for the degree of Doctor of Philosophy

Submitted to the Faculty of Engineering

Churchill College
September 2017

Use of a Purple Non-Sulphur Bacterium, *Rhodopseudomonas palustris*, as a Biocatalyst for Hydrogen Production from Glycerol

Ning Xiao

Abstract

This project was aimed to use a purple non-sulphur bacterium, *Rhodopseudomonas palustris,* as a biocatalyst for hydrogen (H_2) production, from the waste of biodiesel manufacturing, crude glycerol. The goal of this project was to understand the fundamentals relevant to scaling up the process and developing an off-the-shelf product.

The first objective was to determine the ability of *R. palustris* to generate H_2 by non-growing cells in comparison to that by growing cells. Similar average H_2 production rates and energy conversion were found for both processes but a significant difference in the H_2 yield was observed. H_2 production reached ~ 80 % of the theoretical maximum H_2 yield by non-growing *R. palustris*, about eight-fold of that reached by growing *R. palustris*.

The high yield suggested that it is economically appealing to use non-growing *R. palustris* as the biocatalyst for continuous H_2 production. To accomplish the proposed scale-up systems, understanding its product formation kinetics is the key. It was found that the H_2 production rate is not growth-associated and depends solely on the dry cell mass with a non-growth associated coefficient of 2.52 (Leudeking–Piret model $\frac{dP}{dt} = 2.52\,X$).

Light is vital for H_2 production by non-growing *R. palustris*, in terms of light intensity and wavelength range. It was found that excessive or insufficient light intensity may constrain the performance. Only photons of light with appropriate wavelengths can excite cytochrome bacteriochlorophyll complexes II in *R. palustris* to generate H_2. Among white LEDs, infrared LEDs, and incandescent light bulbs, at the same light intensity, infrared LEDs gave the best results in the H_2 production rate and energy

conversion by non-growing cells, 22.0 % ± 1.5 % higher than that with white LEDs and around 25-30 times of that by incandescent light bulbs.

It was found that non-growing *R. palustris* can be immobilised in alginate beads to give similar H_2 production rates as that by cells suspended in media. This preliminary result pointed the direction of developing an off-the-shelf product of immobilised non-growing *R. palustris* as a biocatalyst for continuous H_2 production.

Preface

The work in this dissertation was carried out in the Department of Chemical Engineering and Biotechnology, the University of Cambridge between October 2012 and September 2016. This dissertation is the result of my own work and includes nothing which is the outcome of work done in collaboration except as declared in the acknowledgement and specified in the text.

It is not substantially the same as any that I have submitted, or, is being concurrently submitted for a degree or diploma or other qualification at the University of Cambridge or any other University or similar institution except as declared in the preface and specified in the text. I further state that no substantial part of my dissertation has already been submitted, or, is being concurrently submitted for any such degree, diploma or other qualification at the University of Cambridge or any other University of the similar institution except as declared in the preface and specified in the text.

This dissertation contains 48 figures, 13 tables and 44115 words including references, figures, tables, and equations. It does not exceed the prescribed word limit of 65,000 words for the Engineering Degree Committee.

Ning Xiao

Department of chemical engineering and biotechnology

University of Cambridge

Acknowledgements

Table of Contents

3 NON-GROWING *RHODOPSEUDOMONAS PALUSTRIS* INCREASES HYDROGEN YIELD FROM GLYCEROL 44

4 THE IMPACT OF INITIAL INOCULUM SIZES ON HYDROGEN PRODUCTION BY NON-GROWING *RHODOPSEUDOMONAS PALUSTRIS* 68

List of Figures

List of Tables

Nomenclature and acronyms

A	the area of the incident surface	m^2
aceryl-CoA	acetyl-coenzyme A	
ADP	adenosine diphosphate	
ATP	adenosine triphosphate	
Ar	argon	
c	the speed of light in vacuum	$m\ s^{-1}$
CBB	Calvin-Benson-Bassham	
$CaCl_2 \cdot H_2O$	calcium chloride dehydrates	
$C_3H_8O_3$	glycerol	
$C_6H_9NO_6$	nitrilotriacetic acid	
$C_{10}H_{16}N_2O_8$	ethylenediaminetetraacetic acid (EDTA)	
$CH_{1.8}N_{0.18}O_{0.38}$	*Rhodopseudomonas palustris*	
CO_2	carbon dioxide	
$Co(NO_3)_2 \cdot 6H_2O$	cobalt nitrate hexahydrate	
$CuSO_4 \cdot 5H_2O$	copper(II) sulphate pentahydrate	
Cyt bc1	cytochrome bacterial chlorophyll 1 complexes	
Cyt bc2	cytochrome bacterial chlorophyll 2 complexes	
E	the energy carried by a photon	J
Fe^{2+}	iron (II) ion	
$FeSO_4 \cdot 7H_2O$	iron (II) sulphate heptahydrate	
Fd	ferredoxin	
h	Planck's constant	J s
ΔH	the molar combustion enthalpy of H_2	$kJ\ mol^{-1}$
H^+	hydrogen ion	
H_2	hydrogen gas	
HCl	hydrochloric acid	
$H_2NC_6H_4CO_2H$	4-aminobenzoic acid (PAPB)	
H_2SO_4	sulphuric acid	
I	light intensity	$W\ m^{-2}$
K_2HPO_4	potassium phosphate dibasic	
KH_2PO_4	potassium phosphate monobasic	
LH-I	the light-harvesting complex I	
LH-II	the light-harvesting complex II	
LH-III	the light-harvesting complex III	
Mg^{2+}	magnesium ion	
$MgSO_4$	magnesium sulphate	
$MnSO_4 \cdot H_2O$	manganese(II) sulphate monohydrate	
n	the dilution factor	

	the number of moles of H_2 generated	
N_2	nitrogen gas	
$Na_2B_4O_7 \cdot 10H_2O$	sodium tetraborate decahydrate	
Δn_{C_i}	moles of carbon consumed or generated in carbon containing compound i	
$\Delta n_{e_i^-}$	moles of electrons consumed or generated in electron containing compound i	
Na^+	sodium ion	
NaOH	sodium hydroxide	
$Na_2S_2O_3$	sodium thiosulphate	
NADH	nicotinamide adenine dinucleotide	
NADPH	nicotinamide adenine dinucleotide phosphate	
$(NH_4)_6Mo_7O_{24} \cdot 7H_2O$	ammonium molybdate tetrahydrate	
O_2	oxygen	
OD	optical density	
OD_{660nm}	optical density at 660 nm	
P	the power incident on the surface	W
	the H2 volume per unit volume of the cell culture	mL L^{-1}
PCTFE	polychlorotrifluoroethylene	
PD	1, 3-propanediol	
PEEK	polyether ether ketone	
PHB	polyhydroxybutyrate	
Pi	inorganic phosphate	
PP	polypropylene	
PSU	photosynthetic unit	
Q	quinone	
R. palustris	*Rhodopseudomonas palustris*	
RC	reaction centre	
PTFE	polytetrafluoroethylene	
PNS bacteria	purple non-sulphur bacteria	
RubisCo	ribulose-1,5-bisphosphate carboxylase/oxygenase	
S^{2-}	sulphide	
t	time	h
t_1	initial time	h
TCA	tricarboxylic acid	
UV	ultraviolet	
v	frequency	s^{-1}
$V_{culture}$	the volume of culture	L
$V_{headspace}$	the volume of headspace gases	mL
V_i	the volume of gases at the i-th time	mL
$V_{liquid\ sample}$	the volume of liquid extracted for this test	
V_n	the volume of gases at the n-th time	mL

X	dry cell mass	g L^{-1}
X_1	the initial dry cell mass in the exponential phase	g L^{-1}
$ZnSO_4 \cdot 7H_2O$	zinc sulphate heptahydrate	
α	growth-associated coefficient	
β	non-growth associated coefficient	
θ^{CO_2}	the CO_2 composition	
$\theta_i^{H_2}$	the H_2 composition at the i-th time	
$\theta_n^{H_2}$	the H_2 composition at the n-th time	
$\theta_i^{CO_2}$	the CO_2 composition at the i-th time	
$\theta_n^{CO_2}$	the CO_2 composition at the n-th time	
μ	the specific growth rate	h^{-1}
λ	wavelength	nm

1 Introduction

1.1 Biodiesel and crude glycerol

1.1.1 Biodiesel

The diminishing crude oil reserves, the climbing transport fuel demand, and growing environmental concerns have increased the emphasis on renewable energy for transport sector (Yang *et al.* 2012; Taylor *et al.* 2013). There is currently an unprecedented interest in biofuels, a generic term referring to liquid fuels derived from plant materials. Although such fuels, when combusted, release carbon dioxide (CO_2), a proportion of that CO_2 has been fixed from the atmosphere by photosynthesis. Accordingly, the proportion of fossil-fuel derived CO_2 emitted by a biofuel is less than that produced by a genuine fossil fuel. One biofuel of particular interest is biodiesel, owing to its advantages in terms of environmental sustainability, energy content, and compatibility with current fuel supply infrastructure and diesel engines (Luque *et al.* 2008; Johnson & Taconi 2009).

1.1.2 Crude glycerol from biodiesel manufacturing

The production of biodiesel by esterification of tri-acyl-glycerides, produced in seeds (*e.g.* oilseed rape) or algae, with alcohol is shown in Figure 1-1. Glycerol is generated as a by-product. Roughly, each kilogram of biodiesel generates 0.1 kilogram of crude glycerol.

100 kg of oil + 10.5 kg MeOH = 100 kg methyl esters (biodiesel) + 10.5 kg glycerol
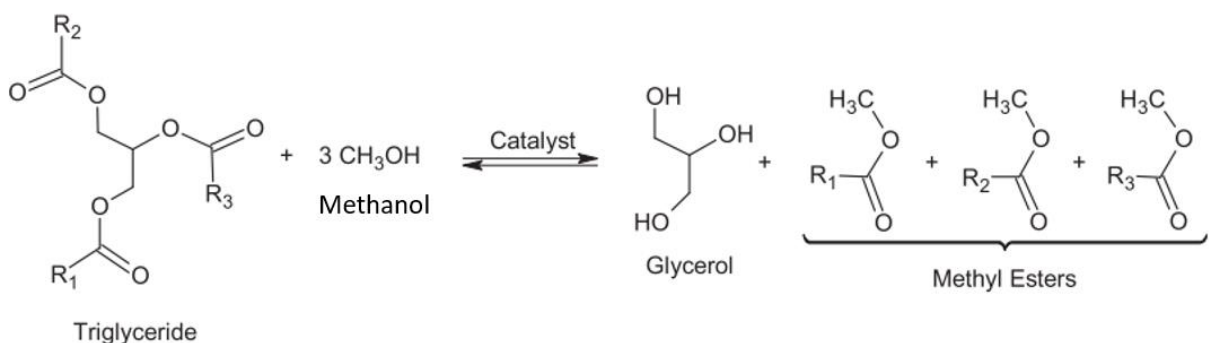
Figure 1-1: Transesterification of a triglyceride with methanol (Ciriminna *et al*. 2014)

1

Biodiesel production is rapidly increasing recently due to the support from government policies and incentives (Ayoub & Abdullah 2012). Accompanying the sharp increase in biodiesel production, the production of glycerol, the by-product of the esterification reaction used to make the biodiesel, has been increased significantly over the years. As shown in Table 1-1, glycerol was traditionally obtained from soap manufacturing, fatty acids and fatty alcohol production, and synthesis from the petroleum industry. From 1992 to 2010, the world glycerol production increased from 0.65 to 2.46 million tonnes per year. Among all the glycerol supply sources, the glycerol from biodiesel manufacturing increased 0 to 1.58 million tonnes per year from 1992 to 2010. Consequently, the glycerol produced from biodiesel manufacturing has far outstripped the existing saturated glycerol demand market. Because of that, there was a significant decline of more than 80 % in its current price. The price of refined glycerol decreased from about 4000 USD per tonne in 2000 (before the expansion of biodiesel production) to less than 500 USD per tonne in 2010 (after the expansion of biodiesel production) (Ciriminna *et al.* 2014). And in 2006, the world production of biodiesel was approximately 30 million tonne per year (BP 2016), which generated 3 million tonne of glycerol per year and triggered the glycerol price dropped to 190 ~ 210 USD per tonne (ICIS 2016).

Table 1-1: Sources of glycerol during 1992-2010 (Ayoub & Abdullah 2012)

Glycerol source	World glycerol production ($\times 10^3$ tonne/ year)							
	1992	1995	1999	2003	2005	2006	2008	2010
Soaps	208	208	198	188	167	146	125	83
Fatty acids	271	292	313	333	396	438	479	521
Biodiesel	0	42	42	167	375	521	1125	1583
Fatty alcohol	83	104	125	104	125	167	250	250
Synthetic	83	83	63	63	21	0	0	0
Others	0	0	42	63	42	0	21	21
Total production	646	729	781	917	1125	1271	2000	2458

1.1.3 Application of crude glycerol

Combustion of glycerol to supply heat could be one option to utilise such a large quantity of crude glycerol. However, the impurities in crude glycerol result in its being treated as a hazardous environmental waste in the European Union and therefore entailing a cost for controlled incineration (Johnson & Taconi 2009).

Alternatively, glycerol is considered as a good energy source for animals due to its high absorption rates, and it could be applied as a supplement to animal feed (Kerr *et al.* 2007). Again, owing to the uncertain nature of the contaminants in crude glycerol, the growth performance could be affected; in more serious cases, some impurities might cause health problems to animals. For example, the high level of potassium might result in wet liver and imbalanced dietary electrolyte for broilers (Cerrate *et al.* 2006), and the high level of methanol is toxic to most animals (Kerr *et al.* 2007; Cerrate *et al.* 2006; Lammers *et al.* 2008; Donkin *et al.* 2009). In addition, compared to the current crude glycerol market price of 0.02 USD per kilogram, the selling price of crude glycerol as animal feed is not appealing (0.016 ~ 0.02 USD per kilogram) (Yang *et al.* 2012).

Thus, crude glycerol from biodiesel production has now become a financial and environmental liability and there is an urgent need to develop crude glycerol purification and conversion technologies (Johnson & Taconi 2009).

1.1.4 Purification of crude glycerol

The purified glycerol is a high-value commercial chemical with a wide range of applications in food, polymer, pharmaceutical, and personal care industries. Hence, this by-product, crude glycerol, was initially considered as a subsidy in the biodiesel industry to lower the manufacturing cost and promote biodiesel industrialisation at large scale (Yang *et al.* 2012; Pott *et al.* 2012). However, the crude glycerol from biodiesel production is usually far from pure. The actual chemical composition of the crude glycerol varies with the type of catalysts and reagents used during the esterification, the conversion and recovery efficiencies of the biodiesel, other impurities in the feedstock, and whether or not the reagents and catalysts are

recovered (Yang *et al.* 2012). Typical compositions of crude glycerol, purified glycerol, and commercial refined glycerol are shown in Table 1-2. The cost to refine crude glycerol with such large number of contaminants can be a major financial issue. In order to achieve highly refined glycerol, apart from neutralisation and recycling processes (Chiu *et al.* 2005), the refining process also has to use expensive vacuum distillation and ion exchange processes (Van Gerpen 2005). In 2007, the selling price of crude glycerol was 110 USD per tonne, and the approximate cost of refining crude glycerol was 330 USD per tonne (Johnson & Taconi 2009), which brought up to a total value of 440 USD per tonne. Compared to the price of refined glycerol in 2010, less than 500 USD per tonne, the profit margin to purify the crude glycerol from biodiesel manufacturing was too low to be economically feasible.

Table 1-2: Quality parameter of different categories of glycerol (Ayoub & Abdullah 2012)

Parameter	Crude glycerol	Purified glycerol	Refined glycerol
Glycerol content (% w/w)	60-80	99.1-99.8	99.2-99.98
Moisture contents (% w/w)	1.5-6.5	0.11-0.8	0.14-0.29
Ash (% w/w)	1.5-2.5	0.054	<0.002
Soap (% w/w)	3.0-5.0	0.56	N/A
Acidity (pH)		Slightly acidic	
Chloride (ppm)	ND	1.0	0.6-9.5
Colour (APHA)	Dark	Moderate	Faint

1.1.5 Convert crude glycerol to other value-added chemicals

Utilising crude glycerol for the synthesis of value-added chemicals plays a key role in biodiesel commercialization and development (Zhou *et al.* 2008; Ayoub & Abdullah 2012). Various approaches for utilising the crude glycerol as a feedstock for chemicals, mainly through chemical conversion and biological conversion, have been investigated, and these are reviewed below.

1.1.5.1 Chemical conversion of glycerol

From a technical point of view, glycerol's multifunctional structure and properties can go through different reaction pathways to form various valuable products as shown in Figure 1-2.
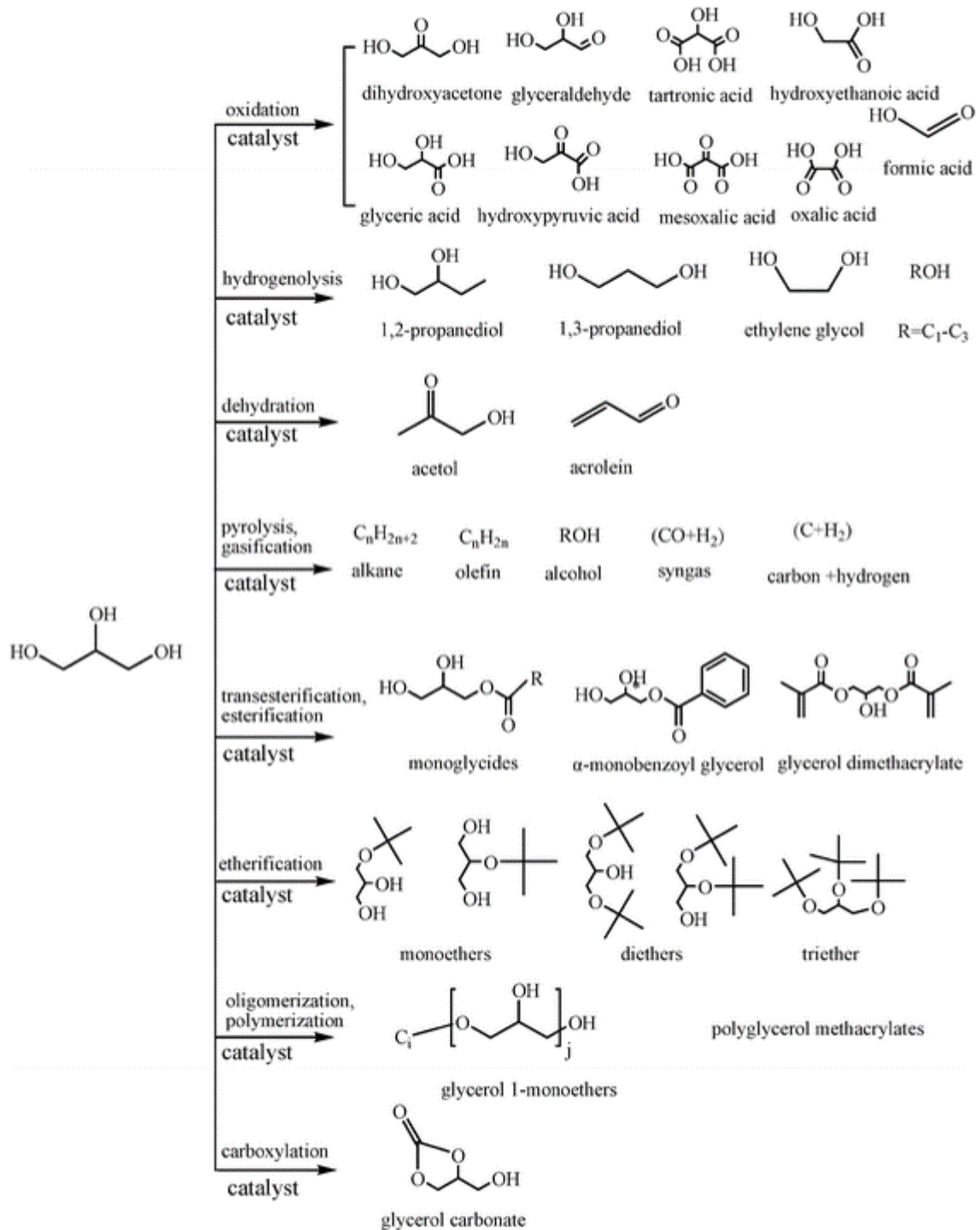
Figure 1-2: Processes of catalytic conversion of glycerol into useful chemicals (Zhou *et al.* 2008)

Compared to hydrocarbons, glycerol is a highly functionalized molecule that can be used as an alternative feedstock for the production of valuable oxygenated derivatives including dihydroxyacetone (Kimura 1993), glyceric acid (Garcia *et al.* 1995; Carrettin *et al.* 2003; Porta & Prati 2004; Dimitratos *et al.* 2005; Dimitratos *et al.* 2006; Demirel *et al.* 2007), hydroxy-pyruvic acid (Abbadi & van Bekkum 1996; Demirel *et al.* 2007), mesooxalic acid, and tartronic pyruvic acid *etc.*.

In the presence of metallic catalysts and hydrogen, glycerol could be converted to valuable 1,2-propanediol (Che 1987; Chaminand *et al.* 2004), 1,3-propanediol (Che 1987; Chaminand *et al.* 2004; Oh *et al.* 2011), or ethylene glycol (Dasari *et al.* 2005) through hydrogenolysis.

Acetal and acrolein can be obtained through acid dehydration of glycerol (Bühler *et al.* 2002; Watanabe *et al.* 2007).

The pyrolysis of glycerol yields liquid fuel at low temperature and gaseous fuel at high temperature (Soares *et al.* 2006). The gasification of glycerol is very similar to pyrolysis but conducted in the presence of oxygen, and it produces syngas and hydrogen (Xu *et al.* 2009).

Mono-glycerides and polyglycerol esters can be obtained from the transesterification or direct esterification of glycerol with acid and/ or base catalysis (Zhou *et al.* 2008; Sonntag 1982). The traditional acid and/ or base catalysis of transesterification and esterification processes will result in a lot of undesired waste chemicals (Márquez-Alvarez *et al.* 2004).

Although glycerol could be used as a burning fuel directly, it could also be converted into valuable fuel additives or solvents through etherification. For example, glycerol tertiary butyl ethers, obtained from glycerol, has a great potential as an alternative oxygenate in diesel (Bradin 1996; Kesling *et al.* 1994).

Poly-glycerols and polyglycerol esters could be produced through the oligomerisation of glycerol and the esterification or trans-esterification of the oligomers with fatty acids or methyl esters (Queste *et al.* 2006; Barrault *et al.* 2004).

Glycerol carbonate is traditionally generated through a reaction with phosgene and an exchange reaction with a dialkyl carbonate, and it could be also produced by reacting glycerol with carbon monoxide and oxygen at high pressure with a catalyst (Teles *et al.* 1994).

In most chemical conversion processes of glycerol, it is difficult to use crude glycerol from biodiesel manufacturing directly with high levels of contaminants. Cost effective pre-treatment of crude glycerol must be studied, and a combination of crude glycerol separation with catalytic conversion is recommended. As the three hydroxyl groups in glycerol are not strongly different in reactivity, the conversion of glycerol and the selectivity of desired products are quite low and highly depend on nature of catalysts and reaction conditions. They always produce a mixture of undesired product, which makes the purification of the desired product complicated and expensive. In addition, the chemical conversion processes are always associated with high pressures and/ or high temperatures. Therefore, chemical conversion of crude glycerol needs to be further developed to make biodiesel industrialisation more practical. Otherwise, other conversion processes, such as biological conversion of glycerol, must be explored and considered.

1.1.5.2 Biological conversion of glycerol

Nath and Das (2004), and Keskin *et al.* (2011) have mentioned that biological conversions have advantages in sustainability and energy requirement, compared to some chemical catalytic conversions. Because most bioconversions are carried at ambient temperatures and pressures, and therefore they require less energy input compared to catalytic conversions. The development of an economic biological conversion of inexpensive glycerol into higher value products is expected to make biodiesel production more economic and will thus help to establish more bio-refineries (Dharmadi *et al.* 2006).

There is a wide range of microorganisms capable of metabolising glycerol or crude glycerol and generating valuable products. Glycerol can be metabolised through both reductive and oxidative pathways as shown in Figure 1-3.
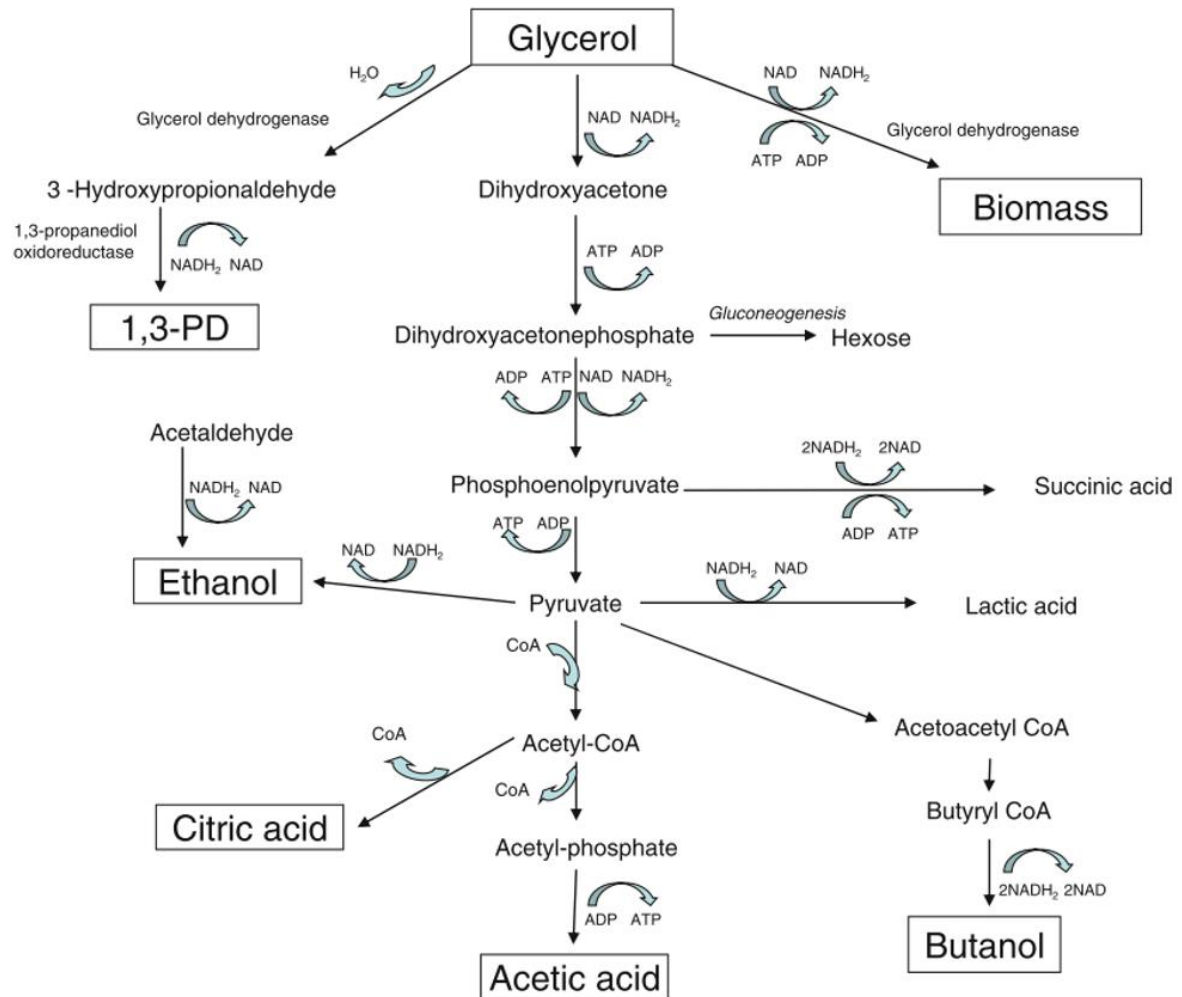
Figure 1-3: Glycerol metabolism to produce value-added products (Dobson *et al.* 2012)

As seen in Figure 1-3, in the reductive pathway, glycerol is initially dehydrated to form 3-hydroxypropionaldehyde, and 3-hydroxypropionaldehyde is then reduced to form 1, 3-propanediol (PD) and regenerate NAD^+. On the other hand, most value-added products are generated through the oxidative pathway. Glycerol is dehydrogenated by NAD-linked glycerol dehydrogenase to form dihydroxyacetone (DHA). DHA is phosphorylated to dihydroxyacetone phosphate (DHA phosphate), and then converted to the intermediate product pyruvate through glycolysis. Organic

8

alcohols and acids, such as citric acid, acetic acid, succinic acid, lactic acid, ethanol, butanol *etc.*.

Most research has focused on the bioconversion of glycerol and crude glycerol to hydrogen (H_2) and 1, 3-propandiol (PD) (da Silva *et al.* 2009). Between H_2 and PD, H_2 is a more desirable product because the production of PD is constrained by low yields and productivity (Saxena *et al.* 2009; Burch *et al.* 2007; Daniel *et al.* 1995; Seifert *et al.* 2001). In addition, H_2 is a clean renewable alternative fuel owing to its high gravimetric energy density, 143 MJ kg^{-1}, and it is easily converted to electricity in fuel cells yielding only water as the final product upon its combustion (Basak & Das 2007). Therefore, it has great potential in the fuel market.

H_2 can be generated with organic acids and alcohols as a by-product during the oxidative dark fermentation of glycerol. Under the photo-fermentation of glycerol, intermediate products, such as acetic acids, ethanol and butyric acids can be further metabolised to hydrogen. The stoichiometric equations showing hydrogen yield during glycerol bioconversion are shown in Figure 1-4.

Dark fermentation

$$C_3H_8O_3 + H_2O \rightarrow CH_3COOH \ (Acetic \ acid) + CO_2 + 3H_2 \qquad \text{Equation 1-1}$$

$$2C_3H_8O_3 \rightarrow C_4H_8O_2(Butyric \ acid) + 2CO_2 + 4H_2 \qquad \text{Equation 1-2}$$

$$2C_3H_8O_3 \rightarrow C_4H_{10}O \ (Butanol) + 2CO_2 + H_2O + 2H_2 \qquad \text{Equation 1-3}$$

$$C_3H_8O_3 \rightarrow C_2H_6O \ (Ethanol) + CO_2 + H_2 \qquad \text{Equation 1-4}$$

Photo-fermentation

$$C_3H_8O_3 + 3H_2O \rightarrow 3CO_2 + 7H_2 \qquad \text{Equation 1-5}$$
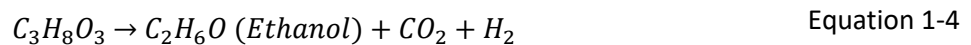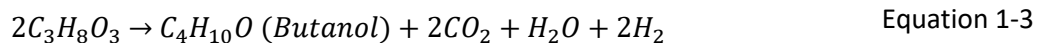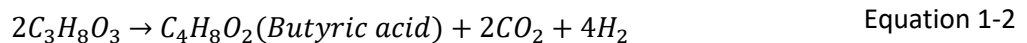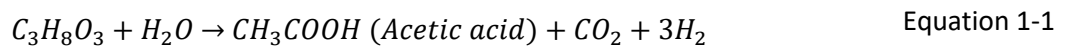
Figure 1-4: Stoichiometric equation showing hydrogen yield during glycerol bioconversion (Sarma, Brar, Sydney, et al. 2012)

As seen in Figure 1-4, the H_2 yield from glycerol through photo-fermentation is much higher than that through dark fermentation, because the incomplete oxidation in dark fermentation results in the production of organic acids as waste products. Therefore,

photo-fermentation of glycerol is more desirable for H_2 production than dark fermentation.

Some typical hydrogen-producing microorganisms are listed in Table 1-3. Amongst microorganisms able to generate H_2 and listed, *Rhodopseudomonas palustris* (*R. palustris*) has the highest H_2 yield, generating 6 moles of H_2 per mole of glycerol (Sabourin-Provost & Hallenbeck 2009; Pott *et al.* 2012). This purple, non-sulphur (PNS) bacterium produces relatively pure H_2, in stoichiometric quantities at a reasonable rate, when grown anaerobically on crude glycerol. It can reduce H^+ ions to H_2 gas by using both reducing powers derived from the organic compounds, such as glycerol, and the energy derived from light. Therefore, cultivating *R. palustris* to utilise the crude glycerol from biodiesel manufacturing and convert it into H_2 is a potential solution to the glycerol problem.

Table 1-3: List of micro-organisms producing H_2 and other products from glycerol (Sarma, Brar, Le Bihan, *et al.* 2012)

Strains	Maximum H_2 yield (mol H_2/ mol glycerol)	Other by-products
Thermotoga neapolitana DSM 4359	2.73	-
Halanaerobium saccharolyticum (subspecies *Saccharolyticum*)	0.62	1,3-propanediol (PD), butyrate, ethanol
Halanaerobium saccharolyticum (subspecies senegalensis)	1.61	acetate
Enterbacter aerogenes HU-101	0.063	ethanol
Klebsiella pneumoniae ATCC 25955	-	PD
Citrobacter freundii ATCC 8090	-	PD
Enterbacter agglomerans CNCM 1210	-	PD
Clostridium butyricum CNCM 1211	-	PD
Rhodopseudomonas plastrius	6	-
Enterbactor aerogenes NBRC 12010	0.77	-
Klebsiella sp. HE1	0.345	-
Klebsiella pneumoniae	-	PD

1.2 Rhodopseudomonas palustris

1.2.1 Taxonomy, ecology, and reproduction

Rhodopseudomonas palustris (*R. palustris*), a common purple non-sulphur (PNS) bacterium, is a gram-negative alpha proteobacterium widely found in the natural environment (Larimer *et al.* 2004). Normally it can be found in warm aquatic environments, which are rich in organic compounds, such as lakes, wastewater ponds and coastal lagoons (Hallenbeck 2012).

Figure 1-5 is a colour image of a single *R. palustris* cell obtained from electron microscopy. From the figure, it is red to brownish-red in colour, rod-shaped to ovoid in shape, and it has a size of 0.6-0.9 × 1.2-2.0 μm. It is motile by means of subpolar flagella. It is normally reproduced by budding (Brenner et al. 2005b). *R. palustris* cells vary in size, shape, and opacity of cells (Whittenbury & McLee 1967).

The "life cycle" of *R. palustris* from a "daughter" cell becoming a "mother" cell and developing a second "daughter" cell is shown in Figure 1-6 (Whittenbury & McLee 1967). From *a* to *d*, the "mother" cell produces a slender prostheca at the pole opposite to that bearing the flagella with a length 1.5 – 2.0 times of the original cell. From *e* to *g*, the end of the prostheca swells, and the "daughter" cell grows, producing a dumbbell-shaped organism. During *h* and *i*, asymmetric division then takes place and results in two "daughter" cells: one motile, classified as a "swarmer"; and one immotile, possessing a stalk. At a the motile "daughter" cell is now turned into a "mother" cell to repeat the cycle again (Brenner et al. 2005a).
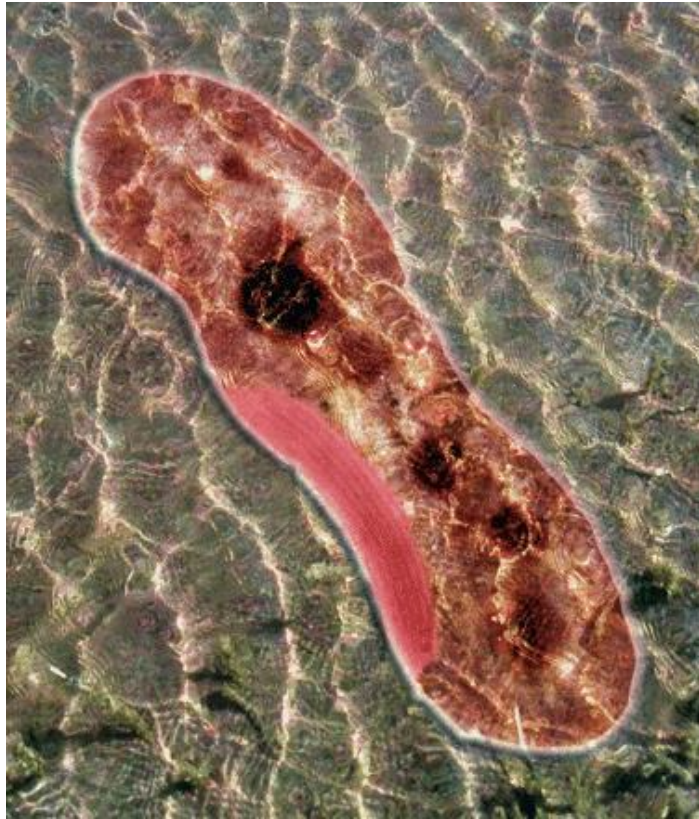
Figure 1-5: A digitally-colorized image of *R. palustris* obtained *via* electron microscopy (obtained from a cover page of Journal of Bacteriology related to (Welander *et al.* 2009))
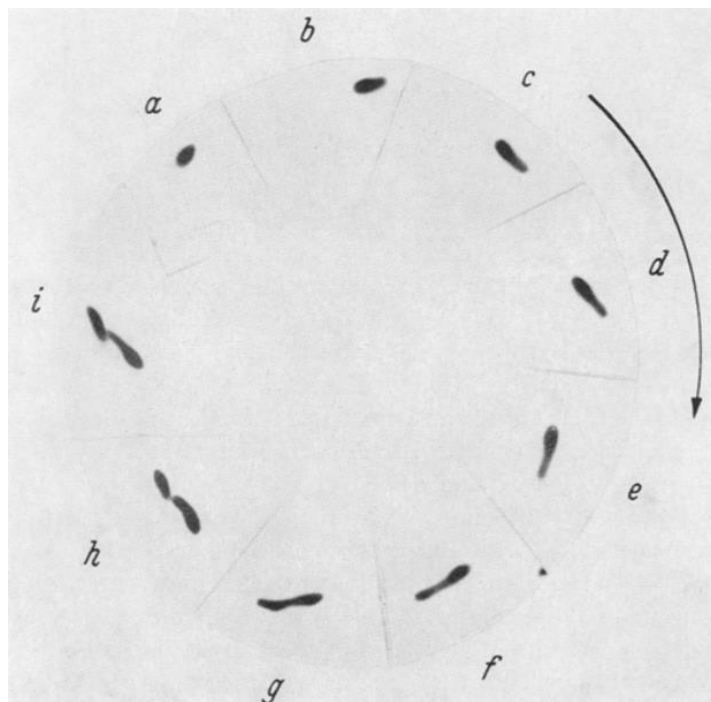
Figure 1-6: "Lifecycle" of *R. palustris*. Phase contrast preparation. Stages in the development of a "daughter" cell in *a*. to the beginning of the development of a second "daughter" cell in *i*. Magnification × 1,700 (Whittenbury & McLee 1967)

1.2.2 Metabolic pathways

R. palustris is the first PNS bacterium had its genome completely sequenced (Larimer *et al.* 2004). The genome sequence has demonstrated that this PNS bacterium is metabolically diverse, and it can grow by any one of the four pathways of metabolism that support life: photoheterotrophic, photoautotrophic, chemoheterotrophic, and chemoautotrophic; as shown in Figure 1-7 (Larimer *et al.* 2004). For example, under anaerobic conditions, in the presence of light, *R. palustris* can utilise the energy from light. It is preferred to grow on organic carbon sources and perform as photoheterotrophs, and this metabolic pathway is well-known to produce H_2 as a side product (Koku *et al.* 2002). In the absence of organic carbon sources, *R. palustris* can also grow on carbon dioxide and perform as photoautotrophs if electron donors, such as H_2, S^{2-}, and Fe^{2+} *etc.*, are provided (Gest 1951; Hallenbeck 2012). Under aerobic conditions, in the dark, *R. palustris* can grow on and utilise energy from organic and inorganic carbon sources and perform as chemoautotrophs and chemoheterotrophs. No H_2 will be generated under aerobic conditions.
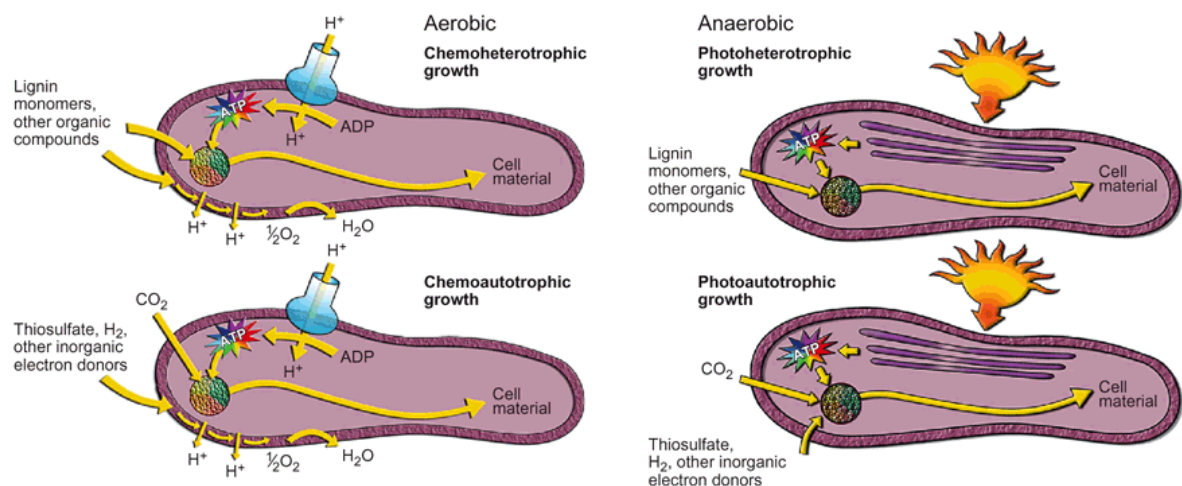
Figure 1-7: Schematic representations of the four types of metabolism of *R. palustris*. The multi-coloured circle in each cell represents the enzymatic reactions of central metabolism. (Larimer *et al.* 2004)

1.2.2.1 Phototrophs: energy from light

R. palustris contains genes *rps1505-rpa1554* for energy generation by photophosphorylation. These genes are required for the biosynthesis of bacteriochlorophyll, carotenoid, reaction centre complex, and light harvesting complex. The light energy is absorbed to initiate the electron transfer in reaction centre (Larimer *et al.* 2004).

1.2.2.2 Chemotrophs: energy from chemicals

In the presence of H_2, S^{2-}, and Fe^{2+} *etc.*, *R. palustris* can use inorganic compounds as electron donors as energy sources for respiratory growth and as sources of reducing power for carbon dioxide and nitrogen fixation (Larimer *et al.* 2004; Hallenbeck 2012). In the absence of organic carbon sources, *R. palustris* can consume hydrogen as electron donors to fix carbon dioxide for chemotrophic growth.

1.2.2.3 Heterotrophs: biodegradation

R. palustris can utilise a wide range of organic carbon sources, including lignin monomers, fatty acids and dicarboxylic acids derived from green plants, animal fats, and seed oils (Larimer *et al.* 2004). Therefore, it is possible for *R. palustris* to utilise organic carbon sources from food waste or industrial wastewater to generate valuable products (Kim *et al.* 2004).

1.2.2.4 Autotrophs: carbon dioxide fixation

R. palustris contains two active forms of ribulose-1,5-bisphosphate carboxylase/oxygenase (RubisCo), they key enzyme of the Calvin-Benson-Bassham (CBB) pathway of carbon dioxide fixation (Larimer *et al.* 2004). In the presence of H_2, S^{2-}, and Fe^{2+} etc., *R. palustris* can use inorganic compounds as electron donors for reductive carbon dioxide fixation during photoautotrophic growth primarily via the CBB pathway (Hallenbeck 2012; Tabita 1995). The simplified Calvin-Benson-Bassham pathway is presented in Figure 1-8, from which it can be seen that this pathway is involved in the photosynthesis of *R. palustris* in two stages. In the first stage, light is absorbed to synthesise adenosine triphosphate (ATP) and nicotinamide adenine dinucleotide phosphate (NADPH), whereas, in the second

stage, carbon dioxide and water are converted into organic molecules, such as glucose via RubisCO enzyme (Helmenstine 2015). The carbon fixation process consumes the energy from both ATP and NADPH, and the overall process can be expressed as:

$$3CO_2 + 9ATP + 6NADH + 5H_2O \rightarrow glyceraldehyde - 3 - phosphate \qquad \text{Equation 1-6}$$
$$+ 9ADP + 8Pi + 6NADP^+ + 2H^+$$
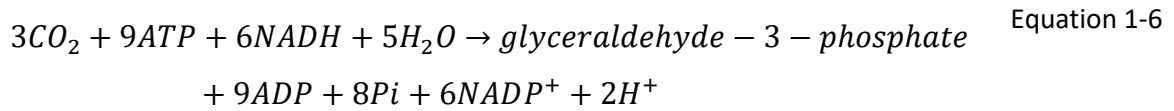
where *Pi* is inorganic phosphate.
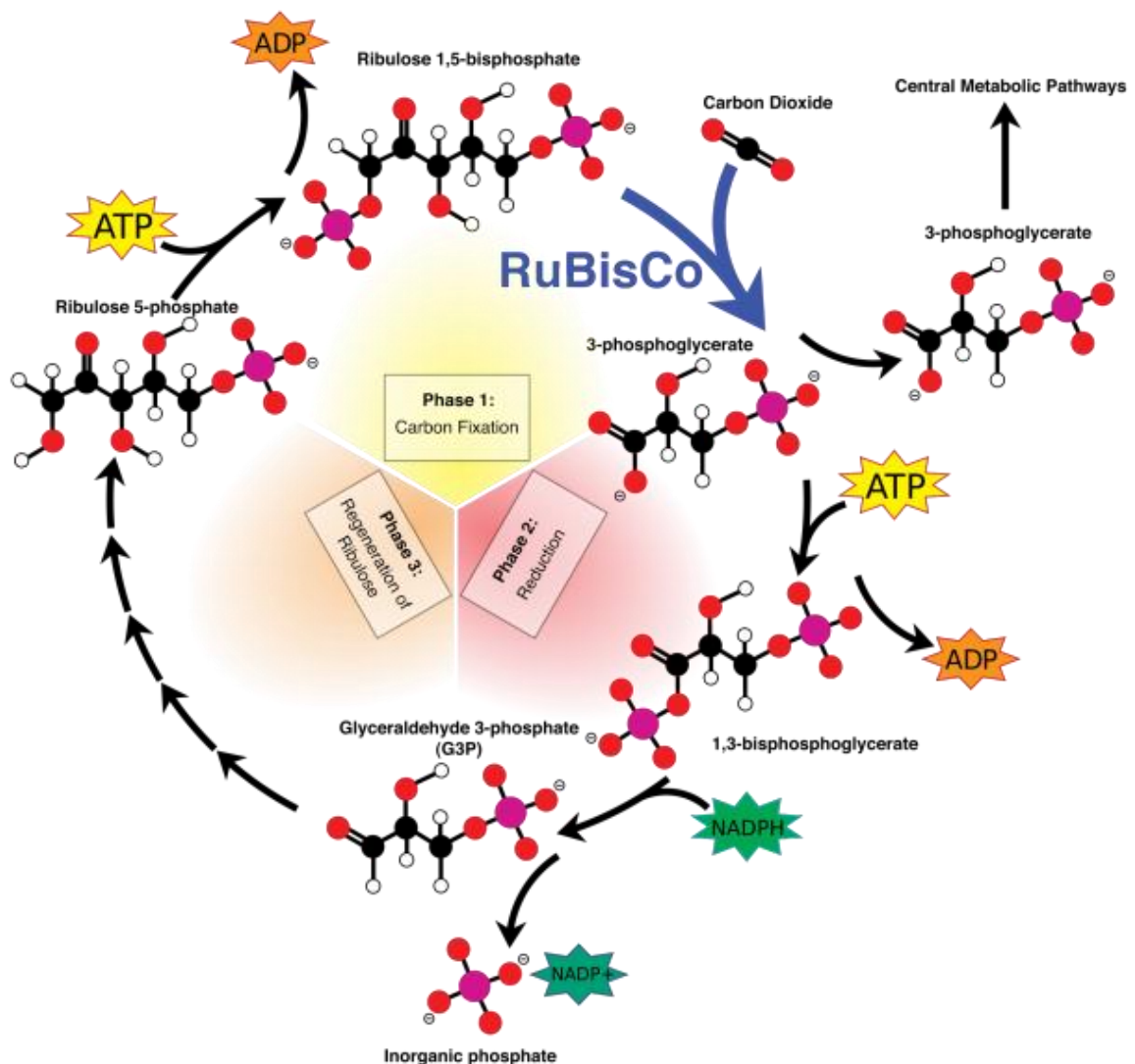
Figure 1-8: Overview of the Calvin-Benson-Bassham pathway (Helmenstine 2015)

1.2.3 Metabolism related to H_2 production

From previous section, *R. palustris* can grow by any one of the four pathways: photoheterotrophs, photoautotrophs, chemoheterotrophs, and chemoautotrophs. Practically H_2 production by *R. palustris* mainly occurs through the photoheterotrophic pathway with an organic carbon source in the presence of light and under anaerobic conditions (Koku *et al.* 2002; Hallenbeck 2012; Kim & Kim 2011). Recently Huang *et al.* (2010a) also found that *R. palustris* grew photoautotrophically with thiosulfate and bicarbonate and produced H_2 when molecular nitrogen was the sole nitrogen source (nitrogen-fixing conditions).

1.2.3.1 Overview

The overall H_2 production process of photoheterotrophic growth in *R. palustris* is illustrated in Figure 1-9.
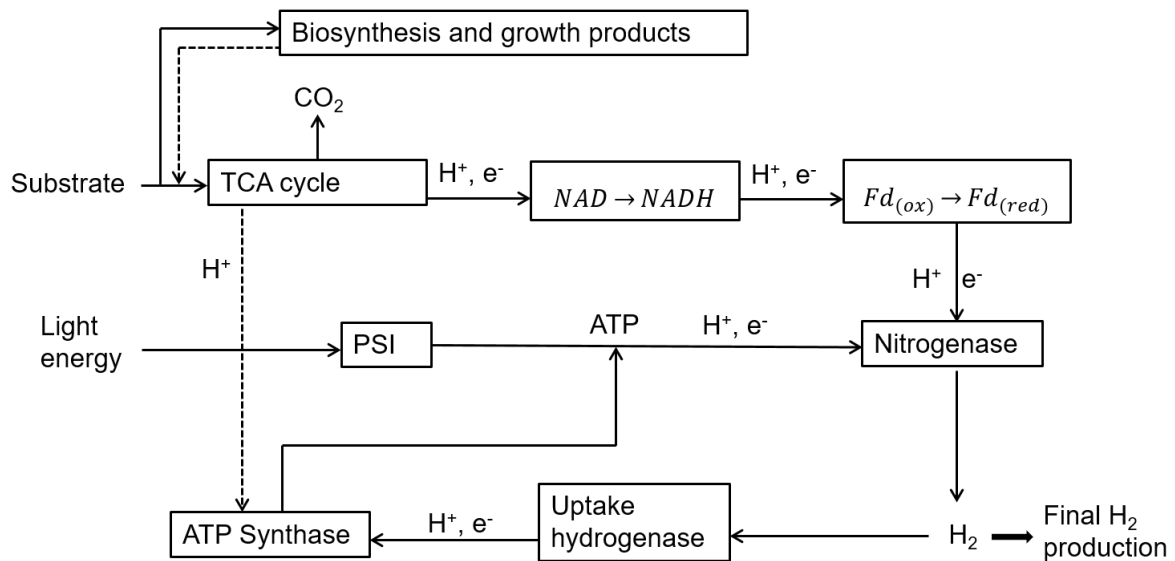
Figure 1-9: Metabolism of *R. palustris* for hydrogen production, modified from (Kim & Kim 2011; Koku *et al.* 2002)

As seen in Figure 1-9, when an organic carbon substrate, such as glycerol, is fed to the bacterium, it is used as both the carbon source for biosynthesis and the electron donor for H_2 production during anaerobic photosynthesis. On the other hand, as an

electron donor, it enters the tricarboxylic acid (TCA) cycle by consuming the energy from adenosine triphosphate (ATP), which generates carbon dioxide, releases protons (H^+) and electrons from the substrates, and reduces quinones in the cell. The reduced quinones then pick up the protons and form an electrochemical gradient between the periplasmic and cytoplasmic space in the cell by the accumulation of protons. This electrochemical proton gradient offers the energy for the nicotinamide adenine dinucleotide (NADH) synthesis. The protons and electrons are then transferred to nitrogenase by ferredoxin (Fd) in the cell. Working in parallel, light is absorbed in the photosynthetic membrane apparatus in photosystem I (PSI) as an energy source to obtain adenosine triphosphate (ATP) from adenosine diphosphate (ADP). This ATP together with the protons and electrons from ATP synthase are also channelled to nitrogenase. H_2 gas is then generated from protons and electrons through the action of the nitrogenase, consuming the energy from both the proton gradient (*i.e.* NADH) and ATP. The hydrogenase in *R. palustris* functions primarily in the direction of H_2 consumption, which consumes hydrogen gas and produces protons and electrons for ATP synthase. Therefore, the overall H_2 production is the balance between the H_2 produced by nitrogenase and the H_2 consumed by uptake hydrogenase.

1.2.3.2 Substrate for hydrogen production

The complete stoichiometric conversion of a substrate to H_2 in *R. palustris* can be described by (Sasikala *et al.* 1990):

$$C_xH_yO_z + (2x - z)H_2O \rightarrow (y/2 + 2x - z)H_2 + xCO_2$$
Equation 1-7
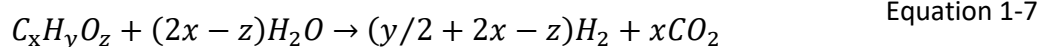
Under photo-fermentative conditions, *R. palustris* can convert glycerol into H_2 using the enzymes nitrogenase and hydrogenase, which catalyse the oxidation as Equation 1-5: $C_3H_8O_3 + 3H_2O \rightarrow 3CO_2 + 7H_2$.

Because *R. palustris* can utilise a wide range of substrates for H_2 production, the feasibility of using wastewater, such as wastewater from dairy plant, sugar refinery, tofu factory, and olive mill *etc.*, as source of nutrients, could be important for the economics of biological H_2 production (Sasikala et al. 1990; Eroglu et al. 2008; Fascetti et al. 1998). Little is known about the metabolism of complex wastes, but

studies of hydrogen production from wastewater are abundant in the literature. However, H_2 production rate from wastewater is still low compared to the case when the pure substrate is used. Therefore, utilising wastewater as the carbon source to cultivate PNS bacteria and generate hydrogen deserves further study.

1.2.3.3 Enzymes involved in hydrogen production

As mentioned in the previous section, *R. palustris* can produce H_2 through the balance of two enzyme systems: nitrogenase and hydrogenase. H_2 is mainly generated through nitrogenase and consumed through uptake hydrogenase. Both the nitrogenase and hydrogenase systems are irreversibly inhibited by the presence of oxygen (Koku *et al.* 2002), therefore, the cultivation of *R. palustris* must be maintained in anaerobic conditions for maximum H_2 production (Ormerod & Ormerod 1961; Schwartz & Friedrich 2006; Nandi & Sengupta 1998).

Nitrogenase

R. palustris has structural genes for three different nitrogenases as well as the related cofactor and assembly genes for these nitrogenases (Larimer *et al.* 2004)

In the presence of molecular nitrogen, *R. palustris* can utilise oxidised nitrogen compounds as electron acceptors to perform denitrification. The most common way to fix molecular nitrogen is to reduce nitrogen to ammonia through a nitrogenase, *via* the following equations (Koku et al. 2002; McKinlay & Harwood 2010a; Hallenbeck 2012), and the regulation between three nitrogenase has been discussed by Oda *et al.* (2005).

$$Mo-nitrogenase: N_2 + 8H^+ + 8e^- + 16ATP \rightarrow 2NH_3 + H_2 + 16ADP$$
<div align="right">Equation 1-8</div>

$$V-nitrogenase: N_2 + 12H^+ + 12e^- + 24ATP \rightarrow 2NH_3 + 3H_2 + 24ADP$$
<div align="right">Equation 1-9</div>

$$Fe-nitrogenase: N_2 + 24H^+ + 24e^- + 48ATP \rightarrow 2NH_3 + 9H_2 + 48ADP$$
<div align="right">Equation 1-10</div>

Nitrogenase also functions in the absence of molecular nitrogen by utilising protons as electron acceptors to dissipate the excessive reducing power in the bacteria (McKinlay et al. 2014a) *via* the following equation:

$$2H^+ + 2e^- + 4ATP \rightarrow H_2 + 4ADP + 4Pi$$
<div align="right">Equation 1-11</div>
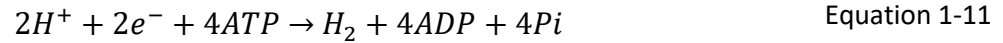
Hydrogenase

The hydrogenase acts to establish the equilibrium between H^+ and H_2:

$$2H^+ + 2e^- \leftrightarrow H_2$$
<div align="right">Equation 1-12</div>

The forward reaction is catalysed by H_2 evolving hydrogenase, and the backwards reaction is catalysed by uptake hydrogenase. However, under most conditions, the uptake hydrogenase dominates the process and actively consumes H_2, in contrast to the action of the nitrogenase. Therefore, H_2 is mainly generated *via* nitrogenase and consumed *via* uptake hydrogenase.

1.2.3.4 Relationship between H_2 and polyhydroxybutyrate

R. palustris grows on organic carbon source, such as glycerol, and produces internal storage products when the environment is not optimal (McKinlay *et al.* 2014b). Those internal storage products include glycogen, trehalose, and mainly (polyhydroxybutyrate) PHB.

PHB is an energy and carbon storage compound found in different microorganisms when the nitrogen source is not sufficient. It can be stored and used for survival when the carbon source becomes a limiting resource (Wu, Liou, *et al.* 2012). However, PHB synthesis consumes many metabolites and reducing power that are required for the H_2 production in PNS bacteria. Therefore, several studies indicated that PHB accumulation in PNS bacteria should compete with H_2 production for electrons and energy distribution (Wu, Liou, *et al.* 2012; Hustede *et al.* 1993; McKinlay *et al.* 2014a).

1.3 Aims and Objectives

The current project is concerned with developing aspects of the work carried out by a previous Ph.D., Robert Pott, in our department (Pott *et al.* 2012; Pott *et al.* 2014), particularly to understand the fundamentals relevant to scale-up and off-the-shelf products development. The overall goal of the current project is to assess the process feasibility and process potential for using *R. palustris* as a biocatalyst for H_2 production from glycerol.

The actual chemical composition of the crude glycerol varies with the type of catalysts and reagents used during the esterification, the conversion and recovery efficiencies of the biodiesel, other impurities in the feedstock, and whether or not the reagents and catalysts are recovered (Yang *et al.* 2012). And the effects of these variation would add additional complexity into understanding the mechanism and optimisation of *R. palustris* for H_2 production. With this in mind, all experimental work in this dissertation was carried out using pure glycerol.

In general, the U.K. has strong restrictions on genetic modification work. Genetic modification of *R. palustris* was again explored and discussed by Robert Pott, hence not discussed further in this project.

Accordingly, the measurable objectives are:

- To study, experimentally and theoretically, the growth and H_2 production characteristics of *R. palustris* when grown on glycerol and nitrogen gas.
- To study, experimentally and theoretically, the H_2 production characteristics of non-growing *R. palustris* under nitrogen starvation conditions.
- To optimise H_2 production rate from glycerol by using non-growing *R. palustris* in nitrogen starvation conditions, in particular, with various dry cell masses.
- To investigate the light impact on H_2 production from glycerol by non-growing *R. palustris*, in particular, the impact of light intensities and light wavelength ranges.
- To investigate organic supports on which the organism could be immobilised in order to protect and retain the organism within a chemical reactor.

The dissertation is organised as follows:

Chapter 1 introduces the background and the relevant literature regarding to this project.

Chapter 2 illustrates the materials and methods used in this project. The culture preparation, storage, and recovery is discussed in cell cultivation section. Most work is done in a custom-made photobioreactor cultivating anoxygenic $R.\ palustris$ and collecting H_2 generated. Different analytical methods are employed to determine bacteria absorbance, light emission and intensity, dry cell mass, glycerol and PHB assays, and gas composition.

Chapter 3 investigates the H_2 production by growing $R.\ palustris$ and explores the possibility of H_2 production by non-growing cells. The H_2 production performance, especially the H_2 yield, by both growing and non-growing $R.\ palustris$ are analysed and compared both qualitatively and quantitatively.

Chapter 4 investigates the H_2 production by non-growing $R.\ palustris$ with a range of optical density from 0.2 to 2.0. The H_2 production performance, particularly the H_2 production rate and energy conversion, is measured and analysed with its corresponding dry cell mass. A regression analysis is carried out to identify the relationship between the H_2 production rate and the dry cell mass. The Leudeking–Piret model is employed to fit the experimental data, and the product formation kinetics is discussed.

Chapter 5 and 6 investigates the H_2 production by non-growing $R.\ palustris$ with illumination provided by three different light sources at various light intensities. The emission spectra of different light sources and the absorbance spectrum of $R.\ palustris$ are compared to identify the suitable light source for $R.\ palustris$. The H_2 production performance, particularly the H_2 production rate and energy conversion, is measured and analysed. Through which, the light requirement for optimal energy conversion from H_2 production by non-growing $R.\ palustris$ is explored and identified.

Chapter 7 investigates the H_2 production by non-growing *R. palustris* in suspension and in immobilisation of alginate and *k*-carrageenan. The H_2 production performance, particularly the H_2 production rate and energy conversion, is measured and analysed to identify the suitable immobilisation material. It also investigates the H_2 production by alginate immobilised non-growing *R. palustris* with a range of dry cell mass. The results are compared with those from Chapter 4 to explore the possibility of H_2 production by immobilised non-growing cells. A regression analysis is carried out to identify the relationship between the H_2 production rate and the dry cell mass, and the Leudeking–Piret model is employed.

Chapter 8 draws the conclusion of the dissertation and gives the recommendation for future work.

2 Materials and methods

2.1 Cell cultivation

All chemicals and accessories used were obtained from Sigma-Aldrich and were of technical grade. Media and container used for culture were sterilised by autoclaving at 121°C for 21 minutes with a cooling fan. Most work was carried out in class 2 biosafety cabinet (Astec Microflow, Andover, U.K.). Suitable eye protection, gloves, and laboratory coat must be worn.

2.1.1 Strain

Rhodopseudomonas palustris (*R. palustris*) with strain designations of ATH 2.1.37 (ATCC® 17007™, NCIB 11774) was ordered from ATCC® as a freeze-dried axenic sample.

2.1.2 Solid medium

112 Van Niel's yeast agar medium (ATCC 2012) was used and consisted (per litre) of 1.0 g potassium phosphate dibasic (K_2HPO_4), 0.5 g magnesium sulphate ($MgSO_4$), 10.0 g yeast extract, and 20.0 g bacterial agar. The agar solution was adjusted to pH 7.0 with hydrochloric acid (HCl) or sodium hydroxide (NaOH) solution.

The autoclaved agar solution was cooled down at around 55 - 60 °C before pouring into 50 mm petri dish. Care was taken to not lift the lid off excessively and the plate was swirled in a circular motion to distribute agar on the bottom completely. The agar plate was left to cool in a class 2 biosafety cabinet (Astec Microflow, Andover, U.K.) for about 2 hours until solid.

The lids were replaced on the agar plates labelled on the bottom (name, date, agar type). The labelled agar plates were kept upside down in sterile plastic bags and stored in the fridge at 5 °C until needed. Prior to use, agar plates were warmed for half an hour in a 37 °C incubator.

2.1.3 Liquid medium

A defined liquid medium as described by Gosse *et al.* (2007) was used with a small modification. Potassium phosphate dibasic was used instead of sodium phosphate dibasic due to the availability in the lab. The liquid medium consisted (per litre) of 12.5 mM potassium phosphate dibasic (K_2HPO_4), 12.5 mM potassium phosphate monobasic (KH_2PO_4), 0.100 mM sodium thiosulphate ($Na_2S_2O_3$), 0.0145 mM 4-aminobenzoic acid (PAPB, $H_2NC_6H_4CO_2H$), and 1 mL concentrated base solution.

Concentrated base solution was composed of (per litre): 20 g nitrilotriacetic acid ($C_6H_9NO_6$), 28.9 g magnesium sulphate ($MgSO_4$), 6.67 g calcium chloride dehydrate ($CaCl_2 \cdot H_2O$), 18.5 mg ammonium molybdate tetrahydrate (($NH_4)_6Mo_7O_{24} \cdot 7H_2O$), 198 mg iron(II) sulphate heptahydrate ($FeSO_4 \cdot 7H_2O$), 100 mL metal 44 solution.

Metal 44 solution was composed of (per litre): 2.5 g ethylenediaminetetraacetic acid (EDTA, $C_{10}H_{16}N_2O_8$), 10.95 g zinc sulphate heptahydrate ($ZnSO_4 \cdot 7H_2O$), 5.0 g iron(II) sulphate heptahydrate ($FeSO_4 \cdot 7H_2O$), 1.54 g manganese(II) sulphate monohydrate ($MnSO_4 \cdot H_2O$), 392 mg copper(II) sulphate pentahydrate ($CuSO_4 \cdot 5H_2O$), 250 mg cobalt nitrate hexahydrate ($Co(NO_3)_2 \cdot 6H_2O$), 177 mg sodium tetraborate decahydrate ($Na_2B_4O_7 \cdot 10H_2O$), and a few drops of concentrated sulphuric acid (H_2SO_4) to prevent precipitation.

The pH of the defined medium was adjusted to pH 7.0 by hydrochloric acid (HCl) or sodium hydroxide (NaOH) solution.

Based on the cultivation conditions, different sterile nitrogen and carbon sources with different concentrations were added to the medium afterwards. Glycerol was used as the only carbon source in this project, and it was sterilised by autoclaving at 121 °C for 21 minutes with a cooling fan. Sodium glutamate and nitrogen gas were used as nitrogen sources. The 2 M sodium glutamate solution was prepared and filtered sterile through Millex® syringe filter units. And the nitrogen gas was filtered sterile through a HEPA filter before sparging into the culture bottles.

2.1.3.1 Pre-culture medium

Pre-culture medium was used for pre-culture in this project. 100 µL of 2M filtered sodium glutamate and 100 µL of autoclaved pure glycerol was added into 15mL medium. As the viscosity of pure glycerol is too high to be transferred through pipetting at room temperature, the glycerol was preheated in the microwave for 30 seconds before adding to the medium. The tube was then sealed by its cap, and the solution was mixed by inversion.

2.1.3.2 Growing medium

Growing medium was used to produce H_2 with growing cells in Chapter 3. 200 mL of the cell suspension was then supplemented with 10 mM glycerol in a 250 mL bottle and sparged with filtered sterile N_2 for ten minutes.

2.1.3.3 Non-growing medium

Non-growing medium was used to produce H_2 with non-growing cells in chapters 3, 4, 5, and 6. 200 mL non-growing cell suspension with the right optical density was then cultivated in a 250 mL bottle and supplemented with 10 mM glycerol. Argon was bubbled through the suspension for ten minutes.

2.1.4 Rehydrating freeze-dried sample

R. palustris was ordered from ATCC as a freeze-dried sample. The sample was rehydrated according to the methods provided by the supplier (ATCC 2013). The sample ampule was disinfected, then broken as instructed in a class 2 biosafety cabinet (Astec Microflow, Andover, U.K.). 1 mL liquid medium (mentioned in Chapter 2.1.3) was added to the vial by using a pipette, and mixed. The sample was then stored in a sealed sterile 1.5 mL micro-centrifuge tube.

2.1.5 Isolating bacterial colonies on agar plates

112 Van Niel's yeast agar plates were prepared as mentioned in Chapter 2.1.2. A quadrant streak plating technique (Thiel 1999b) was used to plate bacterial sample

and isolate bacterial colonies on an agar plate. A schematic diagram of quadrant streak plate is shown in Figure 2-1.
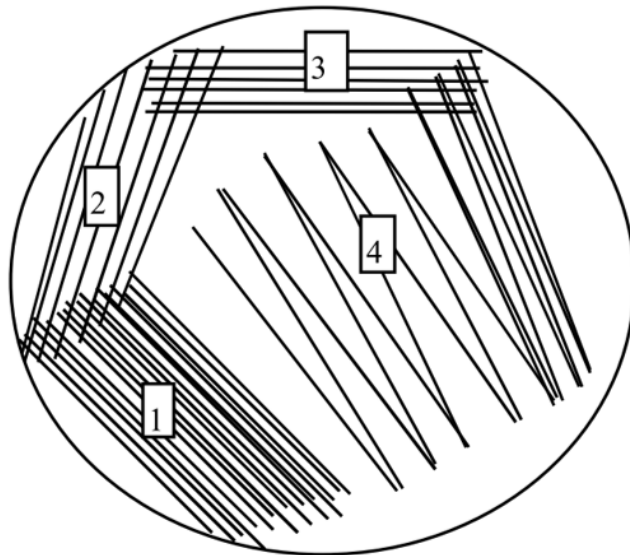
Inoculation of a streak plate

1. Area of initial inoculation and first streaks yield heavy growth
2. Area of second streaks from area 1 yields less dense growth
3. Area of third streaks from area 2 yields weak growth
4. Area of fourth streaks from area 3 yields single colonies

Figure 2-1: Schematic diagram of quadrant streak plating technique (Thiel 1999b).

A small volume of rehydrated bacterial culture was extracted from the micro-centrifuge tube (Chapter 2.1.5). The loopful of culture was gently placed on the surface of the agar, and dragged several times across the surface in region 1. The agar plate was rotated by 90° and a new sterile loop was dragged across the corner of the culture in region 1 before being repeatedly dragged across the surface in region 2. Care should be taken to avoid excursive entry into region 1.

Once again agar plate was rotated by 90° and a new sterile loop was used. The procedure was repeated to create streaks in region 3 and region 4 as shown in Figure 2-1. The streak lines get gradually more spread out to allow individual colonies to form. The agar plate was then covered, and sealed with parafilm to prevent dehydration. All of this was carried out in a class 2 biosafety cabinet (Astec Microflow, Andover, U.K.).

The sealed agar plates were then labelled in the bottom of the plate with the microorganism and incubated upside down at 30 ± 2 °C for two days, whilst illuminated by an incandescent lamp.

2.1.6 Preparing pre-culture

Within a class 2 biosafety cabinet (Astec Microflow, Andover, U.K.), the parafilm on the agar plate was removed. Care was taken to prevent any condensation from dropping from the lid onto the agar plate.

A colony with the right morphology (red or brownish-red in colour, rod-shaped or ovoid in shape) was isolated and transferred into a 15 mL centrifuge tube containing pre-culture media. Care should be taken not to dig the loop into the agar when isolating the colony. Once the colony was successfully transferred, the agar plate was resealed with parafilm and placed up-side-down in the fridge until required. The inoculated centrifuge tube was sealed and then left to culture for a week at 30 ± 2 ºC, whilst illuminated by an incandescent lamp.

2.1.7 Culture storage and recovery

While there are many options for culture storage, it is important to ensure that the strain is compatible with the chosen storage method (Thiel 1999a; Thermo-Scientific 2014). Bacteria can be streaked onto agar plates and stored at 4 °C for up to a month. They can also be stored as a frozen sample with cryoprotectants, typically glycerol for *R. palustris*, at - 20 °C or even - 80 °C for longer time frames. Generally, the viable storage period of bacteria increases as the storage temperature decreases.

2.1.7.1 Short-term storage

For regular use, *R. palustris* can be streaked onto an agar plate and incubated with illumination at 30 ± 2 °C for two days to ensure colony formation. After this the agar plate was sealed with parafilm and stored up-side-down in the dark at 4 °C up to a month. For details in method of streaking bacterial sample on an agar plate, please refer to Chapter 2.1.5.

To re-culture, a right colony can be picked up and cultivated in medium as described in Chapter 2.1.6.

2.1.7.2 Long-term storage

For long-term storage, *R. palustris* can be stored for up to a year at - 20 °C or longer at - 80 °C.

Bacteria not used recently could be stored in liquid medium with a cryoprotectant, such as glycerol at 15 (v / v) %, in a regular - 20 °C freezer up to a year, or stored a special - 80 °C freezer for years (Thiel 1999a; Thermo-Scientific 2014).

Cells were cultivated in a 15 mL centrifuge tubes as described in Chapter 2.1.6 and allowed to grow for a week until they reached lag phase. Cells were then collected by centrifuging (Sigma® 3-16PK, Osterode am Harz, Germany) for ten minutes at room temperature at 4,424 g (Gosse 2008). The call pellet was then re-suspended in 1.5 mL of the 15 (v / v) % glycerol solution. The glycerol-bacteria broth was mixed thoroughly and transferred into a sterile labelled microcentrifuge tube, and stored in a - 20 °C freezer or a - 80 °C freezer. For - 80 °C freezing storage, the cells were snap-frozen by immersing the micro-centrifuge tubes in liquid nitrogen before storing in the - 80 °C freezer.

To re-culture, the frozen sample can be streaked onto a fresh agar plate (Chapter 2.1.5), or cultivated in medium (Chapter 2.1.6). Care should be taken as repeated thawing and refreezing of the bacterial stock will reduce cell viability and should be avoided.

2.2 Experimental set-up

2.2.1 Overview

The experimental set-up for up to 10 culture bottles was designed with a magnetic hotplate stirrer (IKA® RT-10, Staufen, Germany) separated by 1 mm thick filament mica sheets (Langtech, Accrington, U.K.) to prevent light interference. 100 W incandescent lamps (BELL® R80 ES Reflector, London, U.K.) were placed on each side allowing a 40 cm gap between the surfaces of the light bulb and the bottle. A reference bottle (Duran® 250 mL GL 45, Mainz, Germany) with 200 mL water was

placed in the middle of the stirrer. Apart from the reference bottle, this prototype was able to run 9 samples at a time.

The irradiance on the surface of the bottles could be adjusted and controlled by varying the voltage supplied to the light bulbs (Regavolt® variable transformer, Waltham Cross, U.K.). The room temperature was set at 20 °C by air conditioning. The temperature inside the reference bottle was controlled at 30 ± 2 °C by adjusting cooling from fans (Sunon MB40201VX-0000-G99, Kaohsiung City, Taiwan) and heating from the hotplate. The temperature on the surface of each bottle was monitored and recorded continuously (Labfacility L200 digital thermometer, Bognor Regis, U.K.).

This prototype as shown in Figure 2-2 was built by Lee Pratt, our department workshop technician, and all the electrical work was carried out by Weiyao Ma, our senior electrical technician.
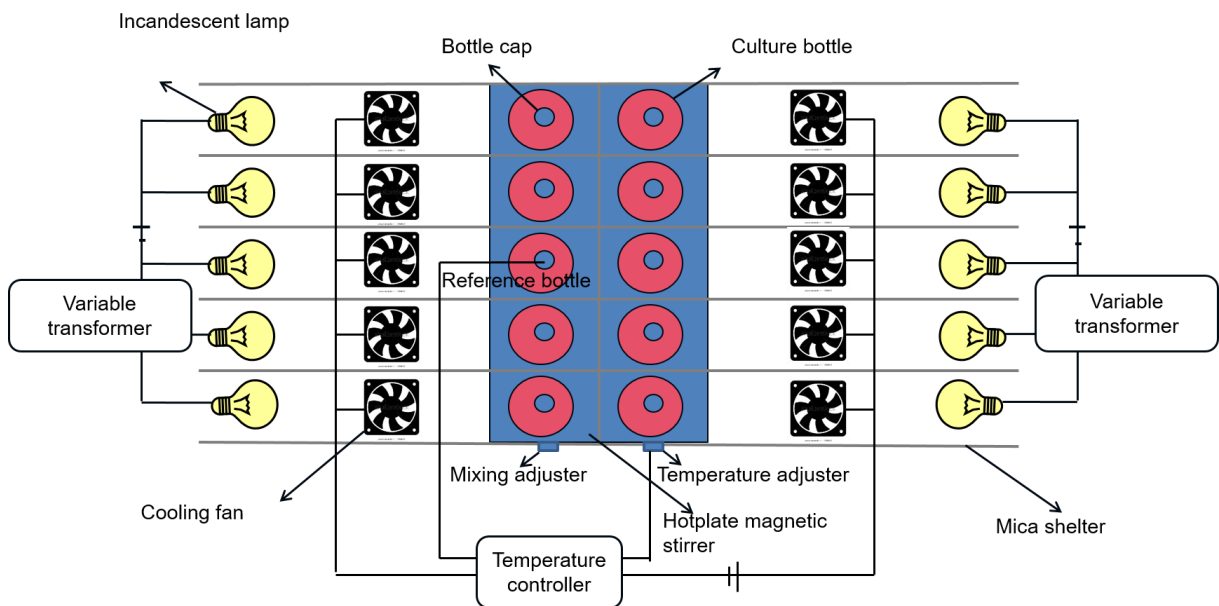
Figure 2-2: Schematic diagram of the overall experimental setup at top view.

2.2.2 Individual unit

A 250-mL laboratory glass bottle (Duran® 250 mL GL 45, Mainz, Germany) together with a specific bottle cap (Kinesis Omnifit® Q-series with on-off valves, Cambridge,

U.K.) were used to cultivate the bacteria and collect hydrogen in each single unit. The culture, inside the bottle, was stirred by a magnetic stir bar (Spinbar® PTFE-coated octagonal 1 / 2" × 1 / 8", New Jersey, U.S.).

The Omnifit® Q-series cap used contains two sampling ports for the collection of gas and liquid, and each port has a built-in on / off valve. The valves of both ports were closed normally to prevent any ingress of air, and they were only open temporarily when extracting gas and liquid samples. To collect the gas produced, each gas port was extended with a 1 / 8" PTFE tube (Kinesis, Cambridge, U.K.) to an inverted Pyrex® 100 ml graduated burette filled with water and submerged in a water bath, where the cumulative volume of gas produced could be measured by the displacement of water.

A water tank was made-to-order (Engineering & Design Ltd, Cambridge, UK) as the water bath for the unit. The tank was made of 2 mm thick acrylic sheet with a dimension of 10 cm × 5 cm × 10 cm (length × width × height). An aluminium burette stand was made by the department workshop to hold the burette by clamps and lift the water tank 6mm above the workbench. A 1 / 4" hole was drilled with the thread at the bottom of the water tank.

The end of the gas port tube was inserted into the burette through that hole, and the hole was sealed with a 1 / 8" O-ring and a 1 / 4"Omnifit® gripper fitting (Kinesis, Cambridge, U.K.).

The schematic diagram of the detailed individual unit is shown in Figure 2-3.
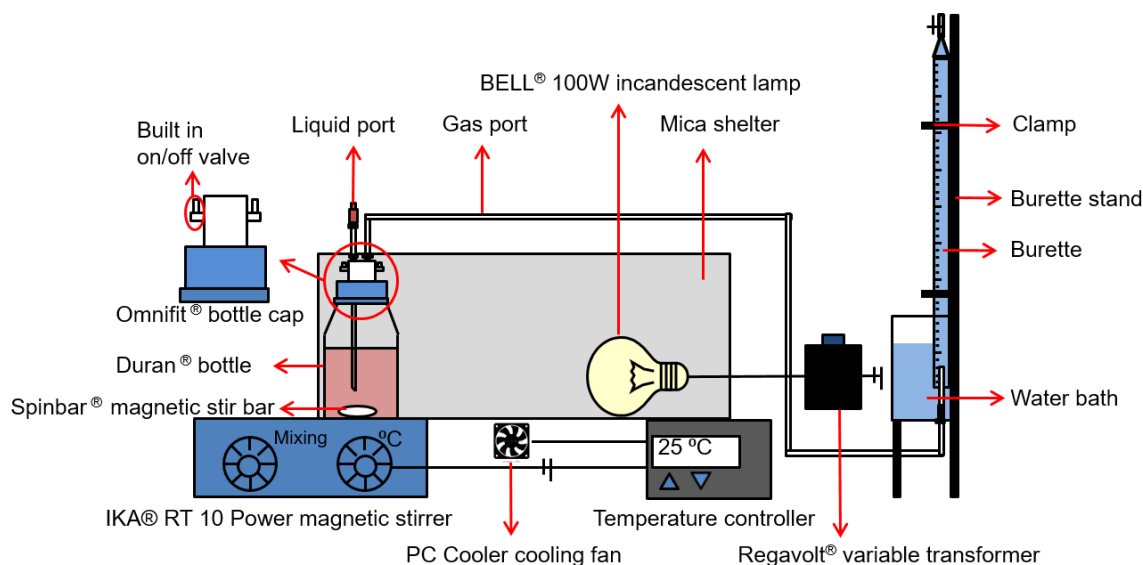
Figure 2-3: Schematic diagram of detailed individual setup at side view

2.2.3 Bottle cap fittings

The bottle caps and fittings were purchased from Kinesis, Cambridge, U.K.. All the components chosen were autoclave-able, and the safe operating pressure ranged from - 10 psi to + 20 psi. Most components were made of PEEK, PTFE, and PCTFE to minimise the hydrogen permeation and leakage.

The Omni-lok^{TM} type P ferrule system was used to build both liquid port and gas port in the bottle cap. To build the Omni-lok^{TM} system, the PTFE tubing was inserted through the gripper fitting and then installed with the ferrule.

The PEEK-cased ferrule contains a PTFE internal face to ensure perfect sealing with the external surface of the PTFE tubing. It also contains a PEEK external casing with a size bigger than the internal size of the gripper fitting. The 1 / 4" PEEK gripper fitting with 1 / 8" thread was then screwed tightly to the bottle cap to complete the system.

For the liquid port, the Omni-lok^{TM} system was applied at the other end of the PTFE tubing as well and screwed tight with the female lure adaptor. For the gas port, the

31

other end of the tubing was inserted into the burette through the hole drilled at the bottom of the water tank, and the hole was sealed with a 1 / 8" O-ring and an Omnifit® gripper fitting (1 / 4", with thread inside) the same way as the Omni-lok™ system.

The schematic diagram of different Omnifit® gas port fitting components is shown in Figure 2-4, and the materials and properties of those fitting components are summarised in Table 2-1.

Figure 2-4: Schematic diagram of different gas port fitting components

Table 2-1: Materials and properties of gas port fitting components (Omnifit 2013a; Omnifit 2013b; DURAN 2014)
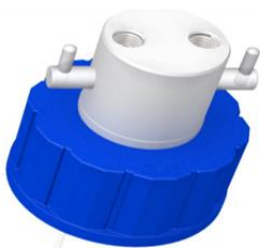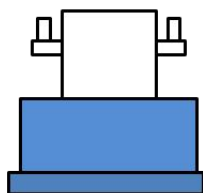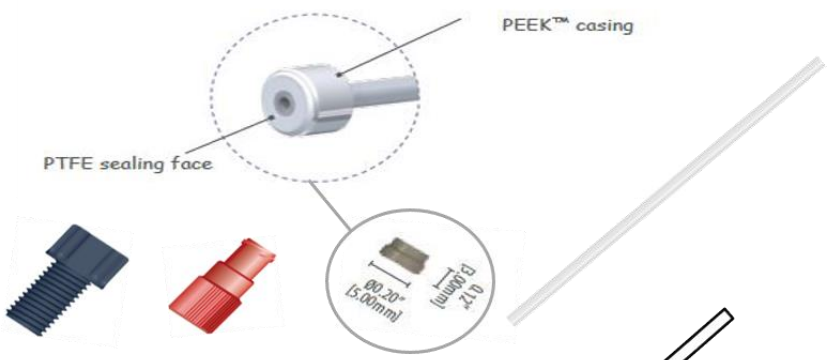
Component	*Materials*		*Operating pressure (psi)*		*Autoclave-able*
			+ve	-ve	
250 ml Duran® GL45 pressure plus laboratory glass bottle	Glass		- 10	+20	Yes
Omnifit® Q-series cap (GL45 cap, 2 port, on-off valves)	Outer cap	PP	-10	+20	Yes
	Body	PTFE			
	Internal rotor (caps with on/off valves)	PCTFE			
Gripper fitting (1/4", 1/8")	PEEK		-	-	Yes
Female lure adaptor (1/4")	PEEK		-	-	Yes
PEEK cased ferrule (1/8")	Internal sealing face	PTFE	-	600	Yes
	External casing	PEEK			
The Omni-lok™ type P ferrule system	-		Up to 1000		
Tube (1/8" 3.2 mm×1.5 mm)	PTFE		-	-	Yes

2.3 Analytical methods

2.3.1 Bacteria absorbance spectrum

The absorbance spectrum of *R. palustris* was measured by an ultra-violet spectrophotometer, ThermoSpectronic UV1 (Thermo Electron Corporation, Rugby, U.K.), as a function of wavelength ranging from 300 nm to 1000 nm.

2.3.2 Light source emission spectrum

The emission spectrum of a light source was measured by an imaging spectrograph (Chromex 250is, High Peak, U.K.) as a function of wavelength ranging from 300 nm to 1000 nm. The signal was received and transferred by a 200 nm fibre optic to the imaging spectrograph. The schematic diagram of imaging spectroscopy is shown in Figure 2-5, and the dark lines indicated light signal.
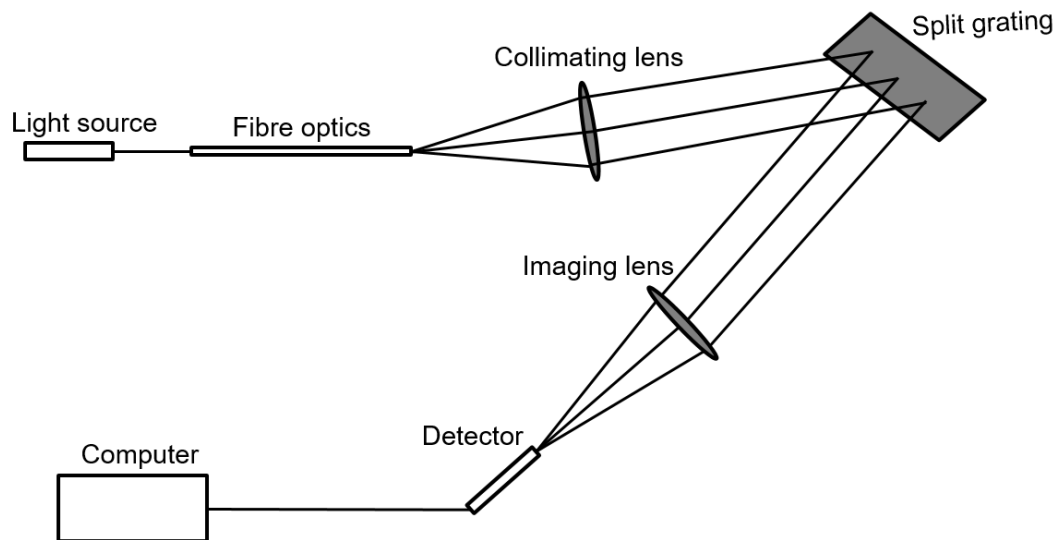
Figure 2-5: Schematic diagram of imaging spectroscopy

2.3.3 Light intensity

Since light intensity is defined as $I = \frac{P}{A}$ where I is the light intensity (W m^{-2}), P is the power incident on the surface, and A is the area of the incident surface, the light intensity on an incident surface could be measured by the power received at the surface if the area of the incident surface is known.

The power received on the surface of the culture bottles was measured by a power meter, Integrated 2-Watt Broadband Power and Energy Meter System (Melles Griot, Rochester, U.S.A.). The detector was placed exactly on the location of the culture bottles, and the energy output was selected as mW.

This power meter measures power from 10 µW to 2 W, and it covers the power generated by photons with wavelengths ranging from 200 nm to 20 µm. The 10-mm-diameter large-area thermopile was used as its detector. Therefore, the area of the incident surface could be calculated as the surface area of the detector. Hence, the light intensity could be calculated accordingly.

2.3.4 Dry cell mass assay

As it was not feasible to measure the dry cell mass of *R. palustris* in liquid suspension directly, the optical density of the liquid sample was measured using a spectrophotometer at a fixed wavelength and was correlated to the cell concentration. The wavelengths of 550 nm and 660 nm were chosen for assay development initially as there were not peaks at those wavelengths.

The correlation was derived by drying a series of 20mL cell suspensions with different known optical densities at 550nm or 660nm to determine the dry cell mass. A few 200 mL samples of cell culture at early stationary phase was centrifuged (Sorvall RL-5B, CE005110) for ten minutes at room temperature at 4,424 g (Gosse 2008) and the supernatant was removed. The pellets were then re-suspended in sufficient de-ionised water and mixed together so that the optical density, determined with a spectrophotometer (ThermoSpectronic, UV1, 005086) of the suspension at 660 nm (OD$_{660}$) was about 2.40. A sequence of dilutions of this was prepared in

triplicate, namely 20, 19, 18... 3, 2 and 1 ml of cell suspension with OD_{660nm} = 2.40 in a total of 20 ml, the balance being de-ionised water. The optical densities of these solutions were measured and recorded at 550 and 660 nm separately. Each of the dilutions was stored in a pre-weighed dry clean glass tube and heated at 90 ºC for

80 h. The final mass of each glass tube was measured to determine the dry cell mass. A graph of the dry cell mass against the optical density at both 550 nm and 660 nm was plotted in Figure 2-6 and a better fit by linear regression is seen at 660 nm. This graph is used as the correlating value for inferring dry cell mass by optical density.
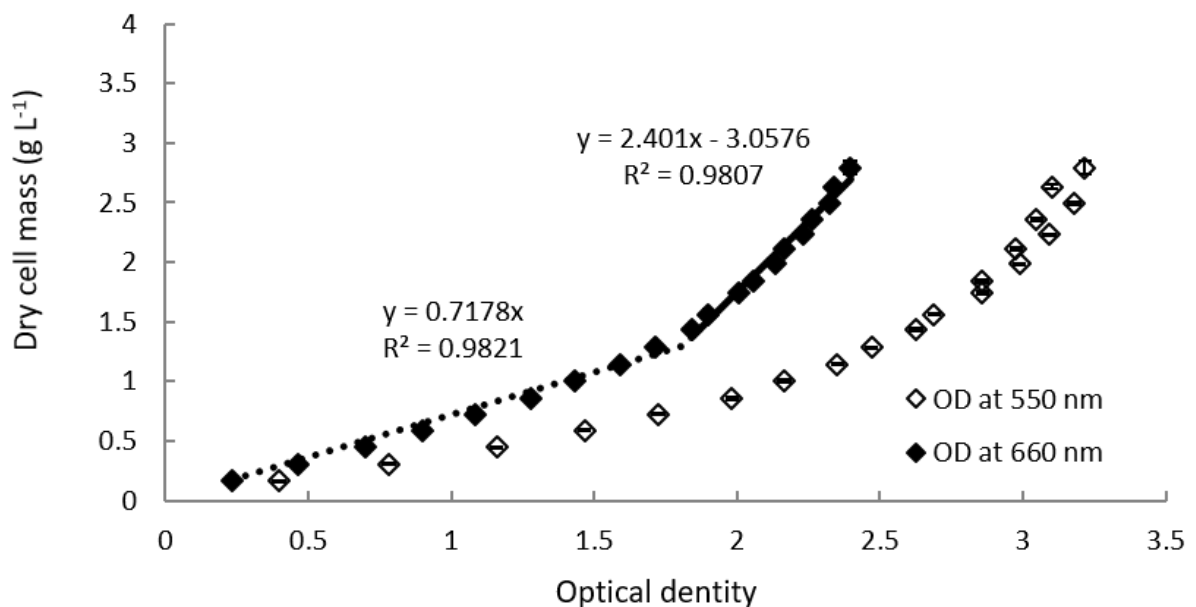
Figure 2-6: Dry cell mass correlation for *R. palustris* at early stationary phase

As the graph had two distinct linear regions, the correlations used were split based on the initial optical density. From the culture bottle, 1 mL sample was extracted and the optical density at 660 nm was measured on a spectrophotometer (Thermo Spectronic UV1, Madison, U.S.A.), and the cell concentration was determined by the following equations.

$$if\ OD_{660nm} < 1.8,\quad cell\ concentration\ (g\ L^{-1}) = OD_{660nm} \times 0.7175 \qquad \text{Equation 2-1}$$

$$if\ OD_{660nm} \geq 1.8,\quad cell\ concentration\ (g\ L^{-1}) = OD_{660nm} \times 2.401 - 3.0576 \qquad \text{Equation 2-2}$$

2.3.5 Glycerol assay

The concentration of glycerol in aqueous solutions was determined by adapting the method of Bondioli and Della Bella (2005a), which was originally used to determine the glycerol concentration in biodiesel. The ethanol solution used in the original assay was replaced volumetrically by de-ionised water to avoid the distortion of the assay when aqueous solutions of glycerol rather than solutions of glycerol in biodiesel were used. The new glycerol assay exhibited good reproducibility.

For this assay, 1.6 M aqueous acetic acid and 4.0 M ammonium acetate solutions were prepared as stock solutions at room temperature, and 0.2 M acetylacetone and 10 mM sodium periodate solutions were prepared daily. 0.2 M acetylacetone solution was prepared by adding 200 μL acetylacetone to a mixture of 5 mL of 1.6 M aqueous acetic acid solution and 5 mL of 4.0 M ammonium acetate solution. 10 mM sodium periodate solution was prepared by dissolving 21 mg of sodium metaperiodate in 5 mL of 1.6 M aqueous acetic acid solution, followed by the addition of 5 mL of 4.0 M ammonium acetate solution.

The correlation was derived by obtaining optical densities at 410nm of a series of 2mL glycerol solutions with known concentrations. A standard glycerol solution with a concentration of 0.06 mg / mL or 48.2 µL / mL was made with de-ionised water. A sequence of dilutions of this was prepared in triplicate, namely 0.2, 0.4, 0.6… 1.6, 1.8 and 2 mL of the 0.06 mg / mL glycerol standard solution in a total of 2 mL solutions, the balance being de-ionised water. To 2 mL of the diluted glycerol solution in a test tube, 1.2 mL of periodate solution was added and the test tube was shaken for 30 s. Then, 1.2 mL of the acetyl acetate solution was added, and the test tube kept in a water bath at 70 °C for 1 minute. The test tube was subsequently put immediately into another water bath, maintained at room temperature until cool. The absorbance of the resulting solution was determined at 410 nm. The glycerol concentration was correlated to the optical density of 3, 5-diacetyl-1, 4-dihydrolutidine in the result solution. The results of glycerol concentrations *vs.* optical densities at 410 nm were plotted in Figure 2-7.
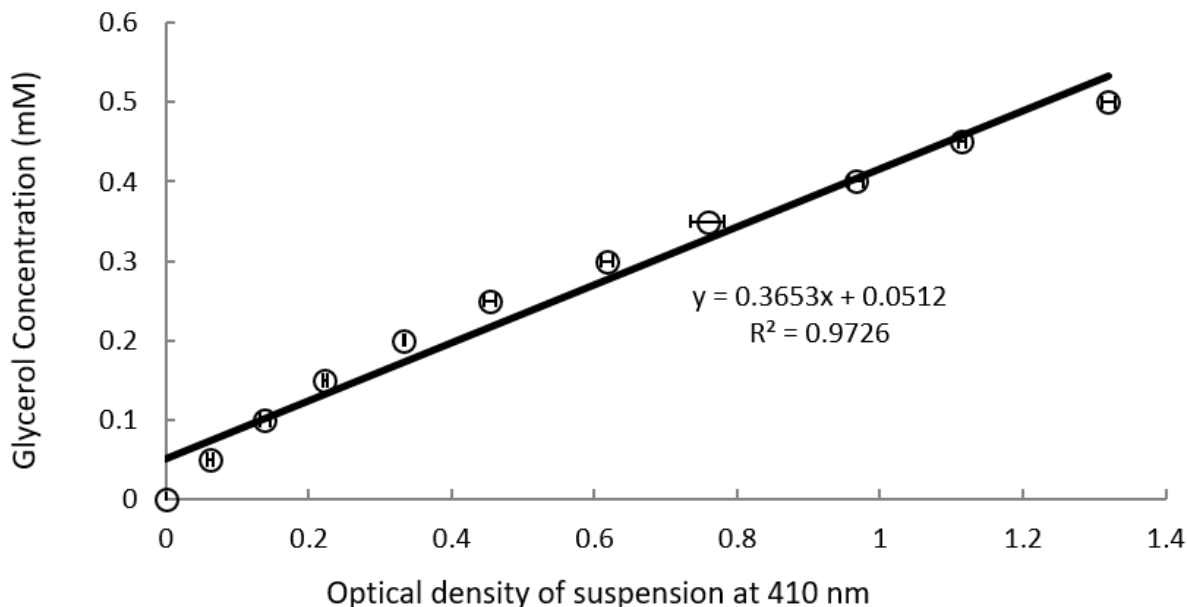
Figure 2-7: Glycerol concentration *vs.* optical density of a solution at 410 nm

Each liquid sample was first filtered through a 0.45 μm filter to remove the cell mass in the sample. The sample was then diluted *n* times to the appropriate concentration so that the final absorbance would lie within the calibration range. Similarly, to 2 mL of the diluted sample in a test tube, 1.2 mL of periodate solution and 1.2 mL of the acetyl acetate solution were added, and the test tube kept in a water bath at 70 °C for 1 minute. The test tube was subsequently put immediately into another water bath, maintained at room temperature until cool. The absorbance of the resulting solution was determined at 410 nm. The glycerol concentration of the liquid sample was then correlated with its optical density at 410 nm *via* Equation 2-3 where *n* is the dilution factor used.

$$Glycerol\ concentration\ (mM) = n(OD_{410nm} \times 0.3653 + 0.0512)$$ Equation 2-3

2.3.6 Polyhydroxybutyrate（PHB） assay

The genome sequence of *R. palustris* (Larimer *et al.* 2004) suggests that it can generate different storage products such as glycogen, trehalose, and polyhydroxy butyrate (PHB). *R. palustris* could generate up to 30 % dry cell weight equivalent PHB under nitrogen starvation condition (McKinlay et al. 2014b). Law and Slepecky's method (1961) was widely applied to estimate polymer extracted from various organisms and under a variety of conditions. And it was applied to measure PHB

concentration in the cell culture in this project. PHB was converted into crotonic acid in hot concentrated sulphuric acid, the optical density of the crotonic acid solution was measured at 235nm, and the concentration of PHB was correlated accordingly.

The correlation was derived by obtaining optical densities at 235 nm of a series of treated 10 mL PHB solutions with known concentrations. A standard PHB solution with a concentration of 5 mg/ L was made by adding 1 mg of PHB into 200 mL of concentrated sulphuric acid. The standard solution was then heated at 100 °C for 10 minutes in a silicon oil bath to convert all PHB into crotonic acid. The solution was then cooled and mixed thoroughly by a magnetic stirrer. A sequence of dilutions of this was prepared in triplicate, between 1 and 10 mL of the standard solution in a total of 10 mL solutions, the balance being concentrated sulphuric acid. The absorbance of the resulting solutions was determined at 235 nm. The PHB concentration was correlated to the optical density of crotonic acid in the result solution. The results of PHB concentrations *vs.* optical densities at 235 nm were plotted in Figure 2-8.
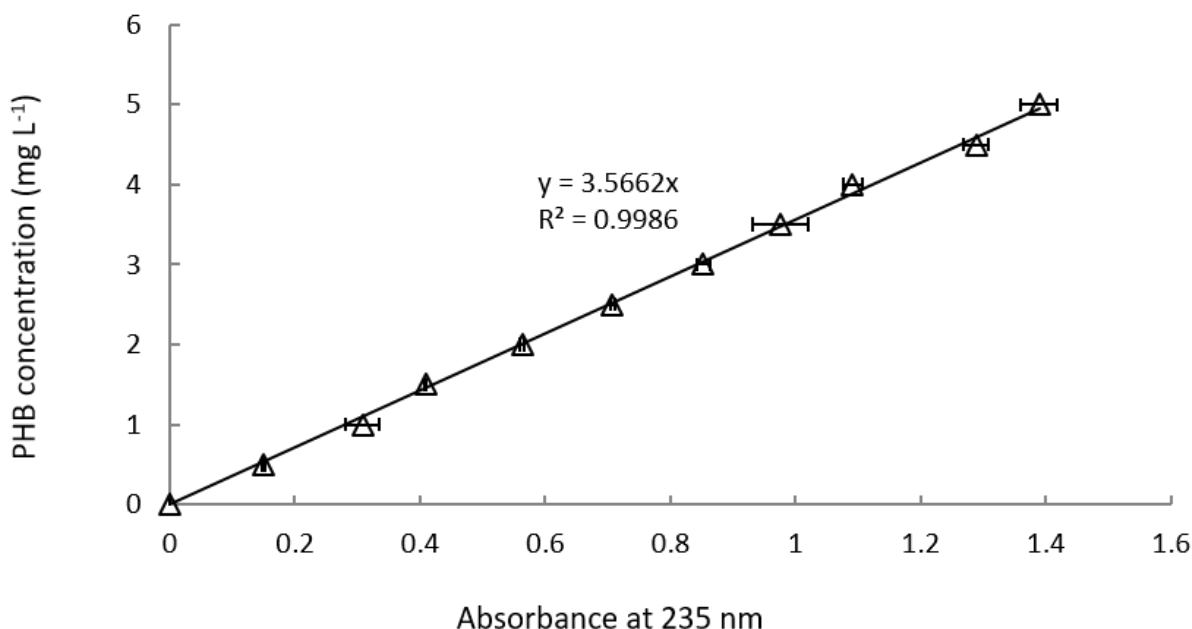
Figure 2-8: PHB concentration *vs.* optical density difference between sample and sample blank at 235 nm

For this assay, PHB was extracted from cell culture and converted into crotonic acid in hot concentrated sulphuric acid. To extract PHB in cell culture, 15 mL Greiner® polypropylene centrifuge tubes and 50 mL Duran® glass bottles were used. To avoid the interference with result, the centrifuge tubes had been previously washed thoroughly with ethanol and hot chloroform to remove plasticisers.

10 mL cell culture was centrifuged in 15 mL centrifuge bottles at 5,000 g for 10 minutes. The supernatant was removed to test the carbon dioxide dissolved in the culture media. The cell pellet was suspended in 10 mL of commercial sodium hypochlorite solution and incubated at 37 ºC for an hour in a water bath. In this project, Tesco® Everyday Value Thin Bleach containing 1.5 (w / w) % hypochlorite was used instead of Clorox® containing 4.5 (w / w) % hypochlorite in the original publication.

After incubation, the lipid granules were centrifuged, washed with water, and then washed with acetone. The pellet was then suspended in 10 mL alcohol and transferred into a clean glass laboratory bottle. PHB formed a precipitate in the alcohol solution, and nitrogen gas was blown on the surface of the solution to encourage the evaporation of alcohol. Finally, the dry PHB precipitate was dissolved by extraction with three small portions of boiling chloroform at 61ºC, the chloroform solution was filtered, and the filtrate was used for PHB assay. In cases where the considerable polymer was present, the acetone and alcohol washings were unnecessary, but they served to remove water which interferes with the extraction of PHB into chloroform. Chloroform will dissolve most polymers; make sure use glass containers.

For the spectrophotometric assay, a sample containing PHB in chloroform was transferred to a clean glass bottle. 10 ml of concentrated sulphuric acid were added. The solution was kept in a silicon oil bath at 100 ºC for 10 minutes to convert all PHB to crotonic acid. The chloroform was evaporated during the hot silicon bath. The solution was cooled and then diluted n times with concentrated sulphuric acid to the appropriate concentration so that the final absorbance would lie within the calibration range, 0 ~ 5 mg L^{-1}. After thorough mixing, a small portion of the resulting solution

was transferred to a silica cuvette (Hellma®, Suprasil® quartz, limit 200-2,500 nm spectral range) and the absorbance at 235 nm was determined against a concentrated sulphuric acid blank. The PHB concentration in the cell culture was then correlated with its optical density at 235 nm *via* Equation 2-4 where *n* is the diluting factor used.

$$PHB\ concentration\ (mgL^{-1}) = n(OD_{235nm} \times 3.5662)$$

<div align="right">Equation 2-4</div>

2.3.7 Gas composition

The gas composition was determined by using a gas chromatograph (Agilent 7890A, Santa Clara, U.S.A.) fitted with a thermal conductivity detector. When the gas sample was rejected into the gas chromatograph, argon was used as the carrier gas and a HayeSep column fitted with a molecular sieve (Agilent 19001A-MX1, Santa Clara, U.S.A.) was employed to give different retention times of different components in the gas sample. The components were analysed using the thermal conductivity detector, where the thermal conductivity of the eluted gas sample is compared to that of the pure carrier gas and is correlated to the percentage of different components in the gas sample using the existing calibrations (Pott *et al.* 2012).

2.3.8 H$_2$ volume

At regular intervals, the gases generated were released to the graduate burette, the volume was measured by water displacement in the burette and recorded as V_1, V_2, V_3, …, V_n; and the H$_2$ composition was determination by injecting the gas sample into the gas chromatography and recorded as $\theta_1^{H_2}$, $\theta_2^{H_2}$, $\theta_3^{H_2}$, …, $\theta_n^{H_2}$. As the H$_2$ solubility in water is extremely low, it was assumed that H$_2$ is insoluble in water in this study. Hence the total H$_2$ volume was equal to the H$_2$ volume in gases collected, and it could be predicted as the equation below:

$$V_{H_2} = \sum_{i=1}^{n-1}(V_i \times \theta_i^{H_2}) + \left(V_n + V_{headspace}\right) \times \theta_n^{H_2}$$

<div align="right">Equation 2-5</div>

where *n* denotes different time to release the gas, V_i denotes the volume of gases at the i-th time, V_n denotes the volume at the n-th time, $\theta_i^{H_2}$ denotes the H$_2$ composition

at the i-th time, $\theta_n^{H_2}$ denotes the H_2 composition at the n-th time, $V_{headspace}$ is the volume of the headspace in the culture bottle.

2.3.9 CO_2 volume

When H_2 was generated from glycerol by *R. palustris*, partial of CO_2 was released to the gases, and partial of CO_2 was dissolved in the media. For the CO_2 in the gases, similarly to H_2, its volume could be determined by the total cumulative gas volume corrected by its gas composition.

$$V_{CO_2 in\ gases} = \sum_{i=1}^{n-1}(V_i \times \theta_i^{CO_2}) + (V_n + V_{headspace}) \times \theta_n^{CO_2}$$

Equation 2-6

where *n* denotes different time to release the gas, V_i denotes the volume of gases at the i-th time, V_n denotes the volume at the n-th time, $\theta_i^{CO_2}$ denotes the CO_2 composition at the i-th time, $\theta_n^{CO_2}$ denotes the H_2 composition at the n-th time, $V_{headspace}$ is the volume of the headspace in the culture bottle.

For the CO_2 in the media, it was measured experimentally by adding a small amount of strong acid into the sample culture (McKinlay et al. 2014b). When the *R. palustris* stopped to produce H_2, 10 mL of cell culture was extracted and centrifuged at 5000 g, room temperature, for ten minutes. After centrifuge, the supernatant was transferred into a 100 mL glass bottle with two-valve-port bottle cap to measure the CO_2 dissolved in the media. 1 mL concentrated sulphuric acid was injected into the supernatant through the liquid port, both valves for liquid and gas ports were closed, and the solution was mixed by a magnetic stirrer for an hour. A gas sample was extracted from the gas port, and the gas composition was detected by injecting the gas sample into the gas chromatograph (7890A Agilent) fitted with a thermal conductivity detector. The volume of the CO_2 in the media could be calculated *via* the equation below.

$$V_{CO_2 in\ media} = \frac{V_{culture}}{V_{liquid\ sample}} \times V_{headspace} \times \theta^{CO_2}$$

Equation 2-7

where $V_{culture}$ denotes the volume of culture, $V_{liquid\,sample}$ denotes the volume of liquid extracted for this test, $V_{headspace}$ is the volume of the headspace in the test bottle, θ^{CO_2} denotes the CO_2 composition of the test sample.

3 Non-growing Rhodopseudomonas palustris increases hydrogen yield from glycerol

3.1 Introduction

Owing to its high gravimetric energy density, 143 MJ kg^{-1}, hydrogen (H_2) is an attractive alternative fuel. It is easily converted to electricity in fuel cells leaving only water as the final product upon its combustion (Basak & Das 2007). Compared to thermochemical H_2 production methods (e.g. steam reforming, cracking, and gasification), biological H_2 production results in lower greenhouse gas emission and requires ambient temperatures and pressures, making it more environmentally friendly and less energy intensive (Chen *et al.* 2008; Basak & Das 2007). Bio-hydrogen generated by purple non-sulphur (PNS) bacteria through photo-fermentation is particularly promising as the bacteria can achieve high yields of H_2 in the absence of oxygen (O_2) with a wide spectrum of sunlight (Huang et al. 2010a). These bacteria are also able to utilise a range of organic compounds from food waste or industrial wastewater during H_2 generation (Kim *et al.* 2006).

Rhodopseudomonas palustris (*R. palustris*), a type of PNS bacteria, generates H_2 through two main route: as a side product of cell growth through nitrogen-fixation (Basak & Das 2007; Lee *et al.* 2011), and as a direct product from adenosine triphosphate (ATP) reduction under nitrogen-depleted conditions (Piskorska et al. 2013; Gosse et al. 2010; Huang et al. 2010a; Melnicki et al. 2008). The simplified metabolic routes of H_2 production by *R. palustris* is shown in Figure 3-1.

R. palustris, a nitrogen-fixing bacterium, can convert molecular nitrogen (N_2) into ammonia (NH_3) during cell growth for use in protein synthesis. Both protons (H^+ ions) and electrons released from organic carbon sources are converted to H_2 by a nitrogenase enzyme (Basak & Das 2007; Ormerod & Ormerod 1961; Lee *et al.* 2011). For growing H_2 production, H_2 is generated as an obligatory but not necessarily advantageous by-product under nitrogen-fixing conditions (Rey *et al.* 2007).

Under nitrogen-depleted conditions, all reductants and energy (*i.e.* ATP) are theoretically directed towards H_2 production without cell growth, *i.e.* converting H^+ from the reductants exclusively to H_2 (McKinlay & Harwood 2010b). Some research

suggests that the non-growing *R. palustris* in nitrogen-depleted conditions act as a biocatalyst for continuous H₂ production (Piskorska et al. 2013; Gosse et al. 2010; Huang et al. 2010a; Melnicki et al. 2008).

Nitrogen-fixation: $N_2 + 8H^+ + 8e^- + 16ATP \rightarrow 2NH_3 + H_2 + 16ADP$

Nitrogen-depleted: $8H^+ + 8e^- + 16ATP \rightarrow 4H_2 + 16ADP$
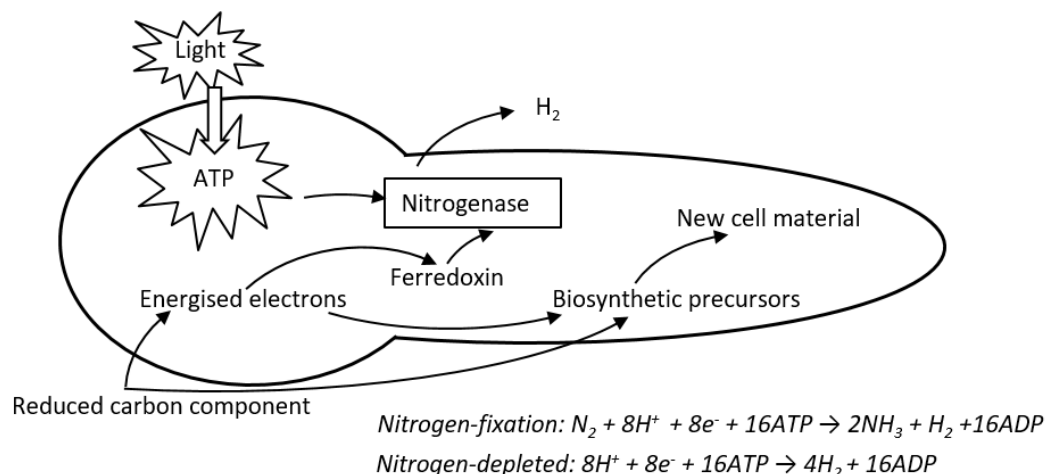
Figure 3-1: Metabolic route of H₂ production by *R. palustris* under growing and non-growing conditions (modified from Rey *et al.* (2007)).

In this chapter, the H₂ production performance by both growing and non-growing *R. palustris* was compared qualitatively and quantitatively. For both processes, the carbon input and carbon output were tracked, carbon balances were carried out, and the carbon recovery as well as the electron recovery were estimated accordingly. H₂ yield (in terms of % theoretical maximum H₂ yield), average H₂ production and energy conversion efficiency for both processes were qualitatively and quantitatively analysed and compared. Through the analyses, it is aimed to understand the mechanism of H₂ production under both conditions.

3.2 Materials and methods

3.2.1 Strain and medium

R. palustris with strain designations ATH 2.1.37 (NCIB 11774) was obtained from ATCC® as a freeze-dried sample. A defined medium was used in this chapter as described by Gosse *et al.* (2007), for details please refer to Chapter 2.1.3. All gases used in this chapter were at atmospheric pressure and 30 °C unless otherwise stated.

All containers and media were autoclaved prior to use and all gases bubbled through the media were filtered with GE Healthcare Whatman® HEPA filter to maintain sterility.

3.2.2 Cultivation conditions

The optimal reaction temperature plays an important role in shifting the metabolic pathway towards H_2 production. It was found out that the optimal H_2 production temperature by PNS bacteria varied from 30 °C to 36 °C (Basak & Das 2007). Cells were cultivated in 250 mL laboratory bottles (Duran® 250 mL GL 45, Mainz, Germany) at 30 ± 2 °C. Illumination was provided by incandescent light bulbs (BELL® R80 ES Reflector, London, U.K.) with a light intensity of 230 ± 7 Wm^{-2}. For details in experimental setup, please refer to Chapter 2.2.

At regular intervals, the gases generated were released to the graduate burette, the volume was measured by water displacement in the burette and recorded, and a gas sample was extracted for gas composition determination by a gas chromatography. As the H_2 solubility in water is extremely low, it is assumed that H_2 is insoluble in water. The total H_2 volume was equal to the H_2 volume in gases released in the burette and gases in headspace of the culture bottle. Equally a liquid sample was extracted from the bottle at the same time to monitor cell growth and glycerol consumption. When the *R. palustris* stopped to produce H_2, a liquid sample was extracted and centrifuged. The supernatant was removed to measure CO_2 volume dissolved in the media, and the cell pellet was used to measure the polyhydroxybutyrate (PHB) generated by the bacteria.

When H_2 was generated from glycerol by *R. palustris*, partial of CO_2 was released to the gases, and partial of CO_2 was dissolved in the media. For the CO_2 in the gases, similarly to H_2, its volume could be determined by the total cumulative gas volume corrected by its gas composition. For the CO_2 in the media, it was measured experimentally by adding a small amount of strong acid into the sample culture and testing the gas composition of the gases released 1 hour later (McKinlay et al. 2014b).

3.2.3 Growing H_2 production

Freeze-dried sample was rehydrated and the pre-culture was prepared. For details, please refer to Chapter 2.1. The pre-culture was cultivated at 30 ± 2 °C for a week in a 15 mL centrifuge tube with defined medium, 100 µL of 2M filtered sodium glutamate, and 100 µL of autoclaved pure glycerol. The cells were then centrifuged for ten minutes at room temperature at 4424 g (Gosse *et al.* 2007), and re-suspended in fresh medium to an optical density of 0.15 at 660 nm (OD_{660nm} = 0.15). 200 mL of the cell suspension was then supplemented with 10 mM glycerol in a 250 mL bottle and sparged with filtered sterile N_2 for ten minutes.

3.2.4 Non-growing H_2 production

It has been found that the PNS bacteria at their late exponential and early stationary phases of growth are suitable for H_2 production at a high yield (Sasikala *et al.* 1995; Basak & Das 2007). *R. palustris* was initially cultivated in 10 mM glycerol and N_2 under nitrogen-fixation conditions for 10 days. Cells were harvested at its early stationary phase. The culture was centrifuged (Beckman® JA-10 rotor, California, U.S.A.) in a wide mouth sealing bottle (Beckman® Polypropylene 250 mL, California, U.S.A.) for ten minutes at room temperature at 4424 g. The pellet was washed and re-suspended in fresh medium to an optical density of 0.80 at 660 nm (OD_{660nm} = 0.80) to maintain early stationary phase (Gosse *et al.* 2007). 200 mL of the non-growing cell suspension was then cultivated in a 250 mL bottle and supplemented with 10 mM glycerol for the non-growing H_2 production. Argon (Ar) was bubbled through the suspension for ten minutes to remove the air inside.

3.2.5 Analytical methods

The optical density of the cell suspension was measured by a Thermo® UV1 spectrophotometer against a blank solution of de-ionised water at a fixed wavelength of 660 nm, and the equivalent dry cell mass was correlated with the optical density (Pott *et al.* 2012).

Glycerol concentration was determined using a modified method as described by Bondioli & Della Bella (2005). The ethanol solution used in the original assay was

replaced volumetrically by distilled water to avoid the distortion of the assay when aqueous solutions of glycerol rather than solutions of glycerol in biodiesel were used.

Law and Slepecky's method (1961) was used to measure PHB concentration in the culture media.

The gas composition of the gases generated was determined using a gas chromatograph (Agilent® 7890A, Wilmington, U.S.A.) with a thermal conductivity detector. A HayeSep Q column was used with Ar as the carrier gas. The components were identified and analysed using existing calibrations (Pott *et al.* 2012).

For details in analytical methods, please refer to Chapter 2.3.

3.3 Numerical methods

3.3.1 Carbon recovery

To track the movement of carbon from the input sources to the output products, all the carbon-containing substrates and products were measured for both growing and non-growing processes. Moles of carbon consumed or generated was calculated experimentally and recorded as Δn_{C_i} where *i* could be any carbon containing compound. The total difference in carbon input and carbon output was calculated and the carbon recovery could be calculated *via* the following equation:

$$\text{Carbon recovery \%} = \frac{\sum_{output} \Delta n_{C_i}}{\sum_{input} \Delta n_{C_i}} \times 100 \text{ \%}$$
Equation 3-1

As an example, it was assumed that within the cell culture the carbon containing end products were the biomass of *R. palustris*, CO_2, and PHB. Therefore, the carbon recovery could be estimated by the following equation:

$$\text{Carbon recovery \%} = \frac{\Delta n_{C_{biomass}} + \Delta n_{C_{CO_2}} + \Delta n_{C_{PHB}}}{\Delta n_{C_{glycerol}}} \times 100\%$$
Equation 3-2

3.3.2 Electron recovery

Both cell growth and H_2 production compete for free electrons donated by the substrate (Huang et al. 2010a; McKinlay et al. 2014b). Like carbon recovery, electron recovery could be calculated by the following equation:

$$\text{Electron recovery \%} = \frac{\sum_{output} \Delta n_{e_i^-}}{\sum_{input} \Delta n_{e_i^-}} \times 100\ \%$$

Equation 3-3

where $\Delta n_{e_i^-}$ denoted moles of electrons consumed or generated, while *i* could be any electron containing compound.

To monitor the electron movement from substrate to product, the electron content of compound was determined by the number of hydrogen atoms available in that substrate or product (Gottschalk 1986). The number of electrons was calculated by oxidising the carbon compound down to CO_2. As such for glycerol, the oxidation with water equals to $C_3H_8O_3 + 3H_2O \rightarrow 3CO_2 + 14H^+ + 14e^-$; therefore, glycerol has 14 moles of electrons available per mole.

R. palustris was assumed to have the biological formula $CH_{1.8}N_{0.18}O_{0.38}$ (Carlozzi & Sacchi 2001); the nitrogen source for the growing H_2 production process was molecular N_2. Therefore, to determine the electrons available in *R. palustris*, McKinlay *et al.*'s (2014) equation was employed, $CH_{1.8}N_{0.18}O_{0.38} + 1.62H_2O \rightarrow 3CO_2 + 5.04H^+ + 5.04e^- + 0.09N_2$ suggesting it carries 5.04 moles electrons per mole.

It was assumed that the products of interest were the biomass of *R. palustris*, H_2, PHB, and glycerol. Therefore, the electron recovery in this process could be estimated by the equation:

$$\text{Electron recovery \%} = \frac{\Delta n_{e_{biomass}^-} + \Delta n_{e_{H_2}^-} + \Delta n_{e_{PHB}^-}}{\Delta n_{e_{glycerol}^-}} \times 100\ \%$$

Equation 3-4

3.3.3 Cell growth kinetics

Rhodopseudomonas palustris grew photo-heterotrophycally on glycerol and N_2 to produce H_2 under nitrogen-fixation conditions. During cultivation, cells experienced different growth phases including lag phase, exponential phase, and stationary phase.

During the exponential phase, assuming the substrate concentration (*i.e.* glycerol concentration), and light intensity stayed constant over this period, cell growth occurred exponentially, and the rate of growth was postulated to be proportional to the dry cell mass, *i.e.*:

$$X = \frac{1}{\mu}\frac{dX}{dt} \qquad\qquad \text{Equation 3-5}$$

where *X* was the bacterial concentration in g L^{-1}, *μ* was the specific growth rate in h^{-1}, and *t* was time in h. Therefore, the specific growth rate *μ* could be obtained from the slope of the straight line representing ln (dry cell mass) *vs.* time:

$$\mu = \frac{ln(X/X_1)}{t/t_1} \qquad\qquad \text{Equation 3-6}$$

where X_1 was the initial dry cell mass in the exponential phase in gL^{-1}, and t_1 was the corresponding time.

3.3.4 H_2 production performance

H_2 production performance from a specific reductant is commonly evaluated against three criteria: H_2 yield in terms of % theoretical maximum H_2 yield, H_2 production rate, and energy conversion efficiency *(*Koku *et al.* 2002; Hallenbeck 2012).

The theoretical maximum H_2 yield is defined as the maximum amount of H_2 produced from electrons made available when the organic reductant (or substrate) is fully oxidised to CO_2 (McKinlay et al. 2014b). For example, *R. palustris* can convert glycerol into H_2 using the enzymes nitrogenase, which catalyses the oxidation through

$C_3H_8O_3 + 3H_2O \rightarrow 7H_2 + 3CO_2$. Hence, the H_2 yield is defined as

$$H_2 \ yield$$

$$= \frac{\Delta n_{H_2 measured}}{7 \times \Delta n_{glycerol} \ measured} \% \ the \ theoretical \ maxium \ H_2 \ yield \qquad \text{Equation 3-7}$$

While, H_2 production rate is defined as the volume of H_2 generated per unit volume of cell suspension per unit time (mL L^{-1} h^{-1}) (Tian *et al.* 2010). For H_2 production by growing *R. palustris* (*i.e.* under nitrogen-fixing condition), the average H_2 production rate was calculated during the exponential phase of growth; whereas for H_2 production by nongrowing *R. palustris* (*i.e.* under nitrogen depleted condition), the average H_2 production rate was obtained during the nongrowing phase.

Finally, the energy conversion efficiency, in terms of light, is defined as the ratio of the combustion enthalpy of H_2 to the total energy input into cell cultivation (Uyar *et al.* 2007) via Equation 3-8.

$$Energy \ conversion \ efficiency = n\Delta H/(IAt) \qquad \text{Equation 3-8}$$

where n is the number of moles of H_2 generated, ΔH is the molar combustion enthalpy of H_2 (-286 kJmol^{-1}), I is the light intensity in Wm^{-2}, A is the irradiated area in m^2, and t is the duration of H_2 production in hours (h).

3.4 Results

The experimental results of tests conducted on growing *R. palustris* (Figure 3-2) and non-growing *R. palustris* (Figure 3-3) are showing in the following figures. All gases used in chapter were at atmospheric pressure and 30 ± 2 °C. Each data point in each figure represents the average value of three experimental repeats with corresponding error bars denoting the standard derivations. The analytical results are presented in Table 3-1, Table 3-2, and Table 3-3.
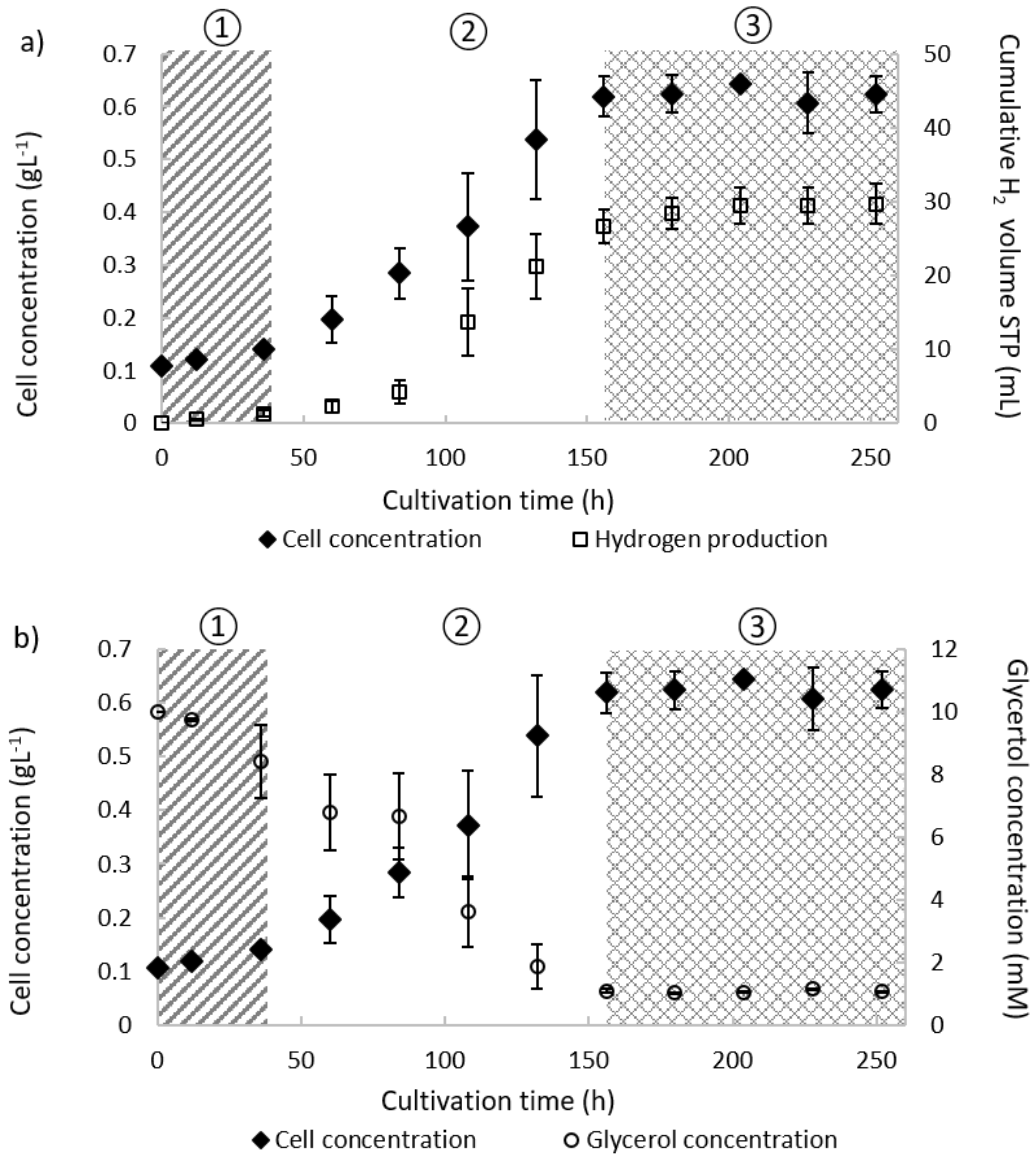
Figure 3-2: H_2 production by growing *R. palustris*. *R. palustris* grown photo-heterotrophycally on 10 mM glycerol and N_2 to produce H_2 under nitrogen-fixing conditions for 10 days. All gases used were at atmospheric pressure and 30 ± 2 °C. Cells grew and experienced different growth phases: lag phase (①), exponential phase (②), and stationary phase (③). Glycerol and N_2 were consumed and H_2 was generated and measured as described. Each data point in each figure represents the average value of three experimental repeats with corresponding error bars denoting the standard derivations.
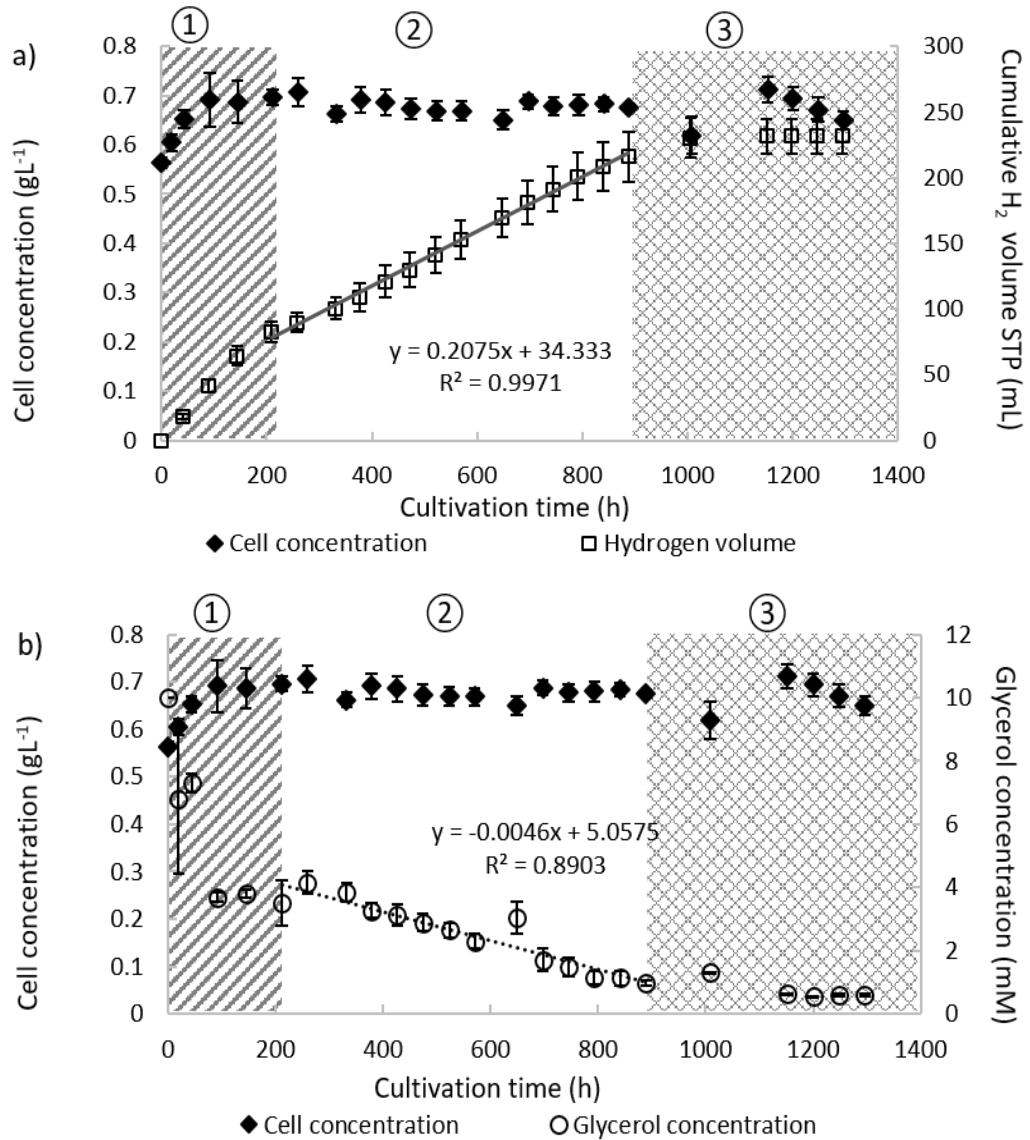
Figure 3-3: H2 production by non-growing *R. palustris*. *R. palustris* was initially cultivated with glycerol and N_2 for 10 days (conditions and results shown in Figure 3-2), harvested at its early stationary phase, centrifuged to remove the nitrogen source, re-suspended in fresh medium to an optical density of 0.80 at 660 nm, and re-cultivated in 10 mM glycerol only for the non-growing H_2 production. Dry cell mass grew from a concentration of 0.563 ± 0.009 gram of dry biomass per litre of suspension (g L^{-1}) to 0.696 ± 0.015 g L^{-1} in the first 211 h (①). Then cells were used as a biocatalyst for the non-growing H2 production for another 678 h (also called the non-growing phase, ②). Eventually cells went to death phase (③) and H2 production stopped when glycerol ran out. Each data point in each figure represents the average value of three experimental repeats with corresponding error bars denoting the standard derivations.

Table 3-1: Conversion of glycerol to biomass, CO_2, and H_2 by growing *R. palustris* [a]

Compound (substrates or products)	mol	mol carbon per mol compound[b]	mol carbon	mol electron per mol compound[c]	mol electron
Glycerol	$-1.78\times10^{-3} \pm 1.06\times10^{-5}$	3	$-5.34\times10^{-3} \pm 3.17\times10^{-5}$	14	$-2.49\times10^{-2} \pm 1.48\times10^{-4}$
Biomass	$4.61\times10^{-3} \pm 3.05\times10^{-4}$	1	$4.61\times10^{-3} \pm 3.05\times10^{-4}$	5.04	$2.32\times10^{-2} \pm 1.54\times10^{-3}$
CO_2	$9.29\times10^{-4} \pm 4.10\times10^{-5}$	1	$9.29\times10^{-4} \pm 4.10\times10^{-5}$	N/A	N/A
PHB	$2.14\times10^{-5} \pm 3.04\times10^{-6}$	4	$8.56\times10^{-5} \pm 1.22\times10^{-5}$	18	$3.85\times10^{-4} \pm 5.47\times10^{-5}$
H_2	$1.30\times10^{-3} \pm 1.20\times10^{-4}$	N/A	N/A	2	$2.61\times10^{-3} \pm 2.39\times10^{-4}$

[a] The values were obtained as the average of three experimental replicates, the errors were obtained as the standard derivations, and the results were presented in scientific notation with two decimal places in this table. The negative sign means consumed and the positive sign means generated. For example, $-1.78 \times 10^{-3} \pm 1.06 \times 10^{-5}$ means it consumed 0.00178 ± 0.0000106 mol of glycerol in this experiment.

Carbon recovered: $[(4.61 \times 10^{-3}) + (9.29 \times 10^{-4}) + (8.56 \times 10^{-5})] / (5.34 \times 10^{-3}) = 105.33 \pm 5.65$ %.

Electron recovered: $[(2.32 \times 10^{-2}) + (3.85 \times 10^{-4}) + (2.61 \times 10^{-3})] / (2.49 \times 10^{-2}) = 105.24 \pm 7.56$ %.

[b] The number of moles of carbon per mole of substrate or product is obtained through SI method from its chemical formula. For example, glycerol has a chemical formula of $C_3H_8O_3$, and it has 3 moles of carbon per mole of glycerol.

[c] The number of moles of electron per mole of substrate or product is obtained through SI method (Gottschalk 1986), for details please refer to Section 3.4.2.

Table 3-2: Conversion of glycerol to biomass, CO_2, and H_2 by non-growing *R. palustris* [d]

Compound (substrates or products)	mol	mol carbon per mol compound[e]	mol carbon	mol electron per mol compound[f]	mol electron
Glycerol	$-1.88\times10^{-3} \pm 1.07\times10^{-5}$	3	$-5.65\times10^{-3} \pm 3.20\times10^{-5}$	14	$-2.63\times10^{-2} \pm 1.49\times10^{-4}$
Biomass	$7.71\times10^{-4} \pm 1.96\times10^{-4}$	1	$7.71\times10^{-4} \pm 1.96\times10^{-4}$	5.04	$3.89\times10^{-3} \pm 9.89\times10^{-4}$
CO_2	$4.63\times10^{-3} \pm 3.42\times10^{-4}$	1	$4.63\times10^{-3} \pm 3.42\times10^{-4}$	N/A	N/A
PHB	$9.54\times10^{-6} \pm 1.44\times10^{-7}$	4	$3.82\times10^{-5} \pm 5.75\times10^{-7}$	18	$1.72\times10^{-4} \pm 2.59\times10^{-6}$
H_2	$1.02\times10^{-2} \pm 5.87\times10^{-4}$	N/A	N/A	2	$2.04\times10^{-2} \pm 1.17\times10^{-3}$

[d] The values were obtained as the average of three replicates, the errors were obtained as the standard derivation, and the results were presented in scientific notation with two decimal places in this table. The negative sign means consumed and the positive sign means generated. For example, $-1.88 \times 10^{-3} \pm 1.07 \times 10^{-5}$ means it consumed 0.00188 ± 0.0000107 mol of glycerol in this experiment.

Carbon recovered: $(7.71 \times 10^{-4} + 4.63 \times 10^{-3} + 3.82 \times 10^{-5}) / 5.65 \times 10^{-3} = 96.30 \pm 8.84$ %.

Electron recovered: $(3.89 \times 10^{-3} + 1.72 \times 10^{-4} + 2.04 \times 10^{-2}) / 2.63 \times 10^{-2} = 92.80 \pm 2.54$ %. The electron recovery was slight lower than 100%. This suggested that there might be some untracked end products such as Alpha Ketoglutarate in the cell suspension.

[e] The number of moles of carbon per mole of substrate or product is obtained through SI method from its chemical formula. For example, glycerol has a chemical formula of $C_3H_8O_3$, and it has 3 moles of carbon per mole of glycerol.

[f] The number of moles of electron per mole of substrate or product is obtained through SI method (Gottschalk 1986), for details please refer to Section 3.4.2.

Table 3-3: H_2 production by both growing and nongrowing *R. palustris*[g]

Experimental conditions		Inoculum size (g L^{-1})	Specific growth rate (h^{-1})[h]	% theoretical max H$_2$ yield[i]	H$_2$ production rate (mL L^{-1} h^{-1})[g]	Energy conversion efficiency[h]
Growing	Initial	0.108 ± 0.001	0.013 ± 0.001	10.43 ± 0.95%	1.06 ± 0.11	0.035 ± 0.004%
	Final	0.624 ± 0.020				
Non-growing	Average	0.679 ± 0.016[g]	N/A	77.41 ± 4.80%	1.04 ± 0.10	0.038 ± 0.003%

[g] The values were obtained as the average of three replicates, the errors were obtained as the standard derivation

[h] Results obtained at the exponential phase for growing H$_2$ production or the non-growing phase for non-growing H$_2$ production.

[i] Results obtained at the end of the whole process.

3.4.1 Growing H_2 production

Rhodopseudomonas palustris grew photo-heterotrophycally on 10 mM glycerol and N_2 to produce H_2 under nitrogen-fixation conditions for about 10 days. From Figure 3-2 and Table 3-3, cells grew from a concentration of 0.108 ± 0.001 gramme of dry biomass per litre of suspension (gL^{-1}) to that of 0.624 ± 0.020 gL^{-1}. In the exponential phase, cells grew at a specific growth rate of 0.013 ± 0.001 h^{-1}, and the average H_2 production rate was 1.06 ± 0.11 mini-litre of gas per litre of suspension per hour ($mL\ L^{-1} h^{-1}$). When the glycerol was completely depleted, H_2 production and N_2 consumption stopped immediately. Along the cell growth, 89.30 ± 0.11 % of glycerol was consumed, and 29.60 ± 1.56 mL of H_2 at standard temperature and pressure (STP) was generated as an obligatory product.

For growing H_2 production, from Table 3-1, only around 1 % of glycerol was utilised for PHB accumulation, and most glycerol was utilised for both H_2 production and cell growth. Among all the carbons and the electrons tracked, the amount of glycerol utilised for cell growth was about eight-fold of that for H_2 production.

3.4.2 Non-growing H_2 production

Non-growing cells were prepared and cultivated with 10 mM glycerol and Ar for 54 days for the non-growing H_2 production. From Figure 3-3 and Table 3-3, cells grew from a concentration of 0.563 ± 0.009 gL^{-1} to 0.696 ± 0.015 gL^{-1} in the first 211 h. The reason for the initial dry cell mass increase was assumed to be the PHB accumulation. When *R. palustris* is under nutrient deficient conditions, it can generate different storage products such as glycogen, trehalose, and PHB (Larimer *et al.* 2004). Under nitrogen depleted conditions, *R. palustris* could generate up to 30% dry cell weight equivalent PHB in the first ~ 100 h, then the dry cell mass remained roughly the same until it reached death phase (McKinlay *et al.* 2014b). The reason of the initial dry cell mass increase will be verified, and the experimental procedures to minimise the impact on H_2 production rate will be discussed in Chapter 4.

Cells were then entering the non-growing phase to generate H_2 for another 680 h. From Figure 3-3 and Table 3-3, the average dry cell mass was 0.679 ± 0.016 gL^{-1},

the cell growth was limited to 4 %, H_2 was produced at a constant rate of 1.04 ± 0.05 mL $L^{-1} h^{-1}$ at STP, and glycerol was also consumed at a constant rate 4.57 ± 0.20 µmol $L^{-1} h^{-1}$ continuously. When the glycerol concentration dropped to a limiting 0.591 ± 0.005 mM, H_2 production was halted, and cells began to aggregate and perish and went to death phase. 94.09 ± 0.31 % of glycerol was consumed.

Unlike the growing H_2 production, most glycerol was utilised to generate H_2 for non-growing H_2 production. *R. palustris* functioned as a biocatalyst (McKinlay & Harwood 2010b); electrons released from glycerol and ATP generated from the light source were used for H_2 production only, *i.e.* converting H^+ ions exclusively to H_2. From Table 3-2, among all the carbons and the electrons tracked, the amount of glycerol utilised for H_2 production was about eight-fold of that for cell growth.

3.5 Discussion

3.5.1 H_2 yield

The H_2 yields for both processes were quite different. From Table 3-3, H_2 production by non-growing *R. palustris* achieved 77.41 ± 4.80% of the theoretical maximum H_2 yield, about 8-fold as that for H_2 production by growing *R. palustris*, 10.43 ± 0.95% of the theoretical maximum H_2 yield. Both results were within the respective ranges predicted and presented in other studies. For the growing H_2 production, even the most electron-rich substrate, butyrate, was used, the H_2 yield was only 25 % of the theoretical maximum as most of the electrons were used for biosynthesis (McKinlay et al. 2014b). On the other hand, for non-growing H_2 production, the H_2 yield could approach more than 40 % of the theoretical maximum, even 78 %, depending on the substrate supplied (McKinlay *et al.* 2014b; Huang *et al.* 2010a).

The difference in H_2 yield for both processes can be explained as the change in metabolic pathways (McKinlay *et al.* 2014b). For growing H_2 production, cells were assumed to use the glyoxylate shunt to bypasses the lower tricarboxylic acid (TCA) cycle, thereby retaining the two carbons in acetyl-coenzyme A (aceryl-CoA) for biosynthesis that would otherwise be lost as CO_2 (McKinlay & Harwood 2011). While, for non-growing H_2 production, cells were assumed to use the whole TCA cycle exclusively to metabolise reductant, glycerol, for H_2 production (McKinlay et al.

2014b). Nitrogenase was suggested to function as an adenosine triphosphate (ATP) powered hydrogenase (McKinlay & Harwood 2010b). The ATP requirement was not a limiting factor because a single electron in the system could be repeatedly energised through cyclic phosphorylation. It could maintain the required H^+ ion gradient and resultant ATP levels (McKinlay & Harwood 2010b). Therefore, all the electrons, released from the reductant, and ATP from light was potentially exclusively directed towards H_2 production, resulting in a much higher H_2 yield.

In addition, electrons are needed to release H_2 from H^+, and the amount of H_2 generated may be directly proportional to the electrons used for this purpose. During both processes, the only electron donating chemical was glycerol. The glycerol input for both processes were identical, and the glycerol consumptions for both processes were quite similar: 89.30 ± 0.11 % for growing H_2 production and 94.09 ± 0.31 % for non-growing H_2 production. Therefore, the total number of electrons available for both processes were similar. However, the number of electrons utilised for H_2 production were quite different.

From Table 3-1, for growing H_2 production, 105.24 ± 7.56 % of electrons were tracked at the end of the process. Among those, 88.59 ± 0.50 % electrons released from glycerol were utilised for cell growth, and only 9.94 ± 0.38 % of electrons were utilised for H_2 production. As the carbon dioxide fixation Calvin cycle for cell growth competes with nitrogenase for electrons under the nitrogen-fixation conditions (McKinlay *et al.* 2014b; McKinlay & Harwood 2011; McKinlay & Harwood 2010a), H_2 production is inefficient, *explains the low* H_2 yield, 0.732 ± 0.068 mole H_2 per mole of glycerol, 10.43 ± 0.95 % the theoretical maximum H_2 yield (Rey *et al.* 2007). Additionally, excess ammonia generated during growing H_2 production may act as an enzyme inhibitor for H_2 production. Lee *et al.*(2011) found that ammonia concentrations as low as 17 mg L^{-1} could inhibit H_2 production by *R. palustris.*

From Table 3-2, for H_2 production by non-growing *R. palustris* with initial $OD_{660nm} = 0.8$, 92.80 ± 2.54 % of electrons were tracked at the end of the process. Among those, 0.65 ± 0.01 % of electrons were utilised for PHB synthesis, 15.90 ± 4.08 %of electrons were utilised to form biomass, and the majority

59

83.40 ± 4.08 % were utilised for H_2 production. Therefore, the non-growing H_2 production showed a significant improvement in H_2 yield, 77.41 ± 4.80% of the theoretical maximum.

3.5.2 Average H_2 production rate

For growing H_2 production, the average H_2 production rate was 1.06 ± 0.11 mL $L^{-1} h^{-1}$ at STP during exponential growth; whereas for non-growing H_2 production, H_2 was produced at a constant rate of 1.01 ± 0.10 mL $L^{-1} h^{-1}$ at STP during the non-growing phase.

The cultivation conditions for both H_2 production by growing and nongrowing *R. palustris* were almost identical except for the headspace gas. N_2 was supplied in the headspace for growing H_2 production, and Ar was supplied in the headspace for non-growing H_2 production. For growing H_2 production, H_2 was generated as an obligatory but not necessarily advantageous by-product of cell growth under nitrogen-fixing conditions (Rey *et al.* 2007). For non-growing H_2 production, nitrogenase was suggested to function as an ATP-powered hydrogenase, and all electrons and energy should be utilised to produce H_2 only (McKinlay & Harwood 2010b). The ATP requirement was not a limiting factor because a single electron in the system could be repeatedly energised through cyclic phosphorylation. It could maintain the required H^+ ion gradient and resultant ATP levels (McKinlay & Harwood 2010b). Therefore, despite nitrogen depletion, the H_2 production rates for both growing and non-growing H_2 production processes were similar.

There was another factor that needed to be considered in the future. For H_2 production by growing *R. palustris*, the dry cell mass grew over time from 0.140 ± 0.004 to 0.619 ± 0.038 gL^{-1} during exponential growth. Whereas for H_2 production by growing *R. palustris*, the average dry cell mass was 0.679 ± 0.009 gL^{-1}, the cell growth was limited to 4 % during the nongrowing phase. The dry cell mass in both processes were quite different, and the similar H_2 production rates might be a coincidence for those dry cell mass. The impact of dry cell mass (inoculum size) will be discussed in Chapter 4.

3.5.3 Energy conversion efficiency

As the cultivation conditions for both growing and nongrowing H_2 were almost identical with the same light intensities and irradiated area; the energy conversion efficiency in this chapter was proportional to the H_2 production rate. Since H_2 production rates were similar, the energy conversion efficiencies for both processes were quite similar: 0.035 ± 0.004 % for growing H_2 production and 0.038 ± 0.003 % for non-growing H_2 production. The energy conversion efficiency determined in this chapter falls within the predicted range for PNS bacteria *(Kothari et al. 2012; Uyar et al.* 2007).

The low efficiency suggests that most of the light emitted from the incandescent lamp used in this chapter was not consumed by *R. palustris* during cultivation. Therefore, further investigation of the light impact on H_2 production, including different intensities and wavelength ranges, needs to be carried out (Basak & Das 2009; Akkerman *et al.* 2002), and it will be discussed in Chapter 5 .

3.5.4 Average daily H_2 production rate

Even though the average H_2 production rates for both growing H_2 production during exponential growth and non-growing H_2 production during the non-growing phase were similar, the instant H_2 production rates for both processes were quite different. The average daily H_2 production rate was predicted from the results in Figure 3-2 and Figure 3-3 and presented in Figure 3-4 and Figure 3-5 for both processes.

From Figure 3-4, for growing H_2 production, the maximum average daily H_2 production rate occurred at the middle exponential growth phase where the H_2 production rate was 1.91 ± 0.35 mL L^{-1} h^{-1} at $OD_{660nm} = 0.519 \pm 0.082$. It was assumed that the excess *ammonia generated afterwards might act as an enzyme inhibitor for H_2 production.* Then it dropped gradually until the cells reached the stationary phase. From the results, apart from cultivation conditions and nutrient concentrations, the average daily H_2 production rate also depended on different cell growth phases. When $OD_{660nm} = 0.862 \pm 0.030$, the average daily H_2 production rate was 1.12 ± 0.580 mL L^{-1} h^{-1}. From the trend of the result, it was predicted that the

average daily H_2 production rate should be higher than 1.12 ± 0.580 mL $L^{-1} h^{-1}$ when $OD_{660nm} = 0.800$.

From Figure 3-5, under the nitrogen-depleted conditions, the average daily H_2 production rate fluctuated in the first 200 hours when cells were stressed by nutrient deficiency and accumulating PHB. This fluctuation in H_2 production rate could be avoided experimentally. For details, please refer to Chapter 4. Then the average daily H_2 production rate maintained roughly constant at 0.96 ± 0.04 mL $L^{-1} h^{-1}$ at the non-growing phase until the cells reached the death phase.
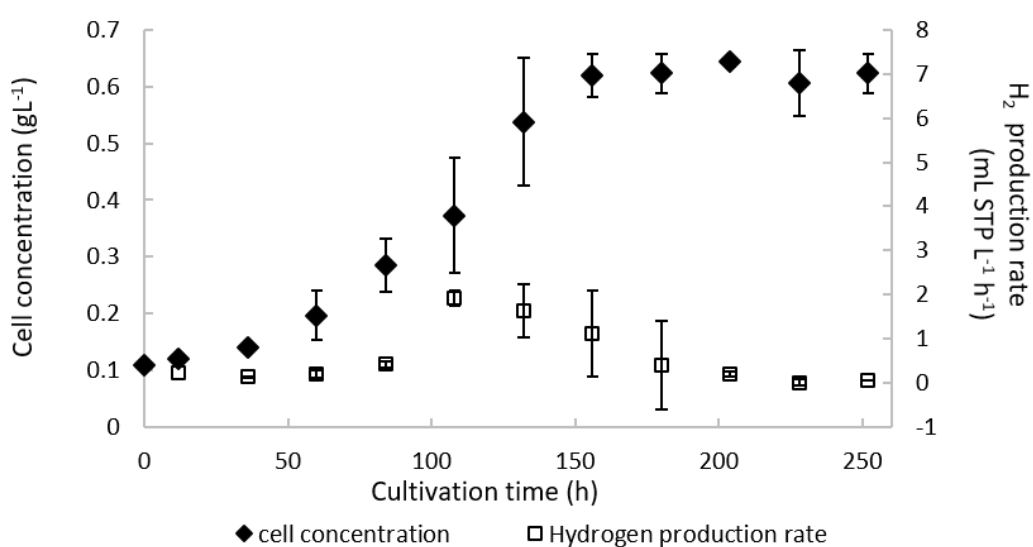
Figure 3-4: The average daily H_2 production rate and dry cell mass *vs.* time for H_2 production by growing *R. palustris*. The H_2 production rate was calculated on daily basis from the results presented in Figure 3-2. Each data point in each figure represents the average value of three experimental repeats with corresponding error bars denoting the standard derivations.
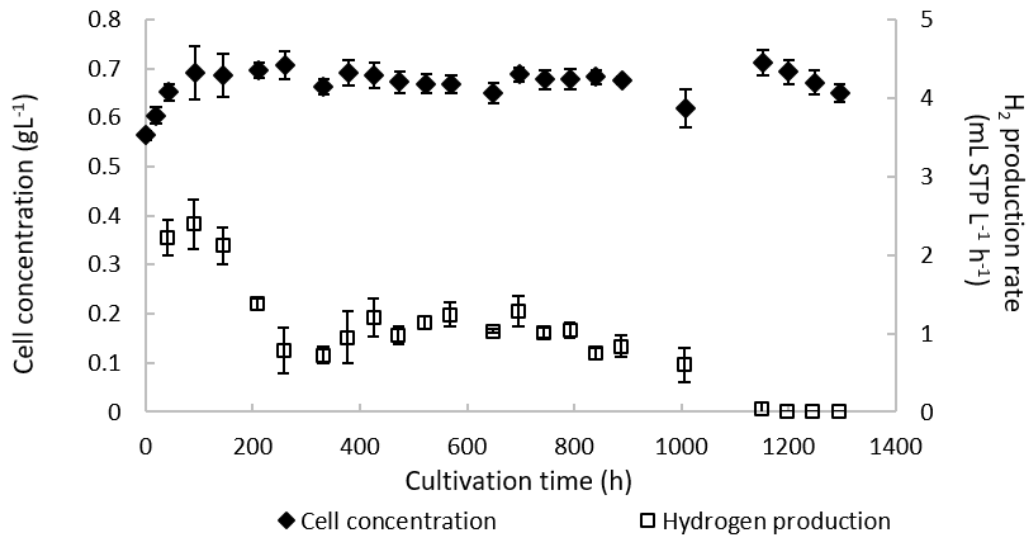
Figure 3-5: The average daily H_2 production rate and cell optical density *vs.* time for H_2 production by non-growing *R. palustris.* The H_2 production rate was calculated every two days from the results presented in Figure 3-3. Each data point in each figure represents the average value of three experimental repeats with corresponding error bars denoting the standard derivations.

3.5.5 Refilling 10 mM glycerol after non-growing H_2 production

As H_2 production by non-growing *R. palustris* demonstrated promising results in H_2 yield compared to that by growing *R. palustris*, it is interesting to know that how long the biocatalyst will last to apply it in industry. For H_2 production by non-growing *R. palustris*, when the glycerol concentration dropped to a limiting 0.591 ± 0.005 mM, H_2 production was halted, and cells began to aggregate and perish and went to death phase. Then another 10 mM of glycerol was added in, H_2 production was immediately recovered and continued for another 1000 hours. The experiment was stopped due to the time constraint during the experiment. By that time, the biocatalyst was still capable of producing H_2 at the constant rate. It was quite fascinating to know that experimentally proven non-growing *R. palustris* was capable to generate H_2 as a biocatalyst for longer than 2000 hours. Gosse *et al.* (2010) also suggested that this biocatalyst could even generate H_2 for longer than 4000 hours. During the refilling process, the average H_2 production was dropped from 0.669 ± 0.007 to 0.515 ± 0.017 gL^{-1}, the constant H_2 production rate dropped from 1.04 ± 0.06 to

0.88 ± 0.07 mL L^{-1} h^{-1}. This again further suggested that the initial dry cell mass (inoculum size) might have impact on H_2 production rate for non-growing H_2 production. It will be further investigated in Chapter 4.
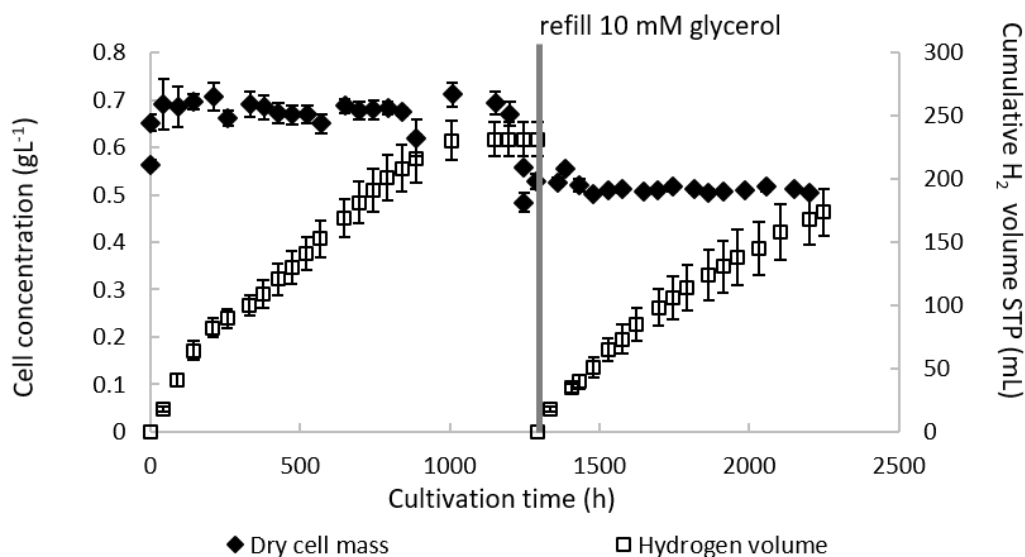
Figure 3-6: Refilling 10 mM glycerol after H_2 production by non-growing *R. palustris*. Non-growing cells were prepared and cultivated with 10 mM glycerol and Ar for 54 days for the non-growing H_2 production. When glycerol ran out and H_2 production stopped at 1300 h, 10 mM glycerol was added in the experimental samples. H_2 production was recovered immediately for another 1000 h. Each data point in each figure represents the average value of three experimental repeats with corresponding error bars denoting the standard derivations.

3.5.6 Preventing interference by polyhydroxybutyrate

It is known that when *R. palustris* is placed under nutrient deficient conditions; stress responses can generate different storage products such as glycogen, trehalose, and polyhydroxybutyrate (PHB) (Larimer *et al.* 2004). Leading on, we see when *R. palustris* is under nitrogen depleted conditions, there is an initial increase in density, in the form of dry cell mass, for the first 200 h prior to it levelling off until death phase. This is demonstrated in Figure 3-7. This initial increase in cell density can be attributed solely to PHB accumulation.

To minimise the interference of PHB accumulation on dry cell mass and H_2 production rate, the following experimental procedures were carried out in this Chapter. *R. palustris* grew photo-heterotrophycally on 10 mM glycerol and N_2 initially until its optical density reached at $OD_{660} = 0.8$, the headspace was replaced by argon to halt the growth and allow PHB accumulation for about 200 hours. The non-growing cells were then harvested and cultivated in fresh medium with 10 mM glycerol and argon. The dry cell mass and cumulative H_2 volume were determined, and the results were shown in figure b). From the results, it was seen that the dry cell mass remained almost constant, and the H_2 production rate was 1.33 ± 0.14 mL L^{-1} h^{-1}. The non-growing H_2 production rate with PHB correction was about 30 % higher than that without PHB correction.
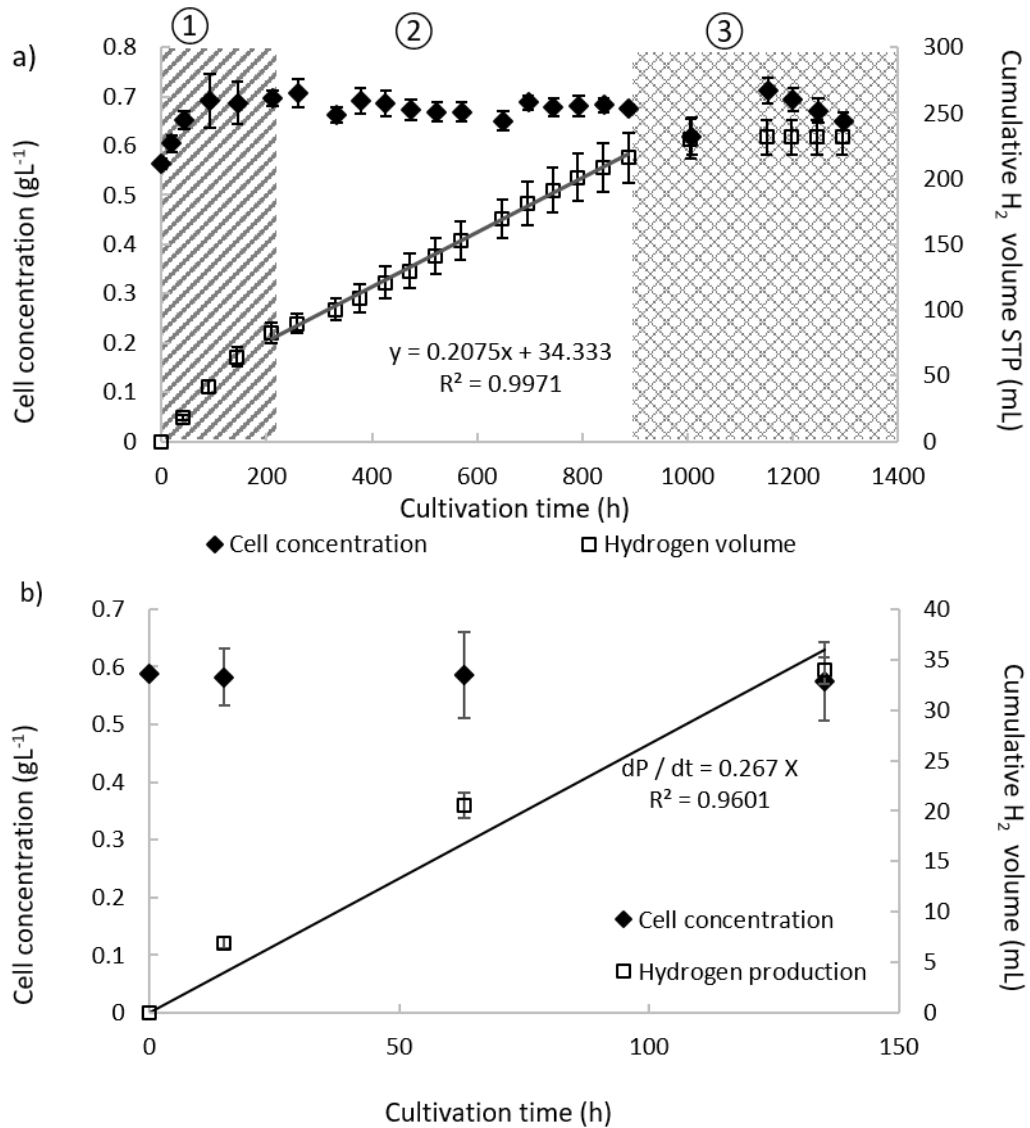
Figure 3-7: H_2 production by non-growing *R. palustris* without and with PHB correction. a) represents the results without PHB correction. The data were obtained from Figure 3-3 in Chapter 3. Cells were cultivated with 10 mM glycerol and N_2 until OD_{660nm} = 0.80, then harvested and cultivated with 10 mM glycerol and argon immediately for non-growing H_2 production. The dry cell mass kept constant in the non-growing phase (②) with a constant H_2 production rate of 1.04 ± 0.06 mL $L^{-1} h^{-1}$. b) shows the results with PHB correction. Identically cells were initially cultivated with glycerol and N_2 until OD_{660nm} = 0.80. The headspace was replaced by argon to halt the cell growth and allow the PHB accumulation for about 200 hours. Then cells were harvested and cultivated with 10 mM glycerol and argon for non-growing H_2 production. The dry cell mass was kept constant over the 140 hours, and the H_2 production rate was 1.33 ± 0.14 mL $L^{-1} h^{-1}$. Each data point in each figure represents the average value of three experimental repeats with corresponding error bars denoting the standard derivations.

3.6 Conclusions

In this chapter, it was demonstrated that H_2 could be generated by non-growing *R. palustris*. Comparing the H_2 production performance for both processes, a significant difference in the H_2 yield was observed; H_2 production by non-growing *R. palustris* reached 77.41 ± 4.80 % of the theoretical maximum H_2 yield, about 8-fold as that reached by H_2 production by growing *R. palustris*, 10.45 ± 0.95 % of the theoretical maximum H_2 yield. In addition, experimentally proven non-growing *R. palustris* was capable to generate H_2 as a biocatalyst for longer than 2000 hours with one refill of glycerol in the half way. Therefore, it was found that for small to medium size batch cultivation, H_2 production by growing *R. palustris* were recommended for the ease of operation, while H_2 production by non-growing *R. palustris* would be more economically appealing in scaled up commercial applications due to the high H_2 yield.

4 The impact of initial inoculum sizes on hydrogen production by non-growing Rhodopseudomonas palustris

4.1 Introduction

Non-growing *Rhodopseudomonas palustris* (*R. palustris*) cultivated with glycerol can generate a more significant H_2 yield than growing *R. palustris* as seen in Chapter 3. Additionally, non-growing *R. palustris* can generate H_2 as a biocatalyst for over 2000 hours. As such H_2 production by non-growing *R. palustris* is economically appealing for scaled-up commercial applications (Piskorska *et al.* 2013; Gosse *et al.* 2010; Huang *et al.* 2010a; McKinlay & Harwood 2010b; Melnicki *et al.* 2008). In order to accomplish the proposed scale-up system, it is important to understand the product formation kinetics for non-growing H_2 production (Das & Veziroglu 2001; Das & Veziroglu 2008; Kumar et al. 2000; Koku et al. 2003).

The photosynthetic apparatus is composed of transmembrane protein complexes and an adenosine triphosphatase (ATPase) complex to allow adenosine triphosphate (ATP) synthesis by consuming the energy from a proton gradient. A comprehensive review of the structure and the operation of the photosynthetic membrane apparatus is covered in Chapter 5. The main processes related to non-growing H_2 production are shown in Figure 4-1.
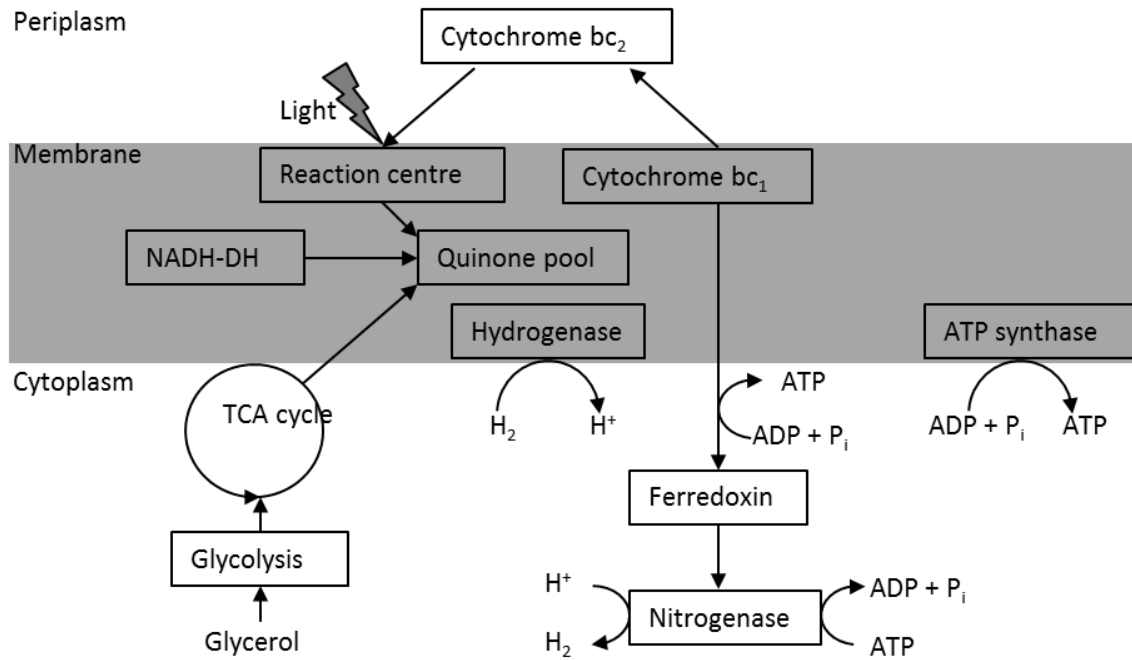
Figure 4-1: Main processes related to hydrogen production by non-growing *R. palustris*: anoxygenic photosynthesis, ATP synthesis, TCA cycle, hydrogenase, and nitrogenase activities, modified from (Hallenbeck 2012; Sarma, Brar, Sydney, et al. 2012). The straight black arrows indicate the electron flow. The lightning symbol indicates light excitation. Abbreviations: Cyt bc_1= cytochrome bacterial chlorophyll 1 complex; Cyt bc_2 = cytochrome bacterial chlorophyll 2; Fd = ferredoxin; RC = reaction centre; NADH-DH = NADH dehydrogenase

When light shines on *R. palustris*, the photon travels through the periplasmic space to reach the reaction centre (RC) in the membrane, in which the photon supplies the energy to stimulate the excitation of cytochrome bacterial chlorophyll 2 complex (Cyt bc2). This energy is used to release an electron from glycerol, the organic substrate and to reduce the quinone (Q). When the second photon releases the second electron, the quinone is reduced twice, and can pick up a proton from the cytoplasmic space and travel through the membrane to reach the cytochrome bacterial chlorophyll 1 complex (Cyt bc1). Electrons are relocated to the Cyt bc2, and protons are accumulated in the periplasmic space to form an electrochemical gradient. Cyt bc2 is able to reduce the oxidised primary electron donor and complete the cycle, whereas the electrochemical gradient formed by the accumulation of protons supplies the energy to the form the ATP-synthase to generate ATP from

adenosine diphosphate (ADP). The reduced quinone can open the cycle to drive the NADH dehydrogenase and succinate dehydrogenase backwards, *i.e.* reduce NAD^+ and fumarate to NADH and succinate respectively (Hallenbeck 2012; Hall & Rao 1999). The electrons are then transferred by ferredoxin in the cell. Hydrogen gas is then generated from the H^+ and electrons through the action of the nitrogenase, consuming the energy from the proton gradient and ATP. When the energy required for the action of the nitrogenase cannot be balanced by the energy supplied by ATP from photosynthesis and proton gradient, hydrogen is consumed by the uptake hydrogenase to release energy and form ATP.

For H_2 production by non-growing cells, the number of cells were assumed to be proportional to the dry cell mass. Hence, the number of light-harvesting antennae, the number of reaction centres, the number of enzymes, and the number of electron carriers including bacterialchlorophylls, quinones and ferredoxins should be directly proportional to the dry cell mass. Providing there is no enzyme inhibitor, no light constraint, and no other environment constraint for the non-growing H_2 production, the H_2 production rate should be proportional to the dry cell mass.

In this Chapter, experiments of non-growing H_2 production with different inoculum sizes were carried out. The results of H_2 production rates and energy conversion regarding to different inoculum sizes were obtained and analysed from the experimental data, through which, it is aimed to understand the product formation kinetics of the non-growing H_2 production.

4.2 Materials and methods

4.2.1 Strain and medium

R. palustris, ATH 2.1.37 (NCIB 11774), was purchased from ATCC® as a freeze-dried sample. A defined medium was used in this study as described by Gosse *et al.* (2007), for details please refer to Chapter 2.1.3.

4.2.2 Preparation of non-growing cells

The freeze-dried *R. palustris* was rehydrated and plated on an agar plate. After one week's incubation, a pure uncontaminated colony from the agar plate was selected for the pre-culture preparation. The selected colony was transferred and cultivated in a 15mL sterile centrifuge tube with 100 μl of 2 M filtered sodium glutamate, 100 μl of autoclaved pure glycerol, and defined medium (Gosse *et al.* 2007) for another week. Both agar plates and centrifuge tubes were incubated up-side-down. The temperature was maintained at 30 ± 2 °C. Illumination was provided by incandescent light bulbs (BELL® 100 W R80 ES Reflector) with a light intensity of 230 ± 7 Wm^{-2}. Full details about culture revival are in Chapter 2.1.

The pre-culture was harvested and centrifuged at 5000 g for ten minutes at room temperature in an Eppendorf® 5800 centrifuge (Model 5810R) (Gosse *et al.* 2007), then re-suspended in 1 L fresh medium, and cultivated in a 1 L Duran® bottle with 10 mM glycerol and filtered sterile N$_2$ as headspace. Liquid samples were extracted from the bottle at a regular interval to monitor cell growth. Once the optical density at 660 nm of the cell suspension reached 0.80 ($OD_{660nm} = 0.80$), the headspace gas was replaced by argon to halt the growth and allow polyhydroxybutyrate (PHB) accumulation for about 200 hours. When *R. palustris* is under nutrient deficient conditions, it can generate different storage products such as glycogen, trehalose, and PHB (Larimer *et al.* 2004).

4.2.3 H$_2$ production by non-growing cells with different inoculum sizes

After PHB accumulation, non-growing cells were harvested and centrifuged at 4424 g for ten minutes at room temperature in a Beckman® JA-10 rotor (Gosse *et al.* 2007). The pellet was washed and re-suspended in fresh medium to the optical density of 0.20, 0.40, 0.80, 1.20, 1.60, and 2.0 at 660 nm respectively. 200 mL non-growing cell suspension with each optical density was then cultivated in a 250 mL bottle and supplemented with 10 mM glycerol and filtered sterile argon as headspace.

Cells were then cultivated at 30 ± 2 °C. Illumination was provided by incandescent light bulbs (BELL® 100 W R80 ES Reflector) with a light intensity of 230 ± 7 Wm^{-2}. For details in experimental setup, please refer to Chapter 2.2.

At regular intervals, the gases generated were released to the graduate burette, the volume was measured by water displacement in the burette and recorded, and a gas sample was extracted for gas composition determination by a gas chromatography. As the H_2 solubility in water is extremely low, it is assumed to be insoluble for this study. The total H_2 volume was equal to the H_2 volume in gases collected from the burette and the H_2 volume in headspace of the culture bottle. Equally liquid samples were extracted from the bottle at the same time to monitor cell growth and glycerol consumption.

4.2.4 Analytical methods

The optical density of the cell suspension was measured by a spectrophotometer (Thermospectronic UV1) against a blank solution of de-ionised water at a fixed wavelength of 660 nm, and the equivalent dry cell mass was correlated with the optical density (Pott *et al.* 2012).

Glycerol concentration was determined by a modified method from Bondioli and Della Bella (2005). The ethanol solution used in the original assay was replaced volumetrically by distilled water to avoid the distortion of the assay when aqueous solutions of glycerol rather than solutions of glycerol in biodiesel were used.

The gas composition was determined by gas chromatograph (Agilent® 7890A) with a thermal conductivity detector employing argon as the carrier gas and a HayeSep Q column. The components were analysed using the thermal conductivity detector and correlated to the percentage of different components in the gas sample using existing calibrations (Pott *et al.* 2012).

For details in analytical methods, please refer to Chapter 2.3.

4.2.5 H_2 production performance

As previously shown in Chapter 3, for non-growing H_2 production, most of the reductant, glycerol, was utilised as the electron donor for H_2 production exclusively. The H_2 yield for non-growing H_2 production was ~ 80 % of the theoretical maximum H_2 yield. Therefore, in this chapter, H_2 production performance from glycerol for non-growing H_2 with different inoculum sizes (Koku *et al.* 2002; Hallenbeck 2012) focused on the other two criteria: H_2 production rate and energy conversion.

H_2 production rate is defined as the volume of H_2 generated per unit volume of cell suspension per unit time (mL L^{-1} h^{-1}) (Tian et al. 2010).

The energy conversion, in terms of light, is defined as the ratio of the combustion enthalpy of H_2 to the total energy input into cell cultivation (Uyar et al. 2007).

For details about the H_2 production performance, please refer to Chapter 2.4.2.

4.2.6 Product formation kinetics

As explained in Chapter 3, most electrons and carbon sources were utilised to generate H_2 in the non-growing phase. It is assumed that the only product of this process is H_2, and the product kinetics could be investigated through the Leudeking–Piret (LP) model (Sarma, Brar, Sydney, et al. 2012).

$$\frac{dP}{dt} = \alpha \frac{dX}{dt} + \beta X \qquad \text{Equation 4-1}$$

where P is the H_2 volume per unit volume of the cell culture (mL L^{-1}), t is time (h), X is the cell concentration (g L^{-1}), and α and β are growth-associated coefficient and non-growth associated coefficient.

Under nitrogen-depleted conditions, the dry cell mass remained roughly the same after PHB accumulation. The cell growth was halted until cell death (McKinlay *et al.*

2014). Thus, it can be assumed that the growth rate is zero during the non-growing H_2 production, *i.e.* $\frac{dX}{dt} = 0$. Simplifying the kinetics to:

$$\frac{dP}{dt} = \beta X$$

Equation 4-2

4.3 Results

The results of H_2 production rate by non-growing *R. palustris* with different initial optical densities were shown in Figure 4-2. The results of initial optical density and its corresponding average dry cell mass was presented in Table 4-1. Instead of optical density, the same results were again represented in terms of different dry cell mass and shown in Figure 4-3. Through which, the corresponding energy conversion was calculated, and the results were displayed in Figure 4-4. Each data point in each figure represents the average value of three repeated experiments, and the corresponding error bar denotes the standard derivation of these results.

4.3.1 H$_2$ production rate
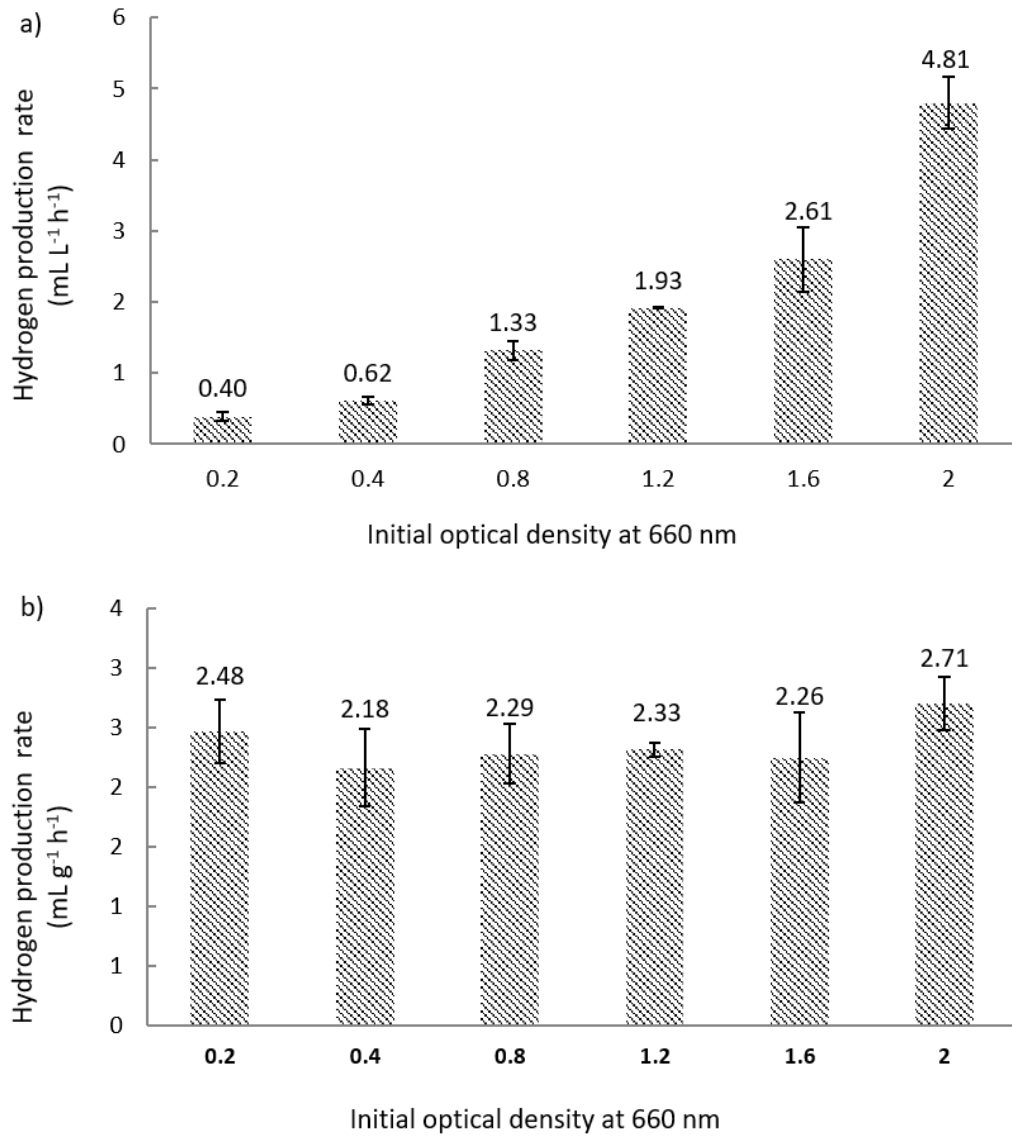
Figure 4-2: H$_2$ production rates by non-growing *R. palustris* with different optical densities. *R. palustris* was cultivated with 10 mM glycerol and filtered sterile N$_2$ as headspace until its optical density reached to 0.8 at 660 nm, the headspace gas was replaced by argon to halt the growth and allow polyhydroxybutyrate (PHB) accumulation for about 200 hours. After PHB accumulation, non-growing cells were diluted or concentrated to different optical density ranging from 0.2 to 2.0 at 660 nm, and the diluted or concentrated culture was then cultivated with 10 mM glycerol and filtered sterile argon for a week. a) represents the hydrogen production rate in terms of the volume of hydrogen gas per unit volume of cell culture per unit time (mL L^{-1} h^{-1}) *vs.* optical density, whereas b) represents the hydrogen production rate in terms of the volume of hydrogen gas per unit mass of the dry cells per unit time (mL g^{-1} h^{-1}) instead. Each data point in each figure represents the average value of three experimental repeats with corresponding error bars denoting the standard derivations.

4.3.2 Initial optical density vs dry cell mass

Table 4-1: Initial optical density *vs*. dry cell mass[a]

Initial OD	Cell concentration (g L^{-1})		
OD = 0.2	0.163	±	0.003
OD = 0.4	0.287	±	0.006
OD = 0.8	0.581	±	0.003
OD = 1.2	0.816	±	0.018
OD = 1.6	1.159	±	0.004
OD = 2.0	1.785	±	0.016

[a] The values were obtained as the average of three experimental replicates, the errors were obtained as the standard derivations

4.3.3 Product formation kinetics
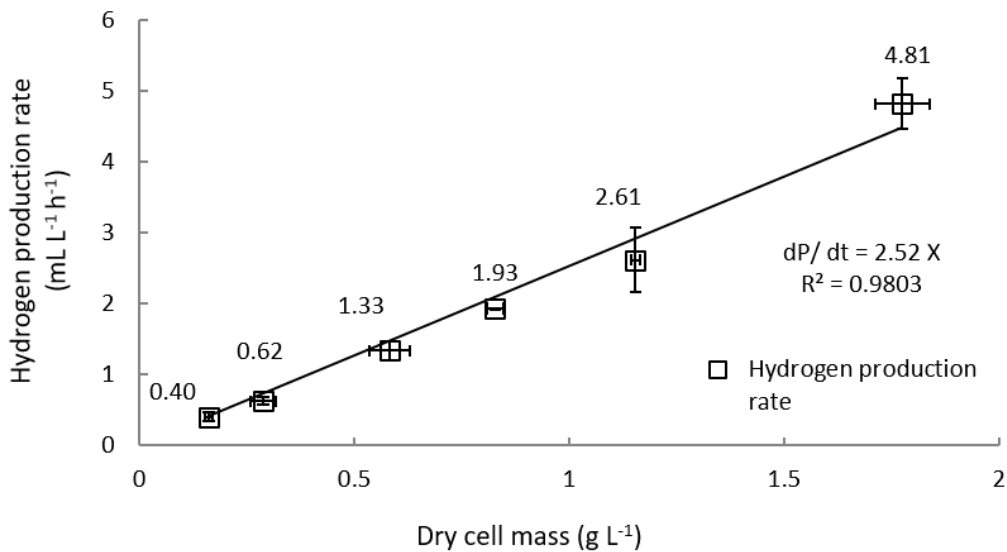
Figure 4-3: H_2 production rates by non-growing *R. palustris* with different dry cell mass. The results of hydrogen production rates, in terms of the volume of hydrogen gas per unit volume of cell culture per unit time (mL $L^{-1} h^{-1}$), *vs.* the dry cell mass, in terms of the mass of the dry cells per unit volume of the culture (g L^{-1}), were presented in the figure above. The experimental data were obtained from Figure 4-2, and the values of optical density were correlated to their corresponding dry cell mass. For the details of this correlation, please refer to Chapter 2.3.4. Each data point in this figure represents the average value of three experimental repeats with corresponding error bars denoting the standard derivations.

Table 4-2: Summary output of regression analysis

Regression Statistics	
Multiple R	0.996
R Square	0.985
Adjusted R Square	0.927
Standard Error	0.301
Observations	18

	Coefficients	Standard error	t Stat	P-value
Intercept	0	-	-	-
Dry cell mass (X)	2.52	0.07	34.44	3.62×10^{-17}

$$H_2 \ production \ rate = 2.52 \ \times \ Dry \ cell \ mass$$
Equation 4-3

4.3.4 Energy conversion
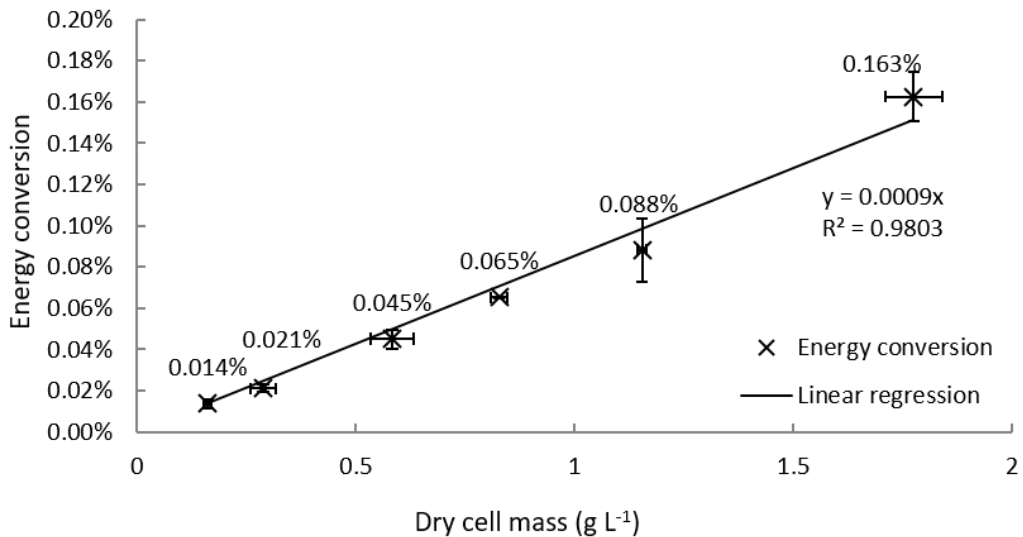
Figure 4-4: Energy conversion of H_2 production by non-growing *R. palustris* with different dry cell mass. The results of hydrogen production rates (mL L^{-1} h^{-1}) *vs.* dry cells mass (g L^{-1}) were obtained from Figure 4-3. The energy conversion was calculated accordingly. The energy conversion, in terms of light, is defined as the ratio of the combustion enthalpy of H_2 to the total energy input into cell cultivation (Uyar *et al*. 2007). Each data point in this figure represents the average value of three experimental repeats with corresponding error bars denoting the standard derivations.

4.4 Discussion

4.4.1 H_2 production rate

After 200 h of PHB accumulation, non-growing cells were diluted or concentrated to their respective densites ranging from 0.2 to 2.0 at 660 nm. The cultures were then cultivated with 10 mM glycerol and filtered sterile argon.

From figure a) in Figure 4-2, the H_2 production rate, in terms of the volume of hydrogen gas per unit volume of cell culture per unit time ($mL\,L^{-1}\,h^{-1}$), increased as the optical density of the culture increased. As the optical density of the cell culture increased from 0.2 to 2.0, the H_2 production rate increased from 0.40 ± 0.06 to $4.781 \pm 0.36\ mL\,L^{-1}\,h^{-1}$.

When the H_2 production rate was represented as the volume of hydrogen gas per unit mass of the dry cells per unit time ($mL\,g^{-1}\,h^{-1}$) instead in figure b), it was almost constant at $2.38 \pm 0.29\ mL\,g^{-1}\,h^{-1}$ regardless of the optical density of cell culture. Only the sample inoculated at $OD_{660nm} = 2.0$ was 14 % higher than the average of $2.71 \pm 0.23\ mL\,g^{-1}\,h^{-1}$. Thus, instead of the volume of hydrogen gas per unit volume of cell culture per unit time ($mL\,L^{-1}\,h^{-1}$), H_2 production rate should be represented as the volume of hydrogen gas per unit mass of the dry cells per unit time ($mL\,g^{-1}\,h^{-1}$) for the H_2 production performance evaluation.

4.4.2 Product formation kinetics

From Chapter 2.3.1, the dry cell mass was linearly correlated to its optical density. As the correlation between the dry cell mass and its optical density had two distinct linear regions, it was split based on the initial optical density and expressed in the equations below.

$$if\ OD_{660nm} < 1.8, \quad cell\ concentration\ (g\ L^{-1}) = OD_{660nm} \times 0.718 \qquad \text{Equation 4-4}$$

$$if\ OD_{660nm} \geq 1.8, \quad cell\ concentration\ (g\ L^{-1}) = OD_{660nm} \times 2.401 - 3.058 \qquad \text{Equation 4-5}$$

As the optical density of 2.0 at 660 nm was just above the boundary of the two distinct linear regions, the result of its dry cell mass might fluctuate. This could also explain the reason that its H_2 production rate was about 14 % higher than the average in Figure 4-2.

Figure 4-3 is a simple translation from Figure 4-2 a) by converting optical density to dry cell mass. A regression analysis was carried out at a confidence level of 95 % with intercept at (0, 0). The "least squares" method was employed to fit a line through the experimental data in Figure 4-3. From Table 4-2, the value of R squared was 0.985, very closed to 1, which indicated that the H_2 production rate was very dependent on the dry cell mass. In addition, the P-value was 3.62×10^{-17}, much smaller than 0.05, therefore the H_2 production rate had a strong linear relationship with dry cell mass, which fitted the Leudeking–Piret (LP) model. From the results, $\frac{dP}{dt} = 2.52\,X$. Therefore, the Leudeking–Piret (LP) model can be further used for the non-growing H_2 production design and optimisation. It also proved that the H_2 production by *Rhodopseudomonas palustris* is not growth associated.

4.4.3 Energy conversion

Energy conversion, in terms of light, was calculated as the ratio of the combustion enthalpy of H_2 to the total energy input into cell cultivation (Uyar et al. 2007). As the cultivation conditions for all non-growing H_2 production were almost identical with the same light intensity and irradiated area; the energy conversion for this chapter was proportional to the H_2 production rate, ranging from 0.014 ± 0.002 % to 0.163 ± 0.012 %. As H_2 production rates increased with the cell inoculum sizes, the energy conversion also increased with the cell inoculum sizes. Again, by regression, a linear correlation was derived and plotted on Figure 4-4. The energy conversion determined falls within the predicted range for PNS bacteria (Kothari et al. 2012; Uyar et al. 2007). The low energy conversion suggests that most of the light emitted from the incandescent lamp used was not consumed by *R. palustris* during cultivation, which is confirmed in other literature studies (Basak & Das 2009; Akkerman *et al.* 2002).

4.5 Conclusions

In this chapter, it was experimentally proven again that H_2 could be generated by non-growing *R. palustris*. A series of non-growing cells with a range of optical densities between 0.2 to 2.0 were cultivated with 10 mM glycerol and filtered sterile argon. It was determined that the H_2 production rate was proportional to the cell inoculum size. By regression analysis, a strong positive linear relationship between the H_2 production rate (mL L^{-1} h^{-1}) and dry cell mass (g L^{-1}) was found, which fitted the Leudeking–Piret model, $\frac{dP}{dt} = 2.52\,X$. Therefore, the Leudeking–Piret model can be further used for the non-growing H_2 production design and optimisation. It also proved that the H_2 production by *R. palustris* is not strictly growth associated. Energy conversion was calculated and found to be very low. Other studies have also indicated that most of the light emitted from incandescent lamps used in this study was not consumed by *R. palustris* during cultivation. Further investigation of the light impact on H_2 production, including different intensities and wavelength ranges, needs to be carried out in Chapter 5 and Chapter 6.

5 The light requirement for hydrogen production by non-growing *Rhodopseudomonas palustris*

5.1 Introduction

Photosynthesis is the process to convert light energy into chemical energy by plants, algae and photosynthetic bacteria (Hu *et al*. 2002; Scheuring *et al.* 2006). It is commonly characterised into two classes. When photosynthesis is carried out in the presence of air, it is called oxygenic photosynthesis (Ort & Yocum 1996). In contrast, when photosynthesis is carried out without the presence of air, it is named anoxygenic photosynthesis which is the opposite (Blankenship *et al.* 2004).

Rhodopseudomonas palustris (*R. palustris*), a type of purple non-sulphur (PNS) bacteria, is a good example of anoxygenic photosynthesis. And its photosynthesis system is the most studied and best characterised in the past 50 years amongst other PNS bacteria (Hu *et al.* 2002). Through the anoxygenic photosynthesis, *R. palustris* reduces organic carbon source and oxidises molecules other than water, *i.e.* this process does not generate molecular oxygen (Blankenship *et al.* 2004).

The photosynthetic membrane apparatus of *R. palustris* is one of the simplest kinds, through which the photons from sunlight stimulate electronic excitation and release protons and electrons for adenosine triphosphate (ATP) synthesis (Hu *et al.* 2002). The schematic diagram and explanation of photosynthetic membrane apparatus in *R. palustris* is presented in Figure 5-1.
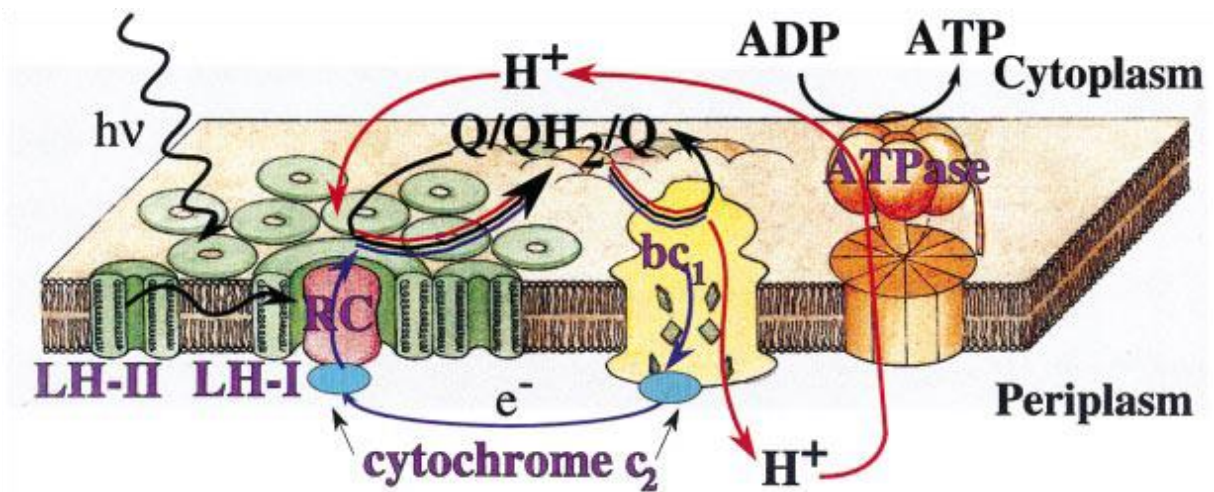
Figure 5-1: Schematic representation of the photosynthetic membrane apparatus in *R. palustris* (Hu *et al.* 2002). The reaction centre (RC, red zone) is surrounded by the light-harvesting complex I (LH-I, green zone), inner antenna, to form the LH-I–RC complex. The LH-I-RC complex is then surrounded by multiple light-harvesting complexes II (LH-II, green zone), outer antenna, forming altogether the photosynthetic unit (PSU). When light shines on *R. palustris*, the photon is harvested by LH-II and transferred *via* LH-I to RC, in which the photon supplies the energy to stimulate the excitation of cytochrome bacterial chlorophyll 2 complexes (Cyt bc2, blue). This energy is used to release an electron from the organic substrate and to reduce the quinone (Q). When the second photon releases the second electron, the quinone is reduced twice, and then it picks up a proton from the cytoplasmic space and travels through the membrane to reach the cytochrome bacterial chlorophyll 1 complex (Cyt bc1, yellow zone). During the process, the electrons are relocated in the Cyt bc2, and the protons are accumulated in the periplasmic space to form an electrochemical gradient. Afterwards the Cyt bc2 is able to reduce the oxidised primary electron donor and complete the cycle, whereas the electrochemical gradient formed by the accumulation of protons supplies as an energy to the ATP-synthase (orange zone) to generate adenosine triphosphate (ATP) from adenosine diphosphate (ADP) (Hu *et al*. 2002; Scheuring *et al.* 2006; Hallenbeck 2012). H_2 is then released by consuming the energy from ATP and electrochemical gradient. Electron flow is presented in blue, proton flow in red, and quinone flow between different membranes in black.

From Figure 5-1, the light requirement is vital for H_2 production by *R. palustris*. Only photons with the appropriate energy levels can trigger the excitation of cytochrome bacterial chlorophyll 2 complexes, and then release electrons and accumulate protons needed for ATP production (Carvalho *et al.* 2011; Hu *et al.* 2002; Hall & Rao 1999; Scheuring *et al.* 2006; Uyar *et al.* 2007). The intensity of a light source is a measure of photons available at that incident surface for bacterial photosynthesis(Carvalho et al. 2011). Excess or insufficient light intensities will limit the optimal H_2 production rate being reached (Basak & Das 2007).

In this chapter, the aim is to understand the light requirement for optimal non-growing hydrogen (H_2) production. Commonly used light source, incandescent light bulbs, was tested and its photosynthetic response was analysed at varying light intensities (10.6 ± 0.7 to 228.9 ± 4.5 Wm^{-2}).

5.2 Materials and methods

5.2.1 Strain and medium

R. palustris with strain designations ATH 2.1.37 (NCIB 11774) was obtained from ATCC® as a freeze-dried sample. A defined medium was used in this chapter as described by Gosse *et al.* (2007), for details please refer to Chapter 2.1.3.

5.2.2 Preparation of non-growing cells

Freeze-dried *R. palustris* was rehydrated, plated and cultivated on an agar plate for one week. A pure uncontaminated colony from the agar plate was selected and cultivated in a 15mL sterile centrifuge tube with 100 µL of 2 M filtered sodium glutamate, 100 µL of autoclaved pure glycerol, and defined medium (Gosse *et al.* 2007) for another week. Both agar plates and centrifuge tubes were incubated up-side-down. The temperature was maintained at $30 \pm 2\,°C$, the illumination was provided by incandescent light bulbs (BELL® R80 ES Reflector, London, U.K.) with a light intensity of 228.9 ± 4.5 Wm^{-2}. For details in culture revival and pre-culture preparation, please refer to Chapter 2.1.

The pre-culture was then harvested and centrifuged at 5000 g for ten minutes at room temperature in an Eppendorf® 5800 centrifuge (Model 5810R) (Gosse *et al.* 2007), then re-suspended in 1 L fresh medium, and cultivated in a 1 L Duran® bottle with 10 mM glycerol and filtered sterile N_2 as headspace. Liquid samples were extracted from the bottle at a regular interval to monitor cell growth. Once the optical density at 660 nm of the cell suspension reached 0.80 (OD_{660nm} = 0.80), the headspace gas was replaced by argon to halt the growth and allow polyhydroxybutyrate (PHB) accumulation for about 200 hours. When *R. palustris* is under nutrient deficient conditions, it can generate different storage products such as glycogen, trehalose, and PHB (Larimer *et al.* 2004).

5.2.3 H_2 production by non-growing cells at different light intensities

After PHB accumulation, non-growing cells were harvested and centrifuged at 4424 g at room temperature in a Beckman® JA-10 rotor for ten minutes (Gosse *et al.* 2007). The pellet was washed and re-suspended in fresh medium to the optical density of 0.80 at 660 nm. 200 mL non-growing cell suspension with 10 mM glycerol and argon was then cultivated in a 250 mL bottle at varying light intensities for a week.

Cells were then cultivated at 30 ± 2 °C. Illumination was provided by incandescent light bulbs (BELL® 100 W R80 ES Reflector). The light intensity on the surface of the bottles could be adjusted and controlled by altering the voltage supplied. Ten different light intensities were applied ranging from 10.6 ± 0.7 to 228.9 ± 4.5 Wm^{-2}. For details in experimental setup, please refer to Chapter 2.2.

At regular intervals, the gases generated were released to the graduate burette, the volume was measured by water displacement in the burette and recorded, and a gas sample was extracted for gas composition determination by a gas chromatography. As the H_2 solubility in water is extremely low, it is assumed that H_2 is insoluble in water. The total H_2 volume was equal to the H_2 volume in gases released in the burette and gases in headspace of the culture bottle. Equally liquid sample was extracted from the bottle at the same time to monitor cell growth and glycerol consumption.

5.2.4 Analytical methods

The emission spectrum of a light source was measured by an imaging spectrograph (Chromex 250is, High Peak, U.K.) as a function of wavelength ranging from 300 nm to 1000 nm. The signal was received and transferred by a 200 nm fibre optic to the imaging spectrograph.

As $I = \frac{P}{A}$ where I is the light intensity (W m^{-2}), P is the power incident on the surface, and A is the area of the incident surface, the light intensity on an incident surface could be measured by the power received at the surface if the area of the incident surface is known. The power received on the surface of the culture bottles was measured by a power meter, Integrated 2-Watt Broadband Power and Energy Meter System (Melles Griot, Rochester, U.S.A.). And the light intensities could be calculated accordingly.

The optical density of the cell suspension was measured by a spectrophotometer (Thermospectronic UV1) against a blank solution of de-ionised water at a fixed wavelength of 660 nm, and the equivalent dry cell mass was correlated with the optical density (Pott *et al.* 2012).

Glycerol concentration was determined by the method modified from Bondioli and Della Bella (2005). The ethanol solution used in the original assay was replaced volumetrically by distilled water to avoid the distortion of the assay when aqueous solutions of glycerol rather than solutions of glycerol in biodiesel were used.

The gas composition was determined by a gas chromatograph (Agilent® 7890A) with a thermal conductivity detector employing Ar as the carrier gas and a HayeSep Q column. The components were analysed using the thermal conductivity detector and correlated to the percentage of different components in the gas sample using existing calibrations (Pott *et al.* 2012).

For details of analytical methods, please refer to Chapter 2.

5.2.5 H_2 production performance

As seen in Chapter 3, for non-growing H_2 production, most of the reductant, glycerol, was utilised as the electron donor for H_2 production exclusively. The H_2 yield for non-growing H_2 production was ~ 80 % of the theoretical maximum H_2 yield. Therefore, in this chapter, H_2 production performance from glycerol for non-growing H_2 at different light intensities focused on the other two criteria: H_2 production rate and energy conversion (Koku *et al.* 2002; Ibrahim *et al.* 2006; Uyar *et al.* 2007; Basak & Das 2007; Carvalho *et al.* 2011).

H_2 production rate is defined as the volume of H_2 generated per unit volume of cell suspension per unit time ($mL\ L^{-1}\ h^{-1}$) (Tian *et al.* 2010).

Energy conversion, in terms of light, is defined as the ratio of the combustion enthalpy of H_2 to the total energy input into cell cultivation (Uyar et al. 2007).

5.3 Results

To test whether or not the incandescent light bulb is appropriate for H_2 production by non-growing *R. palustris*, the emission spectrum of the incandescent light bulb was determined; the result is presented in Figure 5-2.

Non-growing *R. palustris* with an optical density of 0.8 at 660 nm was cultivated with 10 mM glycerol and argon to generate H_2 at varying light intensities. The results of H_2 production rates by non-growing *R. palustris* at different light intensities are shown in Figure 5-3, through which, the corresponding energy conversion was calculated, and the results were displayed in Figure 4-3. Each data point in Figure 5-3 and Figure 4-3 represents the average value of three repeated experiments, and the corresponding error bar denotes the standard derivation of these results.

5.3.1 Light source
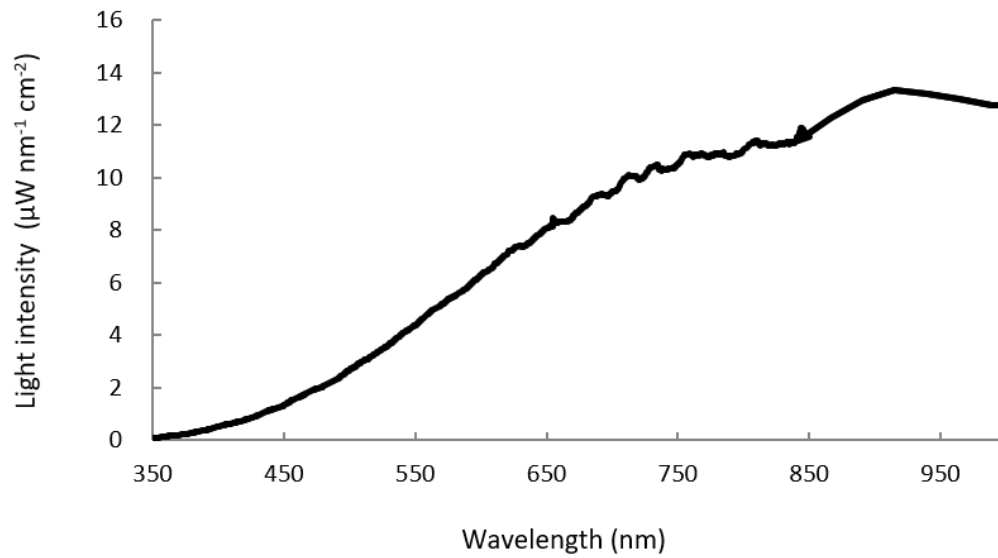
Figure 5-2: The emission spectrum of incandescent light bulb (BELL® R80 ES Reflector, London, U.K.). Incandescent light bulbs (BELL® R80 ES Reflector, London, U.K.) were used in this study. The emission spectrum of the incandescent light bulb was measured by an imaging spectrograph (Chromex 250is, High Peak, U.K.) as a function of wavelength.

5.3.2 Response of photosynthesis to different light intensities
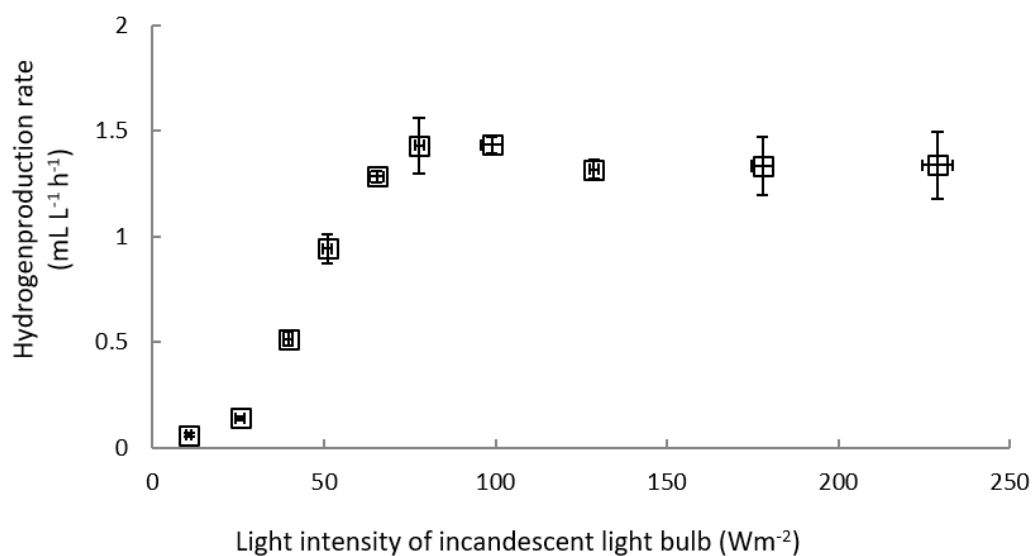
Figure 5-3: H_2 production rates by non-growing *R. palustris* with illumination provided by incandescent light bulb (BELL® R80 ES Reflector, London, U.K.) at different light intensities. *R. palustris* was cultivated with 10 mM glycerol and filtered sterile N_2 as headspace until its optical density reached to 0.8 at 660 nm, the headspace gas was replaced by argon to halt the growth and allow polyhydroxybutyrate (PHB) accumulation for about 200 hours. After PHB accumulation, non-growing cells were then cultivated with 10 mM glycerol and filtered sterile argon at different light intensities. Hydrogen was generated by the non-growing *R. palustris* at different light intensities. The results of the hydrogen production rate in terms of the volume of hydrogen gas per unit volume of culture per unit time ($mL\,L^{-1}\,h^{-1}$) as a function of light intensities were presented in this figure. Each data point in this figure represents the average value of three experimental repeats with corresponding error bars denoting the standard derivations.

5.3.3 Energy conversion at different light intensities
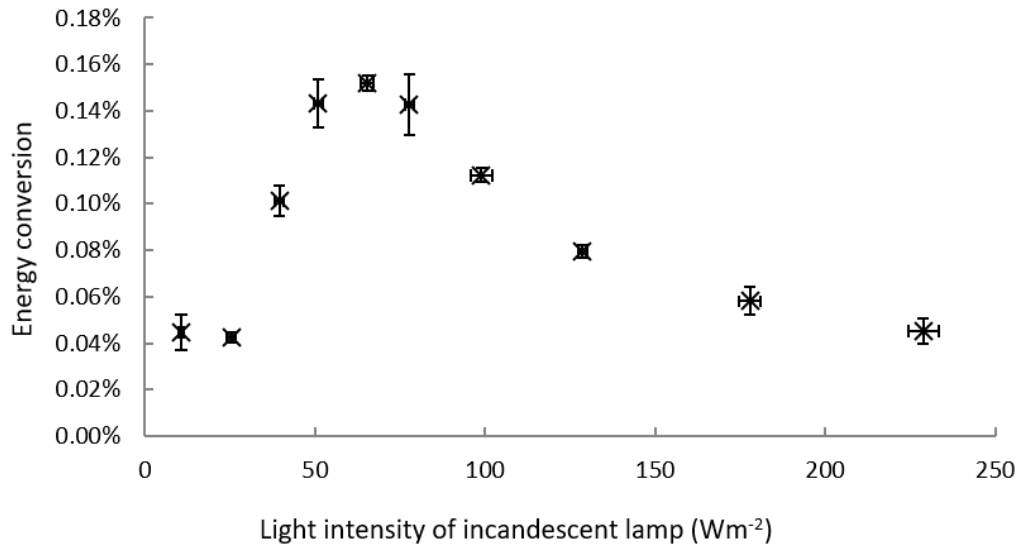
Figure 5-4: Energy conversion of H_2 production by non-growing *R. palustris* with illumination provided by incandescent light bulb (BELL® R80 ES Reflector, London, U.K.) at different light intensities. The results of hydrogen production rates (mL g^{-1} h^{-1}) *vs.* light intensities (W m^{-2}) were obtained from Figure 5-3. The energy conversion was calculated accordingly. The energy conversion, in terms of light, is defined as the ratio of the combustion enthalpy of H_2 to the total energy input into cell cultivation (Uyar *et al*. 2007). Each data point in this figure represents the average value of three experimental repeats with corresponding error bars denoting the standard derivations.

5.4 Discussion

5.4.1 Light source

Light plays a significant role in non-growing H_2 production by *R. palustris*, and the most cost-effective system would be directly using natural light (Hallenbeck 2012). The scattering of sunlight can be illustrated by using the two spectra of blue sky and red sunsets which are presented in Figure 5-5 (Rechtsteiner & Ganske 1998). When the sun is high, the scattering of sunlight would be similar to the spectrum of blue-sky with a high peak in the blue region (360 – 460 nm). When the sun is low, *i.e.* sunrise and sunset, the scattering of sunlight would be close to the spectrum of red sunset with the highest peak at the infrared region. Researchers have proved that the infrared light plays an essential role of photoproduction of H_2, and the H_2 production

rates are optimal during the sunset period (Sierra *et al.* 2008; Adessi *et al.* 2012; Carlozzi *et al.* 2006).
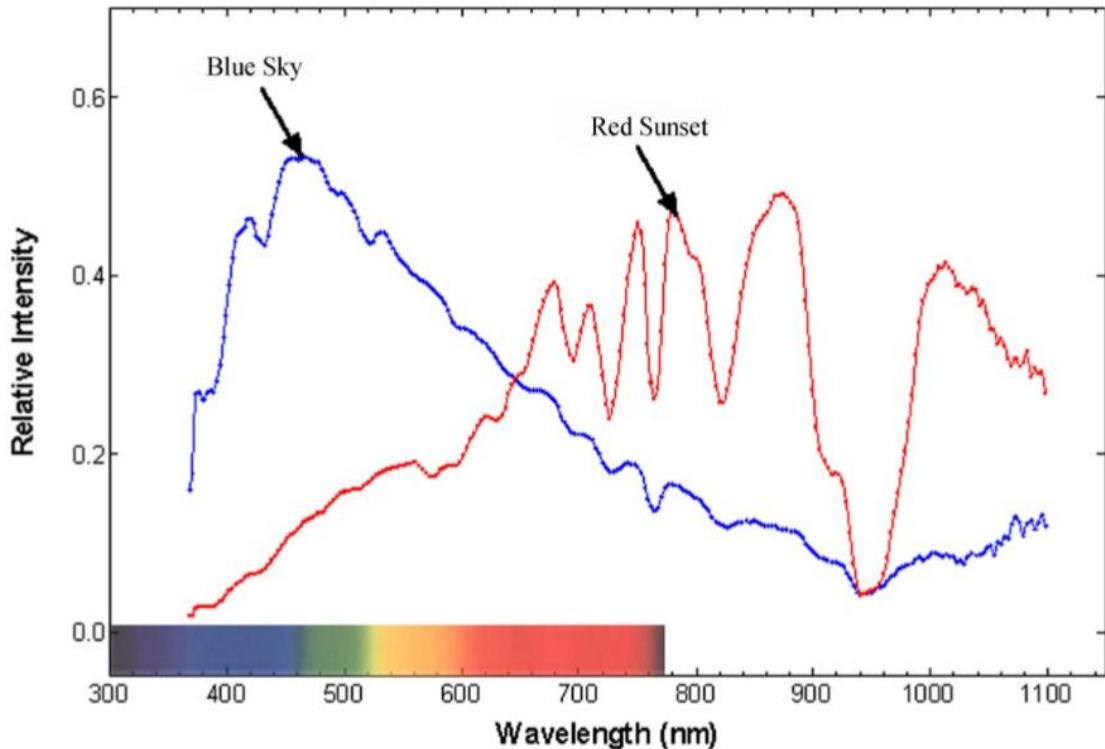
Figure 5-5: The emission spectrum of blue sky (day time) and red sunsets (sun rise and sun set) (Rechtsteiner & Ganske 1998). The emission spectra of the sun at various times of the day were measured outdoor using a Spectron Engineering, Inc. SE590 field-portable, data-logging spectro-radiometer in Malibu, U.S.A. on the November 21st 1996.

BELL® incandescent light bulbs (BELL® R80 ES Reflector, London, U.K.) were used in this chapter. Its emission spectrum was measured, and the result was displayed in Figure 5-2. Comparing the results of both Figure 5-2 and Figure 5-5, both emission spectra share a similar basic trend; the illumination intensity increases as the wavelength increases. The emission spectrum of red sunset has its highest peak at wavelength around 900 nm. Above 700 nm, the intensity of wavelengths fluctuates in natural sunset. Similar to that of the red sunset, the emission spectrum of incandescent light bulb has its highest peak around 900 nm, it also started to fluctuate at wavelengths above 700 nm but at a smaller frequency. Therefore, this

incandescent light bulb with emission spectrum like that of a red sunset could be used to mimic the real scattering of sunlight during the sunset period.

In most Europe (40° -50° N), the light intensity of solar irradiation is up to 850 – 950 Wm^{-2} in a sunny summer day (Uyar et al. 2007). The highest commercially available wattage of BELL® incandescent light bulb is 100W. As the incandescent light bulb is an energy-expensive light source, it might generate too much heat and potentially be harmful to bacterial culture. Using Beer-Lambert's law, where light intensity decreases logarithmically with the distance from light source and the incident surface. A balance of temperature and light intensity requirements could be determined. The incandescent light bulb was placed at 44 cm from the surface of the culture bottle to aid in temperature maintained at 30 ± 2 °C, and allowing for highest light intensity at 228.9 ± 4.5 Wm^{-2}. The light intensity could be further adjusted and controlled by varying the voltage supplied to the light bulbs using a Regavolt® variable transformer (Waltham Cross, U.K.), ranging from 10.6 ± 0.7 to 228.9 ± 4.5 Wm^{-2}.
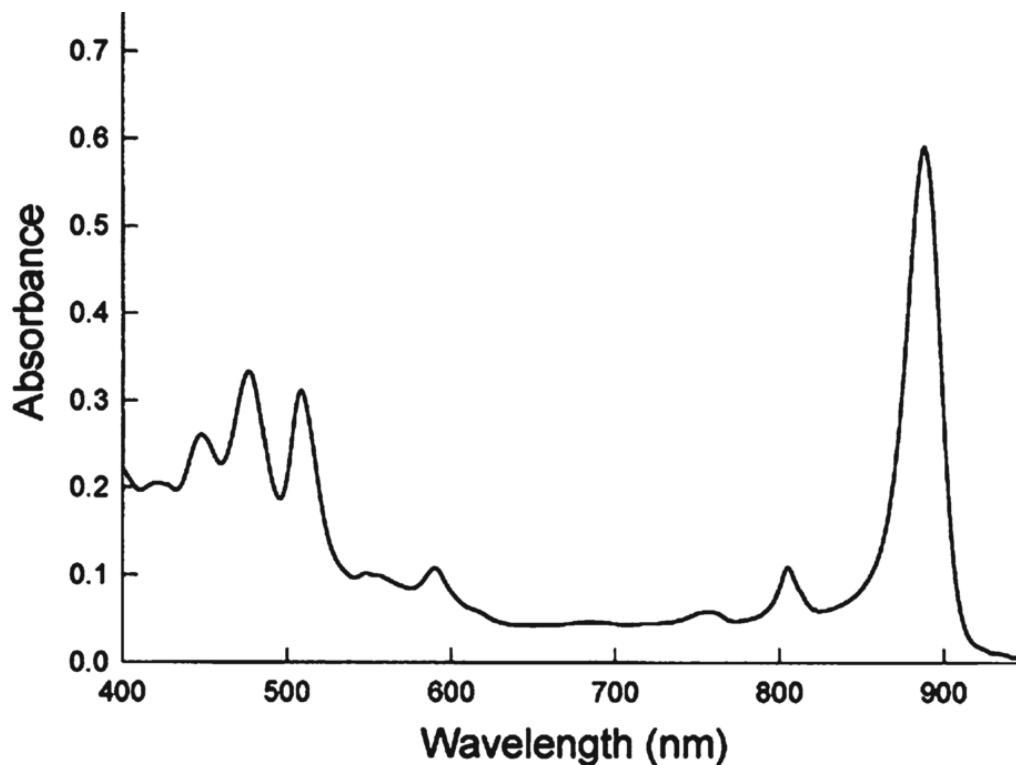
Figure 5-6: Adsorption spectrum of a typical PNSB with maxima at 805 nm and 875 nm due to bacteriochlorophyll *a* (Hallenbeck 2012)

In this chapter, H_2 was generated from glycerol by non-growing *R. palustris* with an optical density of 0.8 at 660 nm. The adsorption spectrum of a typical PNS bacteria was obtained from (Hallenbeck 2012) and shown in Figure 5-6. From the figure, it indicated that the light was absorbed by carotenoids with peaks in the regions of 450 - 550 nm and bacteriochlorophyll a with peaks in at 805 nm and 870 nm).

Compared the results in both Figure 5-2 and Figure 5-6, the emission spectrum of this incandescent light bulb had covered the absorbance spectrum of PNS bacteria including *R. palustris*, and it had high light intensity in the infrared region. Therefore, the incandescent light bulb was suitable for H_2 production by non-growing *R. palustris*.

5.4.2 Dependence of light on non-growing H_2 production

Before scaling up, it is important to understand the dependence of light on non-growing H_2 production, such as the H_2 production at night. Therefore, an experiment was carried out to monitor the H_2 production rate when the light was cycled.

Non-growing *R. palustris* was prepared after poly-hydroxy-butyrate (PHB) accumulation and cultivated with 10 mM glycerol and filtered sterile argon at 228.9 ± 4.5 Wm^{-2} for a week. After a steady H_2 production rate of 2.30 ± 0.23 $mg\,L^{-1}\,h^{-1}$ was reached, the light was switched off for ten minutes and then switched on again for another ten minutes. The cumulative H_2 volume was measured every two minutes, and the H_2 production rate was calculated accordingly as the volume of hydrogen gas per unit mass of the dry cells per unit time ($mL\,g^{-1}\,h^{-1}$). The results of H_2 production rate as a function of time was plotted in Figure 5-7.
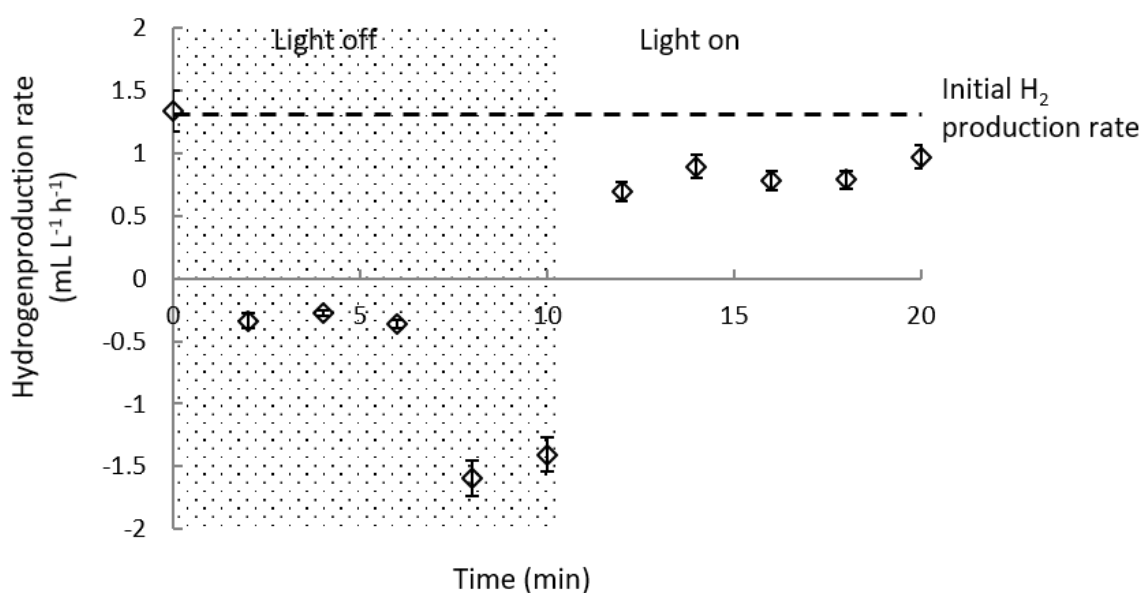
Figure 5-7: H_2 production rate by non-growing *R. palustris* with an optical density of 0.8 at 660 nm at 228.9 ± 4.5 Wm^{-2} *vs.* time, noted the light was turned off at time = 0 min, and was turned on again at time =10 minutes. In this experiment, the gas volume was measured by a fine calibrated capillary tube with a drop of coloured water trapped inside. The gas port tubing of the culture bottle was attached directly to one end of the calibrated capillary tube, and the other end of the capillary tube was exposed to the atmospheric pressure. When H_2 was generated or consumed, the coloured water trapped in the capillary tube would move around. Therefore, H_2 production or consumption could be visualised directly through the movement of trapped water inside the capillary tube.

When the light was switched off, H_2 production stopped immediately as detected by observation of capillary tube. From Figure 5-7, the H_2 production rate was kept around -0.33 ± 0.05 mL $L^{-1} h^{-1}$ for the first six minutes. The reason for the slightly negative value of H_2 production rate could be explained by the connection leakage and hydrogen permeation through the capillary tube. During this period, cells were stressed and trying to stabilise. During the following four minutes, the H_2 production rate dropped to further around -1.50 ± 0.16 mL $L^{-1} h^{-1}$. This is possibly because an alternative metabolic pathway is chosen, and H_2 might be consumed to release energy for cell metabolic maintenance.

When the light was switched on again, H_2 was generated immediately. This was confirmed by observation of the capillary tube. The H_2 production rate recovered around 50% in the first two minutes. Around 70% of the original H_2 production rate

93

was restored when the light was switched on for ten minutes. In that time frame, H_2 production rate was not restored to 100 % of the original production rate. This could potentially be explained by connection leaks and some hydrogen losses by permeation through the capillary tube.

5.4.3   Response of photosynthesis to different light intensities

Light is vital for photosynthesis in *R. palustris*, excessive or insufficient light intensity may constrain the photosynthetic performance – in terms of biomass or metabolite yields (Carvalho *et al*. 2011). For non-growing H_2 production, the major photosynthetic product of *R. palustris* is H_2. Cells acclimated to relatively low light (*i.e.*, shade-adapted) prior to exposure to high light intensity will become photo-damaged at a lower intensity dose than cells which have been high light-acclimated. For bath culture, it is advisable to previously acclimate the cells to high light intensity values (Carvalho *et al.* 2011).

Once again, non-growing *R. palustris* was prepared after poly-hydroxy-butyrate (PHB) accumulation at the highest available light intensity of 228.9 ± 4.5 Wm^{-2}, and then cultivated with 10 mM glycerol and filtered sterile argon at a range of light intensities from 10.6 ± 0.7 to 228.9 ± 4.5 Wm^{-2}. The light intensity was adjusted and controlled by altering the voltage supplied to the light bulbs (Regavolt® variable transformer, Waltham Cross, U.K.). To understand the response of photosynthesis to different light intensities, the H_2 production rates by non-growing *R. palustris* were measured at these different light intensities, and the results were presented in Figure 5-3.

As seen in Figure 5-3, the H_2 production rate at different light intensities could be characterised into two regions. The first region would be light-limiting region with light intensity ranging from 10.6 ± 0.7 to 65.4 ± 1.9 Wm^{-2}, in which the photonic input was fully utilised by photosynthesis to generate H_2. Therefore, as the light intensity increased, the production rate of the photosynthetic product, H_2, also increased. Since the light intensity increased from 10.6 ± 0.7 to 65.4 ± 1.9 Wm^{-2}, H_2 production rate increased from 0.06 ± 0.01 to 1.28 ± 0.03 mL L^{-1} h^{-1}. The second region would be photo-saturation region with light intensity ranging from 65.4 ± 1.9 Wm^{-2} to 228.9 ± 4.5 Wm^{-2}, in which the photosynthetic processing capacity of the culture attained its

maximum values, and the excessive photonic flux provided to the culture was dissipated as heat or fluorescence. When the light intensity went above 65.4 ± 1.9 Wm^{-2}, there was a small fluctuation in the H$_2$ production rate, and the average H$_2$ production rate was maintained at 1.36 ± 0.06 mL L^{-1} h^{-1}. The maximum H$_2$ production rate was 1.43 ± 0.09 mL L^{-1} h^{-1} at 98.9 ± 3.2 Wm^{-2}.

For a batch reactor without agitation, a very high light intensity might eventually be harmful for bacterial photosynthesis by showing a decrease in product rate or growth rate, then it enters to another region: the photo-inhibition region, in which bacteriochlorophylls can be damaged when the enhanced activity of electrons is beyond its capability to process (Glim 1992). For a stirred batch reactor, the photosynthetic performance of microorganism normally switches among light-limiting, photo-saturation and photo-inhibition regions, but it mainly shifts between light-limiting and photo-saturation regions (Carvalho et al. 2011) like the results presented in Figure 5-3.

5.4.4 Energy conversion at different light intensities

The energy conversion based on light was calculated as the ratio of the combustion enthalpy of H$_2$ to the total energy input into cell cultivation (Uyar et al. 2007). The results of energy conversion as a function of different intensities were presented in Figure 4-3.

As the light intensity increased, the energy conversion increased accordingly until a maximum of 0.152 ± 0.003 % at 65.4 ± 1.9 Wm^{-2}. At this stage, the photosynthetic performance was in the light-limiting region. The production rate, *i.e.* H$_2$ production rate, was limited by the photonic flux supplied. As energy conversion was proportional to H$_2$ production rate, in this chapter, the energy conversion was constrained by the light intensity. When the light intensity was increased above 65.4 ± 1.9 Wm^{-2}, the energy conversion started to drop gradually as the light intensity supplied was increased. This could be explained by photo-saturation, in which the photosynthetic capability, *i.e.* H$_2$ production rate in this chapter, maintained its highest value while the excessive photons were released as heat or fluorescence.

Beyond the light limiting region, as the light intensity increased, the energy input increased while the energy output remained constant. Hence the value of energy conversion declined as the light intensity increased in this stage.

5.4.5 Optimisation of energy conversion

In this chapter, the highest energy conversion of 0.152 ± 0.003 % was achieved when the light intensity was 65.4 ± 1.9 Wm^{-2}. Such low energy conversion could be boosted in the following two directions: action on the receptor and action on the source.

5.4.5.1 Improving uptake of light

In this chapter, the photo-saturation occurred at a relatively low light intensity, 65.4 ± 1.9 Wm^{-2}. The highest solar irradiation could reach around 1,000 Wm^{-2} (Uyar et al. 2007; Hallenbeck 2012), far beyond that requirement.

In the photo-saturation region, the photon absorption by the light harvesting antenna was significantly lower than the rate of photosynthetic systems to consume the energy. The energy conversion is defined as the ratio of the combustion enthalpy of H_2 to the total light input into cell cultivation (Uyar et al. 2007). Energy conversion could be improved by making more cells available for H_2 production, *i.e.* more photosynthetic membrane apparatus to absorb and consume photon for electrons transfer and more nitrogenase to consume energy for H_2 production, hence improving the H_2 production rate.

As mentioned in Chapter 4, it was found out that the H_2 production rate was proportional to the cell inoculum size. There was a strong positive linear relationship between the H_2 production rate ($mL\,L^{-1}\,h^{-1}$) and dry cell mass ($g\,L^{-1}$), which fitted the Leudeking–Piret model $\frac{dP}{dt} = 2.52X$ where P is the cumulative H_2 volume, t is time, and X is the dry cell mass. Therefore, energy conversion of non-growing H_2 production could be boosted by increasing the inoculum sizes.

In addition, researcher shows that mutual shading of cells causes steep gradients of light intensity within the culture, *i.e.* cells away from the culture surface would have rather low light intensities available (Uyar et al. 2007). Increasing the illuminated surface-to-volume ratio to the bioreactor could increase the number of cells exposed to light for H_2 production on the light incident surface, *i.e.* enhance the energy conversion (Hallenbeck 2012; Tsygankov et al. 1994; Adessi et al. 2012; Eroglu et al. 2008; Carvalho et al. 2006; Fibler & Kohring 1995; McKinlay & Harwood 2010b; Ratchford & Fallowfield 1992; Akkerman et al. 2002)

5.4.5.2 Focus on the source

The low energy conversion in this chapter suggests that most of the light emitted from the incandescent light bulb was not consumed by *R. palustris* during cultivation. Incandescent light bulbs are energy expensive light source. From Figure 5-2, the incandescent light bulb used in this chapter has a very wide emission spectrum from 350 nm to 1000 nm, with the most intensity distrusted in the infrared and far infrared regions. From Figure 5-6, the wavelength of light is absorbed mostly by carotenoids (peaks in the regions of 450 - 550 nm) and bacteriochlorophylls (peaks in at 805 nm and 870 nm) in *R. palustris*. Comparing the results in both Figure 5-2 and Figure 5-6, while the emission spectrum of incandescent light bulb overlapped the absorption spectrum of *R. palustris*, the rest energy generated by incandescent light bulb was not directed to H_2 production.

While the incandescent light bulb and the solar scattering of sunset have a similar emission spectra, it is also predicted that most solar irradiance would be wasted for photosynthetic H_2 production. To fully utilize the solar irradiance, photosynthetic microorganisms with different absorptions bands could be co-cultured with *R. palustris* to achieve higher overall H_2 production rate, hence higher energy conversion (Melis & Melnicki 2006; Brentner et al. 2010; Rupprecht et al. 2006; McKinlay & Harwood 2010b).

In addition, as mentioned before, H_2 production from glycerol by non-growing *R. palustris* had strong dependence on the availability of light, and H_2 production pauses immediately in the absence of light (Figure 5-7). In fact, cells consume H_2 to release

energy for metabolic maintenance when the light is diminished for any length of time beyond a few minutes. On the other hand, H_2 production is restored quickly upon the return of light. To maintain high H_2 production rate, *i.e.* high energy conversion, throughout day and night, it is advisable to use an appropriate artificial light source for illumination at night (Hallenbeck 2012; Uyar et al. 2007; Koku et al. 2002; Carvalho et al. 2011).

To achieve these objectives, further investigation of the impact of wavelength of light on H_2 production by non-growing *R. palustris* needs to be understood and is carried out in Chapter 6.

5.5 Conclusions

Non-growing *R. palustris* was prepared after poly-hydroxy-butyrate (PHB) accumulation, and then cultivated to generate H_2 at different light intensities. As the light intensity increased, the photosynthetic performance of *R. palustris*, *i.e.* H_2 production rate also increased to a point before stabling. In the initial light-limiting region, the photonic input was fully utilised by photosynthesis to generate H_2, and the H_2 production rate increased from 0.06 ± 0.01 to $1.28 \pm 0.03 \, mL \, L^{-1} \, h^{-1}$ as the light intensity increased between 10.6 ± 0.7 to $65.4 \pm 1.9 \, Wm^{-2}$. When the light intensity reached above $65.4 \pm 1.9 \, Wm^{-2}$, the cells reached the photo-saturation and maintained an average H_2 production rate of $1.36 \pm 0.06 \, mL \, L^{-1} \, h^{-1}$.

As the light intensity increased, the energy conversion increased until it reached to its maximum of 0.152 ± 0.003 % at $65.4 \pm 1.9 \, Wm^{-2}$. Energy conversion started to drop with increasing light intensity due to photo-saturation. In addition, non-growing H_2 production had strong dependence on the availability of light with fast response. Energy conversion of H_2 production by non-growing *R. palustris* could be improved through increasing the inoculum size and increasing the illumination surface-to-volume ration of the bioreactor. To further optimise the energy conversion, investigation of the impact of wavelength on H_2 production by non-growing *R. palustris* is carried out in the following chapter.

6 The impact of light wavelength on hydrogen production by non-growing *Rhodopseudomonas palustris*

6.1 Introduction

As seen in Chapter 5, it is known that *R. palustris*, a kind of PNS bacteria, could generate a good yield of H_2 through anoxygenic photosynthesis, and its photosynthetic system is one of the most studied and best characterised in the past 50 years (Hu et al. 2002).

The photosynthetic membrane apparatus of *R. palustris* is one of the simplest kinds, through which the photons from sunlight stimulate the electron excitation and releases proton and electron for ATP synthesis (Hu et al. 2002).

Based on quantum physics, the energy carried by a photon (E) is proportional to its frequency (v), by a factor of h (Planck's constant, 6.626×10^{34} J s). And the frequency is proportional to the speed of light in vacuum (c, 3×10^8 m s^{-1}) and inversely proportional to its wavelength (λ). $E = hv = h\frac{c}{\lambda}$ (Carvalho *et al.* 2011). Therefore, only photons with the appropriate wavelength can trigger the excitation of cytochrome bacteriochlorophyll complexes II and releases proton and electron (Carvalho et al. 2011; Hu et al. 2002; Hall & Rao 1999; Scheuring et al. 2006; Uyar et al. 2007).

There is a pronounced energetic hierarchy in the light-harvesting system of PNS bacteria (Hu et al. 2002). Unlike green plants and algae, PNS bacteria absorb light mainly at wavelengths of approximately 500 nm through the carotenoids and above 800 nm through the bacteriochlorophylls (Hall & Rao 1999). The energy levels for the key electron excitations in the photosynthetic unit (PSU) in PNS bacteria are shown in the Figure 6-1.
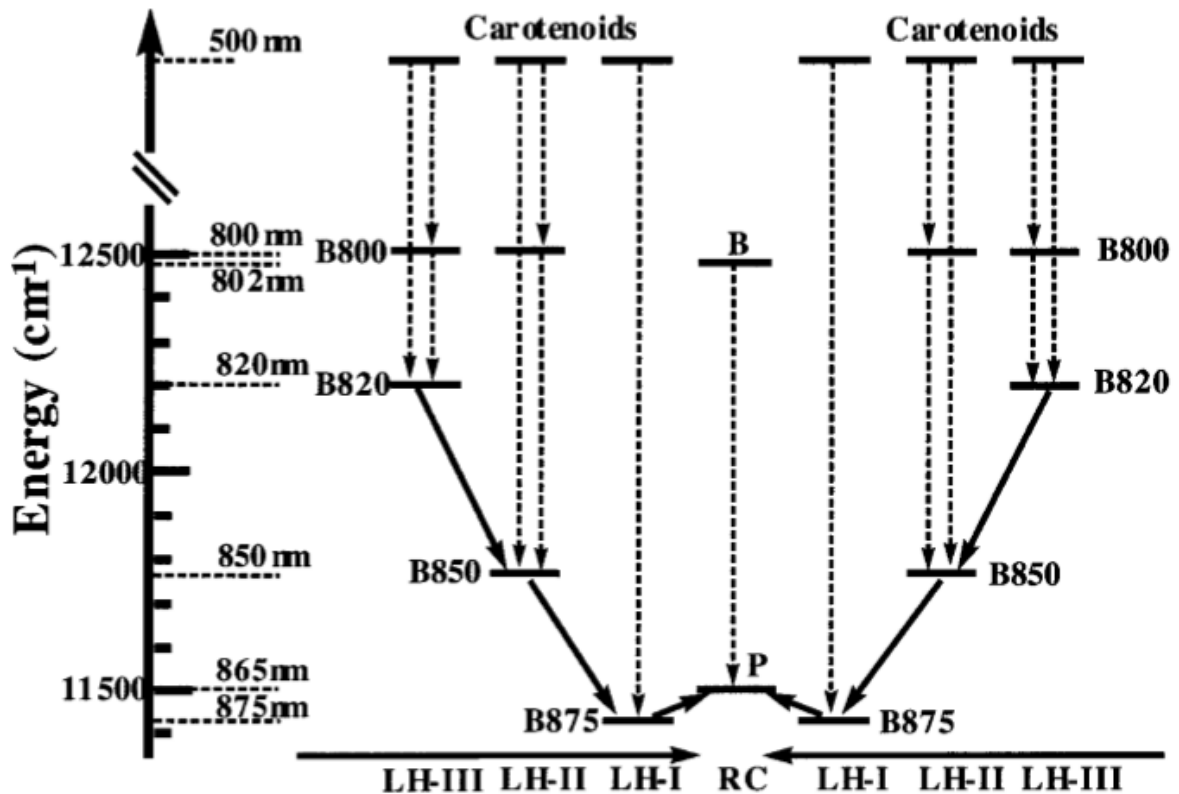
Figure 6-1: Energy levels of electron excitations in the photosynthetic unit of bacteriochlorophylls in purple non-sulphur bacteria (Hu et al. 2002). The diagram demonstrates a series of excitation energy towards the photosynthetic reaction centre. The vertical dashed lines indicate intra-complex excitation transfer; the diagonal solid lines inter-complex excitation transfer. Abbreviations: LH-III = light harvesting complex III; LH-II = light harvesting complex II, LH-I = light harvesting complex I; RC = reaction centre.

From Figure 6-1, pigments of the outer light harvesting complex absorb a higher energy that that of the inner ones. For *R. palustris*, the reaction centre absorbing maximally at 865 nm is surrounded by the light-harvesting complex I (LH-I), mainly absorbing maximally at 875 nm, then the LH-I is surrounded by multiple light-harvesting complexes (LH-II) absorbing higher energy (800 and 850 nm). LH-I exists in all purple bacteria; LH-II exists in most species; light harvesting complex III (LH-III) arises in certain species only and it is usually regulated by ambience light. *R. palustris* only contains LH-I and LH-II, and both LH-I and LH-II are mainly made by bacteriochlorophyll *a*.

Researchers have proved that the bacteriochlorophyll *a*, which absorbs infrared wavelengths (750 ~ 950 nm), is more important for H_2 production by PNS bacteria than the carotenoids which absorb light from blue region (Hallenbeck 2012; Uyar *et al*. 2007). In this chapter, commonly available LEDs generating both wavelength ranges were tested, and the photosynthesis response of *R. palustris* was analysed from these different light sources at different light intensities. The results were compared to that of the incandescent light bulbs in Chapter 5. From this, it is aimed understand the impact of light wavelength for non-growing H_2 production by *R. palustris*.

6.2   Materials and methods

6.2.1   Strain and medium

R. palustris with strain designations ATH 2.1.37 (NCIB 11774) was obtained from ATCC® as a freeze-dried sample. A defined medium was used in this chapter as described by Gosse *et al.* (Gosse et al. 2007), for details please refer to Chapter 2.1.3.

6.2.2   Preparation of non-growing cells

Freeze-dried *R. palustris* was rehydrated, and the pre-culture was prepared and cultivated in a 15mL sterile centrifuge tube with 100 µL of 2 M filtered sodium glutamate, 100 µL of autoclaved glycerol, and defined medium (Gosse *et al.* 2007) for another week. The temperature was maintained at 30 ± 2 °C, the illumination was provided by incandescent light bulbs (BELL® R80 ES Reflector, London, U.K.) with a light intensity of 228.9 ± 4.5 Wm^{-2}. For details about culture revival and pre-culture preparation, please refer to Chapter 2.1.

The pre-culture was then centrifuged at 5000 g at room temperature for ten minutes in an Eppendorf® 5800 centrifuge (Model 5810R) (Gosse *et al.* 2007), re-suspended in 1 L fresh medium, and cultivated in a 1 L bottle with 10 mM glycerol and filtered sterile N_2 as headspace. Liquid sample was extracted from the bottle at a regular interval to monitor cell growth. Once the optical density of the cell suspension

reached to 0.8 at 660 nm, the headspace gas was replaced by Ar to halt the growth and allow PHB accumulation for 200 hours. When *R. palustris* is under nutrient deficient conditions, it can generate different storage products such as glycogen, trehalose, and PHB (Larimer *et al.* 2004).

6.2.3 Non-growing H_2 production with different light sources at same light intensity

After PHB accumulation, non-growing cells were harvested, centrifuged at 4424 g at room temperature for ten minutes in a Beckman® JA-10 rotor (Gosse *et al.* 2007). The pellet was washed and re-suspended in fresh medium to the optical density of 0.80 at 660 nm. 200 mL non-growing cell suspension was then cultivated in a 250 mL bottle with 10 mM glycerol and filtered sterile Ar as headspace for a week.

The temperature was maintained at $30 \pm 2\,°C$. The illumination was provided by different light sources including incandescent light bulbs (BELL® R80 ES Reflector, London, U.K.), white LEDs, and infrared LEDs. The light intensity on the surface of the bottles was adjusted and controlled at $10.5 \pm 0.5\ Wm^{-2}$.

6.2.4 Non-growing H_2 production with different light sources at different light intensities

Similar to chapter 6.2.3., 200 mL non-growing cell suspension was prepared after PHB accumulation, then cultivated in a 250 mL bottle with 10 mM glycerol and filtered sterile Ar as headspace for a week.

The temperature was maintained at $30 \pm 2\,°C$. The illumination was provided by different light sources. The light intensity on the surface of the bottles could be adjusted and controlled by altering the voltage supplied to the light sources. Therefore, instead of one light intensity, non-growing cells were cultivated with illumination provided by different light sources at different light intensities.

6.2.5 Other cultivation conditions for non-growing H$_2$ production

At regular intervals, the gases generated were released to the graduate burette, the volume was measured by water displacement in the burette and recorded, and a gas sample was extracted for gas composition determination by a gas chromatography. As the H$_2$ solubility in water is extremely low, it is assumed that H$_2$ is insoluble in water. The total H$_2$ volume was equal to the H$_2$ volume in gases released in the burette and gases in headspace of the culture bottle. Equally liquid sample was extracted from the bottle at the same time to monitor cell growth and glycerol consumption. For details in experimental setup, please refer to Chapter 2.2.

6.2.6 Analytical methods

The non-growing cells with optical density of 0.8 at 660 nm were prepared. The absorbance spectrum of *R. palustris* was measured by an ultra-violet spectrophotometer, ThermoSpectronic UV1 (Thermo Electron Corporation, Rugby, U.K.), as a function of wavelength ranging from 300 nm to 1000 nm.

The emission spectra of different light sources were measured by an imaging spectrograph (Chromex 250is, High Peak, U.K.) as a function of wavelength ranging from 300 nm to 1000 nm. The signal was received and transferred by a 200 nm fibre optic to the imaging spectrograph.

The power received on the surface of the culture bottles was measured by a power meter, Integrated 2-Watt Broadband Power and Energy Meter System (Melles Griot, Rochester, U.S.A.). And the light intensities could be calculated according to $I = \frac{P}{A}$ where I is the light intensity (W m^{-2}), P is the power incident on the surface, and A is the area of the incident surface

The optical density of the cell suspension was measured by a spectrophotometer (Thermospectronic UV1) against a blank solution of de-ionised water at a fixed wavelength of 660 nm, and the equivalent dry cell mass was correlated with the optical density (Pott *et al.* 2012).

Glycerol concentration was determined by the method modified by Bondioli and Della Bella (2005). The ethanol solution used in the original assay was replaced volumetrically by distilled water to avoid the distortion of the assay when aqueous solutions of glycerol rather than solutions of glycerol in biodiesel were used.

The gas composition was determined by a gas chromatograph (Agilent$^{®}$ 7890A) with a thermal conductivity detector employing Ar as the carrier gas and a HayeSep Q column. The components were analysed using the thermal conductivity detector and correlated to the percentage of different components in the gas sample using existing calibrations (Pott *et al.* 2012).

For details of analytical methods, please refer to Chapter 2.3.

6.2.7 H_2 production performance

As seen in Chapter 3, for non-growing H_2 production, most of the reductant, glycerol, was utilised as the electron donor for H_2 production exclusively. The H_2 yield for non-growing H_2 production was about 80 % of the theoretical maximum H_2 yield. Therefore, in this chapter, H_2 production performance from glycerol for non-growing H_2 with illumination provided by different light sources at different light intensities was mainly focused on the other two criteria: average H_2 production rate and energy conversion (Koku *et al.* 2002; Ibrahim *et al.* 2006; Uyar *et al.* 2007; Basak & Das 2007; Carvalho *et al.* 2011). The average H_2 production rate is defined as the volume of H_2 generated per unit volume of cell suspension per unit time (mL L^{-1} h^{-1}) (Tian *et al.* 2010). The energy conversion, in terms of light, is defined as the ratio of the combustion enthalpy of H_2 to the total energy input into cell cultivation (Uyar *et al.* 2007).

6.3 Results

In order to understand energy levels of electron excitations in *R. palustris*, its absorbance spectrum was measured, and results were presented in and Figure 6-2.

Three different artificial light sources were tested in this chapter, including incandescent light bulb (BELL® R80 ES Reflector, London, U.K.), white LED panel built by high power 12 V white LEDs, and infrared LED panel built by high power 12 V 850 nm infrared LEDs. The emission spectra of those three light sources were measured by an imaging spectrograph (Chromex 250is, High Peak, U.K.) as functions of wavelength, and the results were shown in Figure 6-3.

Non-growing *R. palustris* with an optical density of 0.8 at 660 nm was cultivated to generate H_2 with illumination provided by different artificial light sources at 10.5 ± 0.5 Wm^{-2}. The results of H_2 production rate by non-growing *R. palustris* by different light sources are shown in Figure 6-4. Through which, the corresponding energy conversion is calculated, and the results are displayed in Figure 6-5.

Instead of a single light intensity, results of H_2 production rate and energy conversion by non-growing *R. palustris* with illumination provided by different light sources at a range of light intensities are shown in Table 6-1. Each data point in this chapter represents the average value of three repeated experiments, and the corresponding error bar denotes the standard derivation of these results. The absorbance and emission spectra are obtained from the spectrophotometer and the imaging spectrograph directly, and thus are the average by the built-in software.

6.3.1 Absorbance spectrum of *R. palustris*
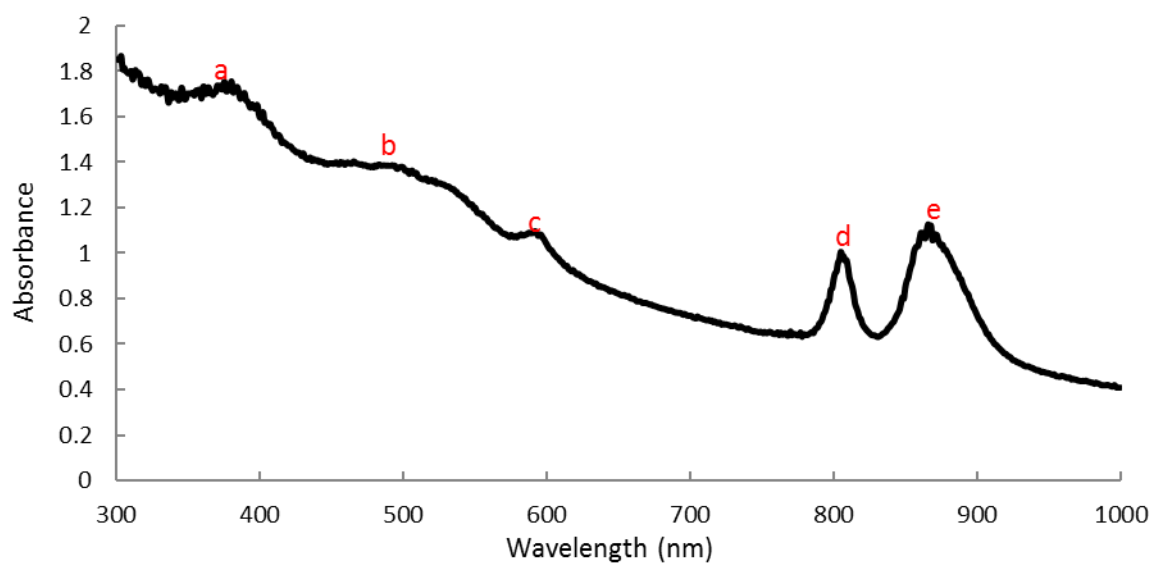
Figure 6-2: The absorbance spectrum of *R.* at stationary phase*. R. palustris* was cultivated with 10 mM glycerol and filtered sterile N_2 until its optical density reached 0.8 at 660 nm, the headspace gas was replaced by Ar to halt the growth and allow poly-hydroxy-butyrate (PHB) accumulation for about 200 hours. After the PHB accumulation, the non-growing cells were harvested and tested. The emission spectrum of the non-growing cell culture was then measured by an ultra-violet spectrometer (Thermo Electron Corporation, Rugby, U.K.) as a function of wavelength. It has peaks at a) 379 nm, b) 491 nm, c) 590 nm, d) 807 nm, and e) 865 nm.

6.3.2 Artificial light source
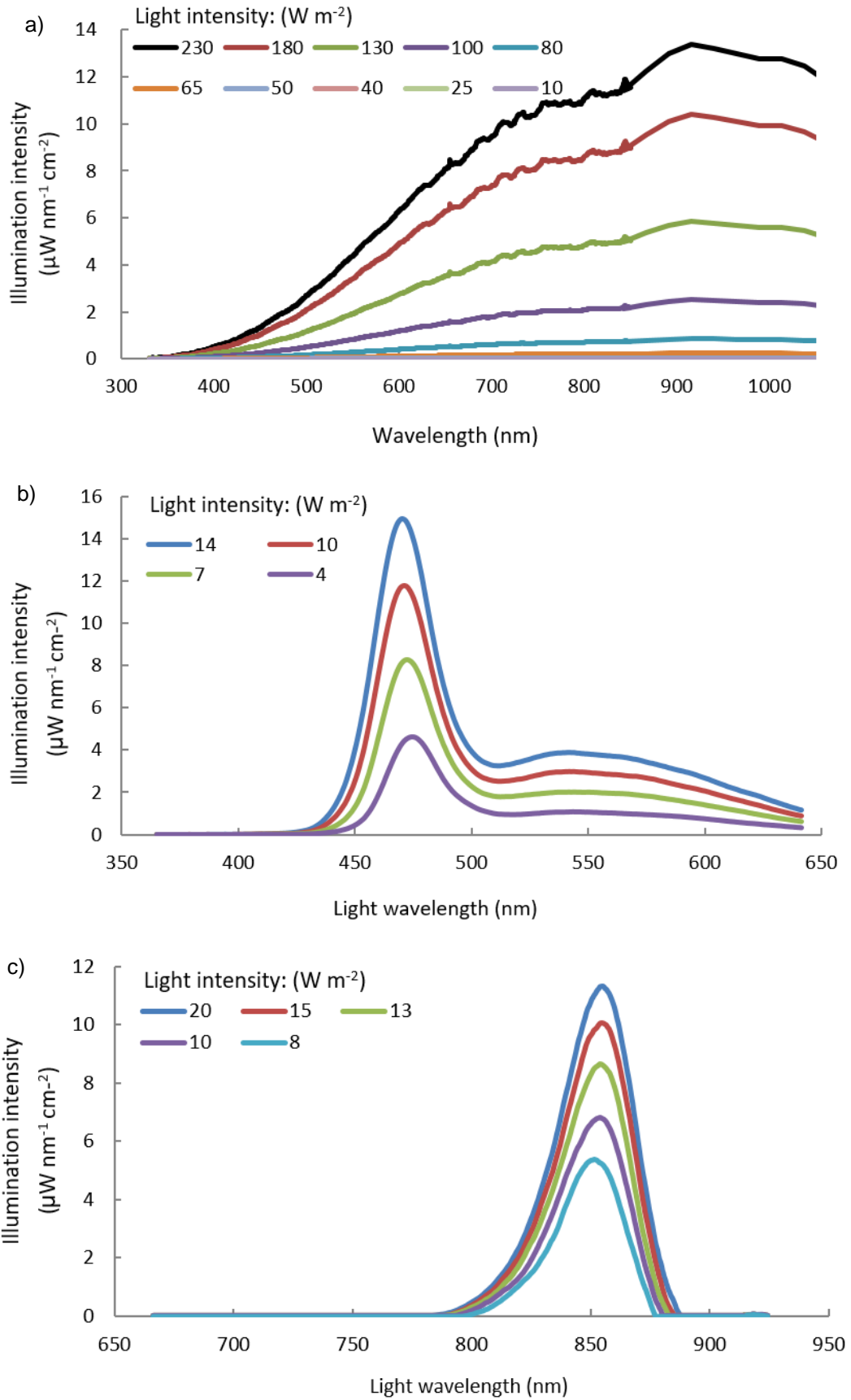
Figure 6-3: The emission spectra of incandescent light bulb (BELL® R80 ES Reflector, London, U.K.) in figure a), white LEDs in figure b), and infrared LEDs in figure c). Incandescent light bulbs (BELL® R80 ES Reflector, London, U.K.) were used. An LED panel was built with high power 12 V white LEDs and high power 12 V 850 nm infrared LEDs. The emission spectra was measured at different light intensities by an imaging spectrograph (Chromex 250is, High Peak, U.K.) as a function of wavelength.

6.3.3   Non-growing H_2 production with different light sources at same light intensity
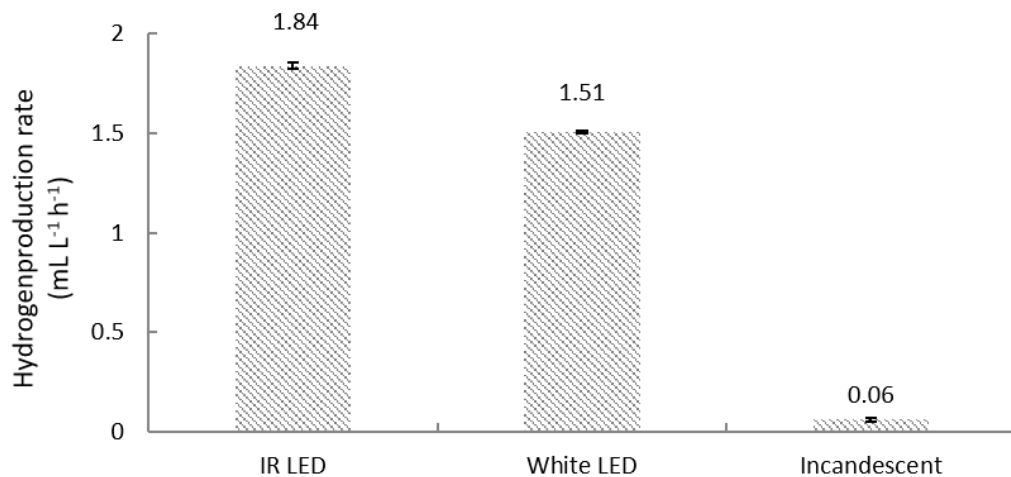
Figure 6-4: H2 production rate generated by non-growing *R. palustris* with illumination provided by different light sources at 10 Wm^{-2}. *R. palustris* was cultivated with 10 mM glycerol and filtered sterile N2 as headspace until its optical density reached to 0.8 at 660 nm, the headspace gas was replaced by argon to halt the growth and allow polyhydroxybutyrate accumulation for about 200 hours. The illumination was provided by incandescent light bulb at its highest light intensity of 228.9 ± 4.5 Wm^{-2}. After PHB accumulation, non-growing cells were then cultivated with 10 mM glycerol and filtered sterile argon. The illumination was then provided by three different light sources including incandescent light bulb, white LEDs, and infrared (IR) LEDs at a common light intensity of 10.5 ± 0.5 Wm^{-2}. Hydrogen was generated by the non-growing *R. palustris* with those three light sources. The results of the average hydrogen production rate in terms of the volume of hydrogen gas per unit volume of culture per unit time (mL L^{-1} h^{-1}) for each light source were presented in this figure. Each data point in this figure represents the average value of three experimental repeats with corresponding error bars denoting the standard derivations.
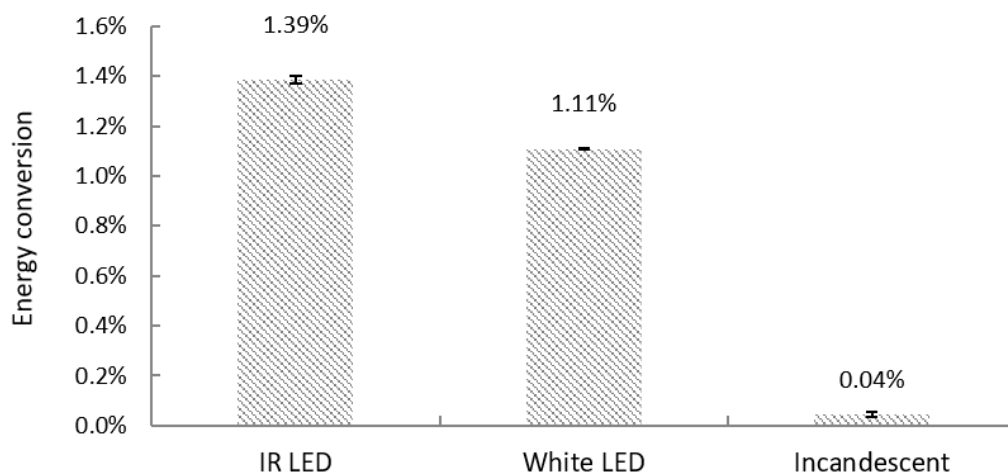
Figure 6-5: Energy conversion from H_2 production by non-growing *R. palustris* with illumination provided by different light sources at 10 Wm^{-2}. The results of hydrogen production rates (mL $L^{-1}h^{-1}$) for each light source were obtained from Figure 6-5. The energy conversion was calculated accordingly. The energy conversion, in terms of light, is defined as the ratio of the combustion enthalpy of H_2 to the total energy input into cell cultivation (Uyar *et al.* 2007). Each data point in this figure represents the average value of three experimental repeats with corresponding error bars denoting the standard derivations.

6.3.4 Non-growing H$_2$ production with different light sources at different light intensities

Table 6-1: H2 production performance by non-growing *R. palustris* with illumination provided by different light sources at different light intensities[a].

Light source	Light intensity	Maximum average H$_2$ production rate	Maximum energy conversion
	(Wm^{-2})	(mLL^{-1}h^{-1})	(%)
Incandescent light bulb[b]	65.4 ± 1.9	1.36 ± 0.06	0.152 ± 0.003
White LEDs[c]	10.5 ± 0.6	1.75 ± 0.07	1.109 ± 0.004
Infrared LEDs[d]	8.3 ± 0.6	2.33 ± 0.05	1.750 ± 0.088

[a] The values were obtained as the average of three experimental replicates, the errors were obtained as the standard derivations

[b] The light intensity of the incandescent light bulb varied from 10.6 ± 0.7 to 228.9 ± 4.5 Wm^{-2}.

[c] The light intensity of the white LED panel varied from 3.7 ± 0.1 to 14.6 ± 0.6 Wm^{-2}.

[d] The light intensity of the infrared LED panel varied from 8.3 ± 0.6 to 20.3 ± 1.3 Wm^{-2}.

6.4 Discussion

6.4.1 Absorbance spectrum of *R. palustris*

From Chapter 5, cells acclimated to relatively low light (*i.e.*, shade-adapted) prior to exposure to high light intensity become photo-damaged at a lower intensity dose than cells which have been high light-acclimated (Carvalho et al. 2011). To avoid photo-damage in the later experiments, non-growing cells were prepared at a high light intensity, 228.9 ± 4.5 Wm^{-2}.

Light-harvesting complexes II (LH-II) (peak at 850 nm), light-harvesting complexes I (LH-I) (peak at 875 nm) and reaction centre (RC) (peak at 865 nm) have very different absorption spectra in the near infrared region. The absorbance spectrum of *R. palustris* in Figure 6-2 represents a convolution of spectra for each LH-II, LH-I and

RC, and it could allow the analysis of the pigment composition in the membrane. The absorbance spectrum showed a sharp band around 800 nm and a more intense broadband between 850 nm and 880 nm, which proved that the spectrum of membranes from high-light adapted cells (Scheuring et al. 2006).

From Figure 6-2, it indicated that the light was absorbed by carotenoids with maxima at a) 379 nm and b) 491 nm, and by bacteriochlorophyll *a* with peaks at c) 590 nm, d) 807 nm, and e) 865 nm.

Other researchers have obtained similar results (Uyar *et al.* 2007; Tian *et al.* 2010). The absorbance of another PNS bacteria, *Rhodopseudomonas sphaeroides* O.U. 001 was determined to have maxima at 450 nm, 482 nm, and 514 nm for the carotenoids; 375 nm, 590 nm, 805 nm and 860 nm for the bacteriochlorophyll *a* (Uyar et al. 2007). In addition, the absorbance of *R. palustris* CQK 01 was determined by (Tian et al. 2010) with peaks at 319 nm and 379 nm for the carotenoids; 590 nm, 806 nm, and 863 nm for the bacteriochlorophyll *a*.

6.4.2 Artificial light source

As mentioned in Chapter 5, since the incandescent light bulb and the solar scattering at sunset have similar emission spectra, it could be used to monitor the optimal H_2 production rate by non-growing *R. palustris* under solar irradiance. However, the incandescent light bulb was an energy-expensive light source, and most energy would be wasted as heat consumption rather than H_2 production. Therefore, apart from the incandescent light bulb with wide wavelength bands, the energy-efficient light-emitting diodes (LEDs) with short wavelength bands were tested in this chapter.

From Figure 6-1, both pigments of carotenoids, absorbing maximally from 350 nm to 550 nm, and bacteriochlorophylls, absorbing maximally from 800 nm to 875 nm, will absorb photons and trigger electronic excitation in the photosynthetic unit of bacteriochlorophylls in PNSB. To test the function of carotenoids and bacteriochlorophylls in photosynthetic H_2 production by non-growing *R. palustris*, the

most commercially available 12 volts 5 mm high-power white LEDs (Honggi Ltd., Shenzhen, China) and infrared LEDs (Honggi Ltd., Shenzhen, China) were selected.

By using those two types of LEDs, two identical LED panels were designed and constructed in cooperation with the High-Pressure Physics Laboratory in Southwest Jiaotong University, China. The schematic diagram of the LED panel was presented in Figure 6-6.
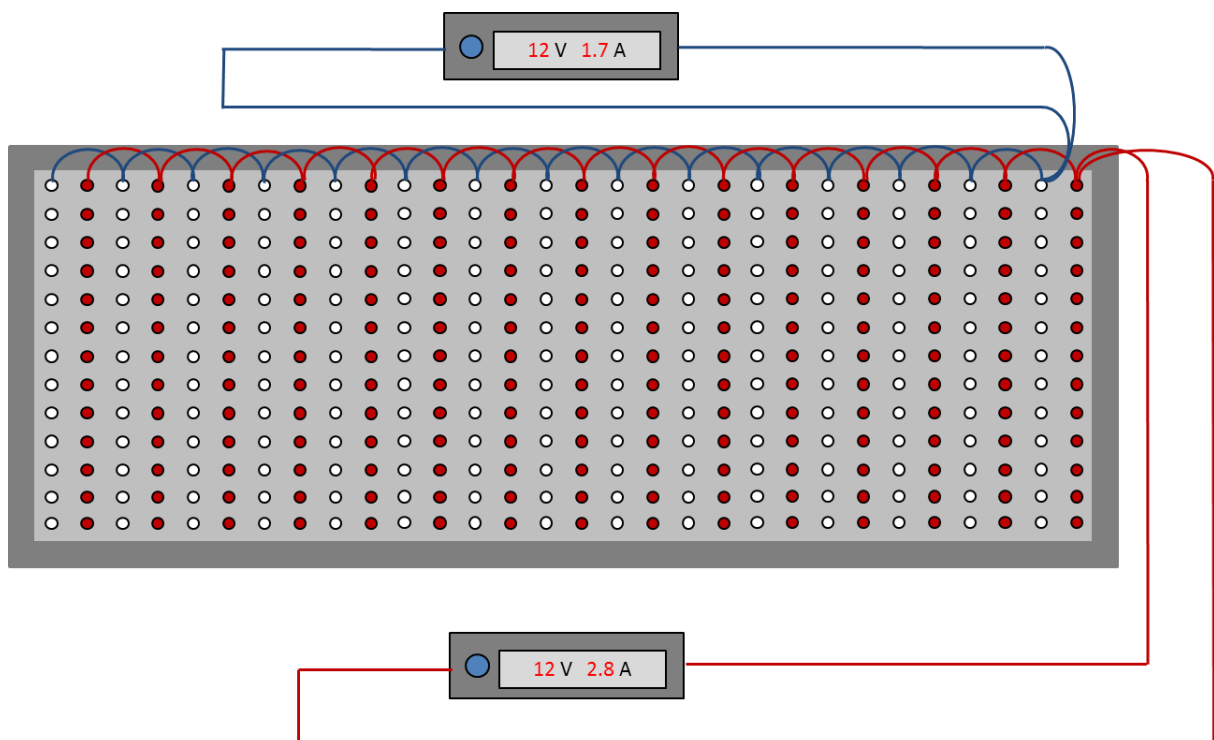
Figure 6-6: Schematic diagram of the LED panel (for demonstration purpose only, not to scales). The LED panel was designed to consist of two types of high-power 12 volts 5 mm LEDs: white LEDs with wavelength band mainly laying in the blue light region, and infrared LEDs with a peak around 860 nm (Hongji Ltd., Shenzhen, China). Both types of LEDs have a diameter of 5 mm and bean angle of $45°$. The white and infrared LEDs were set in columns at 1 cm next to each other, and the layout of the LED panel was shown in the figure. LEDs in each column were connected in parallel with appropriate capacitors. Each type of LED panel was connected to a power source, and the light intensity was controlled by a 12 volts DC transformers. The blue wire was used to connect columns of white LEDs, and the red wire was used to connect columns of infrared LEDs.

As the LEDs used were energy-efficient, they would not generate that much heat to cause photo-damage. Those LEDs had a small diameter of 5 mm and a small bean angle of 45°. To obtain even light distribution, the LED panel was placed at 11 cm from the surface of the culture. The temperature was maintained at 30 ± 2 °C, and the light intensity of each type of LED panel could be adjusted and controlled by varying the voltage supplied through the 12 volts DC transformers.

The emission spectra of different light sources including incandescent light bulb, white LEDs, and infrared LEDs were presented in Figure 6-3.

From Figure 6-3, the emission spectrum of the incandescent light bulb had a wide distribution from 300 nm to 1050 nm, and it had its highest peak at 915 nm. As the emission spectrum of incandescent light bulb was only measured up to 1050 nm, it was predicted that the illumination intensity would continue to drop gradually as the wavelength increased (Rechtsteiner & Ganske 1998). Compared the absorbance spectrum of *R. palustris* in Figure 6-2 and the emission spectrum of the incandescent light bulb in Figure 6-3, most energy generated by incandescent light bulb would be wasted to generate heat rather than produce H_2.

From Figure 6-3, the emission spectrum of white LEDs could be divided into two parts: 450 nm to 500 nm (blue light region), and 500 nm to 650 nm (other visible light regions with green light at 550 nm, yellow light at 600 nm, and orange light at 650 nm). The illumination intensity of the blue light region was about 4 times as that of the other visible light region. The emission spectrum of white LEDs had peaks at 470 nm in the blue light region and at 540 nm in the other visible light region. Compared the results in Figure 6-2 and Figure 6-3 the emission spectrum of the white LEDs covered most absorbance of carotenoids in *R. palustris*. Therefore, white LEDs could be used to test the function of carotenoids in H_2 production by non-growing *R. palustris*.

From Figure 6-3, the emission spectrum of infrared LEDs covered the broadband between 780 nm and 890 nm with a peak at 856 nm. Compared the results in Figure 6-2 and Figure 6-3, the emission spectrum of the infrared LEDs covered most

absorbance of bacteriochlorophyll *a* in *R. palustris*. Therefore, infrared LEDs could be used to monitor the function bacteriochlorophyll *a* in H_2 production by non-growing *R. palustris*.

From the results in Figure 6-3, it was seen that the illumination intensity would drop as the overall light intensity decreased, but the general trends of emission spectra would be similar. Due to different illuminating mechanisms, incandescent light bulb had a much wider range of overall light intensity (10.6 ± 0.7 to 228.9 ± 4.5 Wm^{-2}) compared to that of the white LEDs (3.7 ± 0.1 to 14.6 ± 0.6 Wm^{-2}) and infrared LEDs (8.3 ± 0.6 to 20.4 ± 1.3 Wm^{-2}) used in this chapter. Therefore, a common light intensity of 10.6 ± 0.7 Wm^{-2} was set for all three different light sources to monitor the H_2 production performance by non-growing *R. palustris.*

6.4.3 Non-growing H_2 production with different light sources at same light intensity

Non-growing *R. palustris* at the optical density of 0.8 at 660 nm was prepared after PHB accumulation with illumination provided by incandescent light bulb at its highest available light intensity of 228.9 ± 4.5 Wm^{-2}. The non-growing cells were then cultivated with 10 mM glycerol and filtered sterile Ar. Instead of incandescent light bulb, the illumination was provided by three different light sources including incandescent light bulb, white LEDs, and infrared LEDs. And the light intensity was kept at 10.5 ± 0.5 Wm^{-2} for those three light sources.

To understand the response of photosynthesis to different light wavelength bands, the H_2 production rates and the corresponding energy conversion by non-growing *R. palustris* with illumination provided by those three light sources were measured and calculated, and the results were presented in Figure 6-4 and Figure 6-5.

From Figure 6-4, the average H_2 production rate of non-growing *R. palustris* at the optical density of 0.8 at 660 nm with illumination provided by infrared LEDs at the light intensity of 10.5 ± 0.5 Wm^{-2} was 1.84 ± 0.02 $mL\,L^{-1}\,h^{-1}$, which was $22.0\,\% \pm 1.5\,\%$ higher than that with illumination provided by white LEDs (1.51 ± 0.01 $mL\,L^{-1}\,h^{-1}$). Among those three light sources, the H_2 production rate by non-growing cells with

incandescent light bulb was the lowest (0.06 ± 0.01 mL L^{-1} h^{-1}), which was 3~4 % of that by infrared and white LEDs.

The energy conversion, in terms of light, was calculated as the ratio of the combustion enthalpy of H_2 to the total energy input into cell cultivation (Uyar et al. 2007). The results of energy conversion as a function of different intensities were presented in Figure 6-5. Apart from different light sources, the cultivation conditions for all non-growing H_2 production were almost identical with the same light intensities and irradiated area. Therefore, the energy conversion in this study was proportional to the H_2 production rate. Among those three light sources, the energy conversion from non-growing H_2 production with infrared LEDs was the highest ($1.39 \% \pm 0.01 \%$), then that with white LEDs ($1.11 \% \pm 0.01 \%$), and the lowest energy conversion was obtained from non-growing H_2 production with incandescent light bulb ($0.04 \% \pm 0.01 \%$). From the results, the energy conversion could be improved around 30 times by using energy-efficient LEDs instead of traditional incandescent light bulb.

The results also agreed with other research in this field (Uyar *et al.* 2007; Tian *et al.* 2010). The infrared region (infrared LEDs) where the bacteriochlorophyll *a* absorption maxima exists was important for photosynthetic H_2 production, whereas the blue light region (white LEDs) where the carotenoids absorption maxima occurs was not so significant for photosynthetic H_2 production. Therefore, for photosynthetic H_2 production, it was recommended to place the outdoor bioreactor in the location that it could receive full sunlight during sunrise and sunset period. In addition, infrared LEDs with maxima at 860 nm were suitable as the artificial light source for photosynthetic H_2 production at night.

6.4.4 Non-growing H_2 production with different light sources at different light intensities

As mentioned in Chapter 5, light is essential for photosynthesis in *R. palustris*. Excessive or insufficient light intensity may constrain the photosynthetic performance

(Carvalho *et al.* 2011). For non-growing H_2 production, the major photosynthetic product of *R. palustris* is H_2.

To avoid early stage photo-damage, *R. palustris* was acclimated to high intensity (Carvalho *et al.* 2011). Non-growing *R. palustris* was prepared after PHB accumulation with illumination provided by incandescent light bulb at the light intensity of 228.9 ± 4.5 Wm^{-2}. Then the non-growing cells were cultivated with 10 mM glycerol and filtered sterile Ar, and the illumination was provided at different light sources.

The light intensity was adjusted and controlled by varying the voltage supplied to each light source. Due to different illuminating mechanisms, incandescent light bulb had a much wider range of overall light intensity (10.6 ± 0.7 to 228.9 ± 4.5 Wm^{-2}) compared to that of the white LEDs (3.7 ± 0.1 to 14.6 ± 0.6 Wm^{-2}) and infrared LEDs (8.3 ± 0.6 to 20.4 ± 1.3 Wm^{-2}) used in this chapter. To understand the response of photosynthesis to different light sources at different light intensities, the H_2 production rates by non-growing *R. palustris* were measured accordingly, and the results were presented in Table 6-1. For non-growing H_2 production with incandescent light bulb, the maximum H_2 production rate, 1.36 ± 0.06 mL L^{-1} h^{-1}, and the maximum energy conversion, $0.152 \% \pm 0.003 \%$, obtained at a light intensity of 65.4 ± 1.9 Wm^{-2}. For white LEDs, the maximum H_2 production rate (1.75 ± 0.07 mL L^{-1} h^{-1}) and the maximum energy conversion ($1.109 \% \pm 0.004 \%$) occurred at 10.5 ± 0.6 Wm^{-2}. For infrared LEDs, the maximum H_2 production rate (2.33 ± 0.05 mL L^{-1} h^{-1}) and the maximum energy conversion ($1.750 \% \pm 0.088 \%$) occurred at 8.3 ± 0.6 Wm^{-2}.

In summary, within the test light intensity ranges, the non-growing H_2 production with infrared LEDs achieved the highest values in maximum H_2 production rate and maximum energy conversion at a relatively low light intensity.

For maximum H_2 production rate, the results obtained by white LEDs and incandescent light bulb were around 25 % and 40 % lower respectively compared to that by infrared LEDs. Both non-growing H_2 production with infrared and white LEDs obtained their maximum H_2 production rate at similar light intensities (around

10 Wm^{-2}), but the non-growing H$_2$ production with incandescent obtained its maximum H$_2$ production rate at a much higher light intensity (65.4 ± 1.9 Wm^{-2}).

For maximum energy conversion, the results obtained by white and infrared LEDs were around 10 times as that obtained by incandescent light bulb. Again, both non-growing H$_2$ production with infrared and white LEDs obtained their maximum energy conversion at similar light intensities (around 10 Wm^{-2}), but the non-growing H$_2$ production with incandescent obtained its maximum energy conversion at a much higher light intensity (65.4 ± 1.9 Wm^{-2}).

6.5 Conclusions

Non-growing *R. palustris* was prepared after PHB accumulation, and then cultivated to generate H$_2$ with illumination provided by different light sources including white LEDs, infrared LEDs (with peak at 860 nm), and incandescent light bulb. From the absorbance spectrum of *R. palustris,* the light was absorbed by carotenoids with maxima at 379 nm and 491 nm and bacteriochlorophyll *a* with peaks at 590 nm, 807 nm and 865 nm. At the same light intensity of 10.5 ± 0.5 Wm^{-2}, the H$_2$ production rate and energy conversion by non-growing cells with incandescent light bulb was the lowest among those three light sources, which was around 3~4 % of that by infrared and white LEDs. At different light intensities, within the test light intensity ranges, the non-growing H$_2$ production with infrared LEDs achieved the highest values in maximum H$_2$ production rate and maximum energy conversion at a relatively low light intensity. Therefore, the infrared region (infrared LEDs) where the bacteriochlorophyll *a* absorption maxima exists was important for photosynthetic H$_2$ production, whereas the blue light region (white LEDs) where the carotenoids absorption maxima occurs was not so significant for photosynthetic H$_2$ production. For photosynthetic H$_2$ production, it was recommended to place the outdoor bioreactor in the location that it could receive full sunlight during sunrise and sunset period. In addition, infrared LEDs with maxima at 860 nm were suitable as the artificial light source for photosynthetic H$_2$ production at night.

7 Hydrogen production by cell immobilised non-growing *Rhodopseudomonas palustris*

7.1 Introduction

Immobilisation of whole-cells systems have advantages in terms of reactor operation, product separation, reactor choice, and reusability of the immobilised biocatalyst (van de Velde *et al.* 2002; Bickerstaff 1997). Although some immobilisation has drawbacks in activity, diffusion, and cost, it has proven to be economic and widely applied within the food industry and for the manufacturing of fine chemicals and pharmaceuticals (Krajewska 2004). Therefore, it is appealing to immobilise the whole-cells of non-growing *R. palustris* as a biocatalyst, and the immobilised cells can be applied in scale-up continuous H_2 production systems or sold as an off-the-shelf product.

R. palustris CQK 01 was immobilized in a polyvinyl alcohol-boric acid gel granule to enhance the rate of photo-hydrogen production by *Tian et. al.* (2009). The maximum hydrogen production rate of an immobilized *R. palustris* granule was achieved at 3.6 mmol / g cell dry weight / h. Gosse *et al.* (Gosse et al. 2010; Gosse et al. 2007) reported to immobilise non-growing *R. palustris* in the multi-layer adhesive nano-porous coatings and produce 2.08 ± 0.01 mmol H^2 m^{-2} h^{-1} for 4,000 h.

Compared to the weak interactions in the physical encapsulation, the chemical encapsulation is more stable due to the strong covalent bonds. Among all chemical immobilisation methods, cross-linking method is simple, effective, and durable, and hence attractive in industrial applications. And the most commonly used hydrogels for cross-linking immobilisation method are alginate and *k*-carrageenan.

In this chapter, to test the feasibility of H_2 production by immobilised non-growing *R. palustris*, the same dry cell mass of non-growing cells was immobilised into both alginate and *k*-carrageenan prior to cultivation of cells in those two immobilised agents in media with 10 mM glycerol and Ar as headspace. Based on the requirement of biocompatibility, porosity, transparency, cost, stability, and activity to immobilise non-growing *R. palustris* for H_2 production, the performance of both

hydrogels was analysed and compared. The H_2 production performance was compared with that by suspended cells of the same dry cell mass.

In addition, non-growing cells were immobilised in alginate at a range of inoculum sizes and cultivated in medium with 10 mM glycerol and Ar as headspace. The results of H_2 production rates and energy conversion regarding to immobilised cells with different inoculum sizes were obtained and analysed from the experimental data, through which, it is aimed to understand the product formation kinetics of H_2 production by immobilised non-growing *R. palustris*.

7.2 Materials and methods

7.2.1 Strain and medium

R. palustris, ATH 2.1.37 (NCIB 11774), was purchased from ATCC® as a freeze-dried sample. A defined medium was used in this study as described by Gosse *et al.* (2007), for details please refer to Chapter 2.1.3.

7.2.2 Preparation of non-growing cells

Freeze-dried *R. palustris* was rehydrated, and the pre-culture was prepared. For details in culture revival and pre-culture preparation, please refer to Chapter 2.1.

The pre-culture was then harvested and centrifuged at 5000 g for ten minutes at room temperature in an Eppendorf® 5800 centrifuge (Model 5810R) (Gosse *et al.* 2007), then re-suspended in 1 L fresh medium, and cultivated in a 1 L bottle with 10 mM glycerol and filtered sterile N_2 as headspace. Liquid samples were extracted from the bottle at a regular interval to monitor cell growth. Once the optical density at 660 nm of the cell suspension reached 0.80, the headspace gas was replaced by Ar to halt the growth and allow PHB accumulation for about 200 hours. When *R. palustris* is under nutrient deficient conditions, it can generate different storage products such as glycogen, trehalose, and PHB (Larimer *et al.* 2004).

7.2.3 Immobilisation

For the intermolecular cross-linking of *R. palustris*, functional hydrogels, alginate and *k*-carrageenan, are used as reagents and mixed with the concentrated bacterial solution. The gel-cell suspension then reacts with the gelling agents to form crosslinked covalent bonds. The single-step droplet immobilisation technique is used in this chapter to form immobilised beads.

7.2.3.1 Preparation of the gel solutions and the gelling agents

The alginate gel solution (3 (w / v) % sodium alginate) was prepared by suspending 30 g polymer in 1000 mL distilled water. The suspension was stirred by a magnetic stirrer for 6 hours. The corresponding gelling agent (2 (w / v) % calcium chloride ($CaCl_2$)) was prepared by adding 20 g calcium chloride into 1000 mL distilled water. The solution was mixed by a magnetic stirrer until the calcium chloride powder completely dissolved in the solution. Both well mixed solutions were sterilised by autoclaving at 121°C for 21 minutes with a cooling fan, and stored at room temperature.

Similarly, the *k*-carrageenan gel solution (2.2 (w / v) % *k*-carrageenan) and its gelling agent (3 (w / v) % potassium chloride (KCl)) were prepared and autoclaved for sterile purpose. As *k*-carrageenan has a melting point of 55 °C, the *k*-carrageenan gel solution was removed from the autoclave before it's cooling down and put into a 55 °C orbital incubator to maintain its liquid status.

7.2.3.2 Preparation of the gel-cell suspensions

After PHB accumulation, non-growing cells were harvested and centrifuged at 4424 g at room temperature in a Beckman® JA-10 rotor for ten minutes (Gosse *et al.* 2007). The pellet was washed and re-suspended in fresh medium to the optical density required at 660 nm. The concentrated cell suspension was prepared by centrifuging 200 mL of non-growing cell suspension with required optical density to remove the supernatant and suspending the pellet in a 25 mL of the cultivation medium.

The alginate-cell suspension was prepared by mixing 25 mL of the gel solution (3 (w / v) % sodium alginate) with an equal volume of concentrated cell suspension for 2 minutes. As *k*-carrageenan has a melting point of 55 °C, the *k*-carrageenan-cell suspension was prepared by mixing 25 mL of the gel solution (2.2 (w / v) % *k*-carrageenan) with an equal volume of concentrated cell suspension in a 55 °C water bath for 2 minutes.

7.2.3.3 Droplet immobilisation technique

The gel beads were formed by dripping the gel-cell suspension (50 mL syringes with 18 G needles, about 20 cm from the gelling agent surface) into the gelling agent at room temperature (see Figure 7-1). The beads were left to harden in the gelling agent solutions for 30 min.
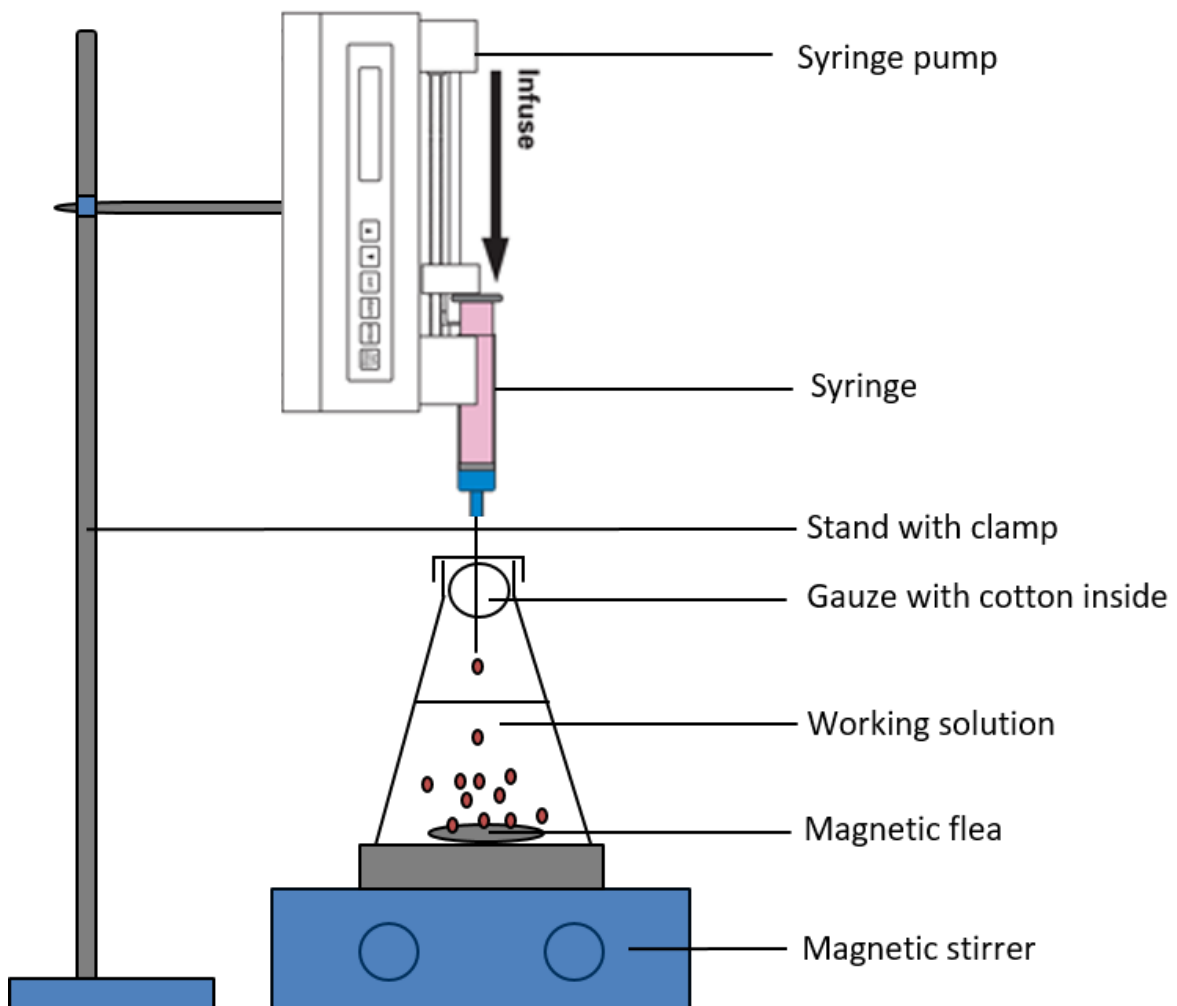
Figure 7-1: General procedures for droplet technique, modified from Smidsrød & Skjåk-Bræk (2000). The gel beads were formed by dripping the 50 mL gel-cell suspension (50 mL syringes with 18 G needles, about 20 cm from the gelling agent surface) into the 150 mL gelling agent. The syringe pump was set at a speed of 100 mL per hour. After dripping, the beads were left to harden in the gelling agent for 30 min. Solutions and containers used for immobilisation were sterilised by autoclaving at 121°C for 21 minutes.

7.2.4 H_2 production by immobilised non-growing cells

After the beads were harden in the gelling agent, the gelling agent was removed, and the cell immobilised beads were washed with cultivation medium. 50 mL cell immobilised beads were transferred into a 250 mL bottle and cultivated in 150 mL medium with 10 mM glycerol and filtered sterile Ar as headspace.

Two hydrogels, alginate and *k*-carrageenan, were used for cell immobilisation in this chapter. For *k*-carrageenan beads, a defined medium was used as described by Gosse *et al.* (2007) for cultivation and H_2 production. Compared to *k*-carrageenan beads, alginate beads has a much lower chemical stability due to its sensitivity towards chelating compounds (phosphate, citrate, and lactate) or anti-gelling cations (sodium ions (Na^+) and magnesium ions (Mg^{2+})) (Smidsrød & Skjåk-Bræk 2000). Therefore, instead of the defined liquid medium (Gosse et al. 2007), Dulbecco's phosphate buffered saline (D-PBS) without calcium chloride ($CaCl_2$) and magnesium chloride ($MgCl_2$) is chosen as the cultivation medium for alginate immobilised beads.

To compare the H_2 production performance of these two hydrogels, the non-growing cells were prepared at an optical density of 0.8 at 660 nm before the cell immobilisation.

7.2.5 H_2 production by alginate immobilised non-growing cells with different inoculum sizes

After PHB accumulation, non-growing cells were harvested and centrifuged (Gosse *et al.* 2007). The pellet was washed and re-suspended in the cultivation medium to the optical density of 0.20, 0.40, 0.80, 1.20, and 1.60 at 660 nm respectively. The

concentrated cell suspension was prepared by centrifuging 200 mL of non-growing cell suspension with required optical density to remove the supernatant and suspending the pellet in a 25 mL of D-PBS.

The concentrated non-growing cells with different inoculum sizes were immobilised in alginate. 50 mL cell immobilised beads were transferred into a 250 mL bottle and cultivated in 150 mL D-PBS with 10 mM glycerol and filtered sterile Ar as headspace.

7.2.6   Other cultivation conditions

Cells were cultivated at $30 \pm 2\,°C$ with illumination provided by incandescent light bulbs (BELL® 100 W R80 ES Reflector) at a light intensity of $228.9 \pm 4.5\,Wm^{-2}$. For details in experimental setup, please refer to Chapter 2.2.

At regular intervals, the gases generated were released to the graduate burette, the volume was measured by water displacement in the burette and recorded; and the H_2 composition was determination by injecting the gas sample into the gas chromatography. As the H_2 solubility in water is extremely low, it was assumed that H_2 is insoluble in water in this study. Hence the total H_2 volume was equal to the H_2 volume in gases released in the burette and the H_2 volume in headspace of the culture bottle. Equally liquid sample was extracted from the bottle at the same time to monitor cell leakage and glycerol consumption.

7.2.7   Analytical methods

The optical density of the liquid sample was measured by a spectrophotometer (Thermospectronic UV1) against a blank solution of de-ionised water at a fixed wavelength of 660 nm, and the equivalent leaked dry cell mass from the immobilised beads was correlated with the optical density (Pott *et al.* 2012).

Glycerol concentration was determined by the method modified from Bondioli and Della Bella (2005). The ethanol solution used in the original assay was replaced volumetrically by distilled water to avoid the distortion of the assay when aqueous solutions of glycerol rather than solutions of glycerol in biodiesel were used.

The gas composition was determined by gas chromatograph (Agilent® 7890A) with a thermal conductivity detector employing Ar as the carrier gas and a HayeSep Q column. The components were analysed using the thermal conductivity detector and correlated to the percentage of different components in the gas sample using existing calibrations (Pott et al. 2012).

7.2.8 H_2 production performance

As seen in Chapter 3, the H_2 yield for non-growing H_2 production was ~ 80 % of the theoretical maximum H_2 yield. Therefore, in this chapter, H_2 production performance from glycerol for cell immobilised non-growing cells was mainly focused on the other two criteria: average H_2 production rate and energy conversion efficiency (Koku *et al.* 2002; Hallenbeck 2012). The average H_2 production rate is defined as the volume of H_2 generated per unit volume of cell suspension per unit time (mL $L^{-1} h^{-1}$) (Tian *et al.* 2010). The energy conversion, in terms of light, is defined as the ratio of the combustion enthalpy of H_2 to the total energy input into cell cultivation (Uyar *et al.* 2007).

7.2.9   Product formation kinetics

As seen in Chapter 4, the non-growing H_2 production rate could be modelled through the Leudeking–Piret (LP) model $\frac{dP}{dt} = 2.52\,X$. Therefore, the same assumption of zero growth rate could be made for immobilised non-growing cells in alginate with different inoculum sizes. And the LP model could also be applied. $\frac{dP}{dt} = \beta X$, where P is the H_2 volume per unit volume of the cell culture (mL L^{-1}), t is time (h), β is the non-growth associated coefficient, and X is the dry cell mass (g L^{-1}) (Sarma, Brar, Sydney, et al. 2012).

7.3   Results

The results of H_2 production rate and energy conversion of immobilised non-growing *R. palustris* are compared to the suspended cells and presented in Table 7-1. To test the H_2 production performance by immobilised non-growing *R. palustris* at various

inoculum sizes, non-growing cells were immobilised in alginate beads at a range of inoculum sizes and cultivated with 10 mM glycerol and Ar as headspace. The results of H_2 production rates (Figure 7-2) and energy conversion (Figure 7-3) are also shown in this section. Each data point in each figure represents the average value of three repeated experiments, and the corresponding error bar denotes the standard derivation of these results.

Table 7-1: H_2 production performance by suspended and immobilised non-growing *R. palustris*[a]

	Average hydrogen production rate (mL L^{-1} h^{-1})			Average glycerol consumption rate (mM h^{-1})			Energy conversion		
Suspended cells	1.33	±	0.14	0.035	±	0.007	0.045%	±	0.005%
Immobilised in alginate	1.67	±	0.27	0.052	±	0.003	0.056%	±	0.009%
Immobilised in *k*-carrageenan	0.10	±	0.01	0.021	±	0.002	0.003%	±	0.009%

[a] The values were obtained as the average of three experimental replicates, the errors were obtained as the standard derivations
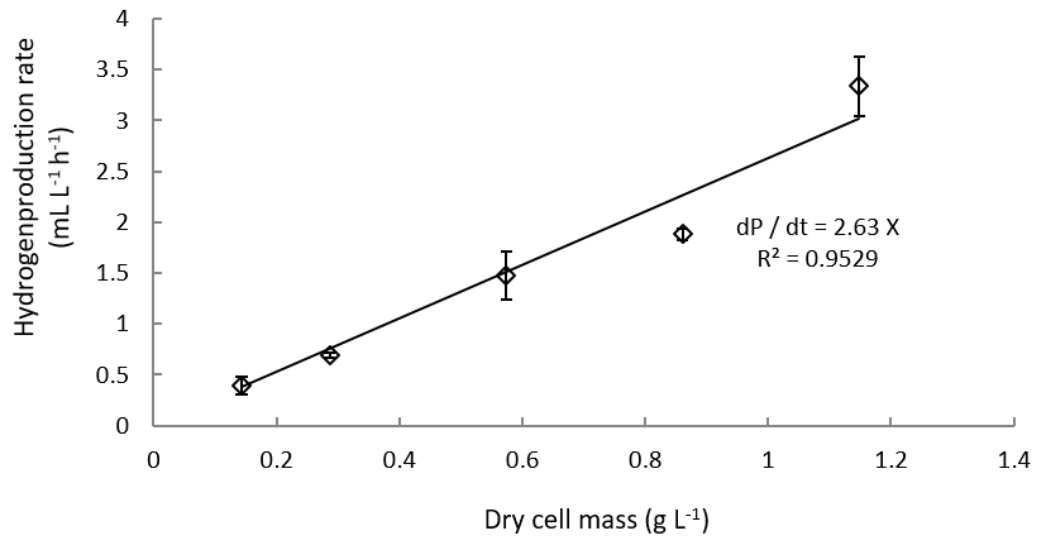
Figure 7-2: H_2 production rates by alginate immobilised non-growing *R. palustris* with different dry cell mass. The results of hydrogen production rates, in terms of the volume of hydrogen gas per unit volume of cell culture per unit time ($mL\,L^{-1}\,h^{-1}$), *vs.* the inoculum size, in terms of the mass of the dry cells per unit volume of the culture ($g\,L^{-1}$), were presented in the figure above. Each data point in this figure represents the average value of three experimental repeats with corresponding error bars denoting the standard derivations.

Table 7-2: Summary output of regression analysis

Regression Statistics	
Multiple R	0.990
R Square	0.980
Adjusted R Square	0.908
Standard Error	0.277
Observations	15

	Coefficients	Standard Error	t Stat	P-value
Intercept	0	-	-	-
X Variable 1	2.63	3.09×10^{-13}	25.94	0.00

$$H_2\ production\ rate = 2.63\ \times\ Dry\ cell\ mass \qquad \text{Equation 7-1}$$
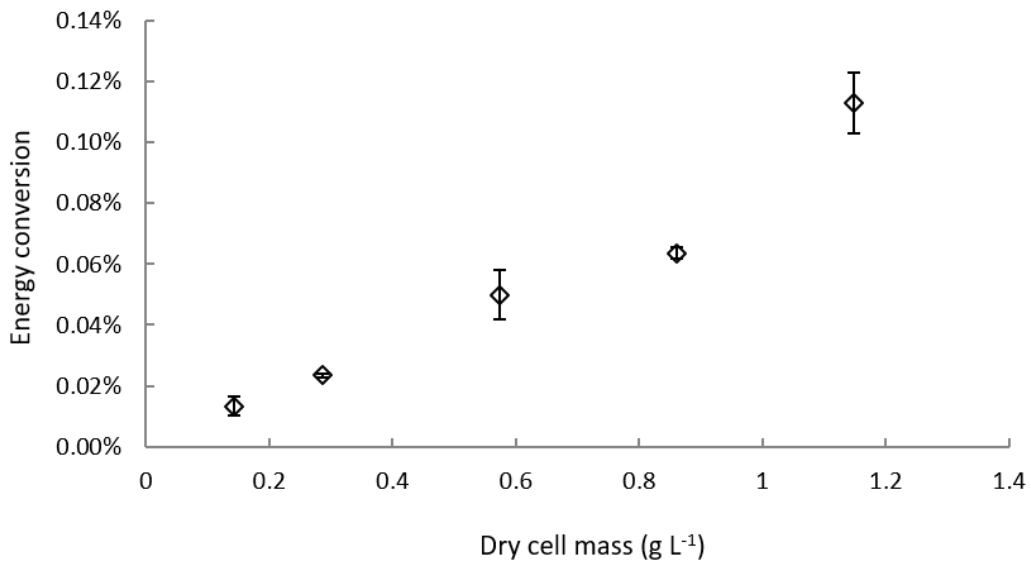
Figure 7-3: Energy conversion of H_2 production by alginate immobilised non-growing *R. palustris* with different dry cell mass. The results of hydrogen production rates (mL $L^{-1} h^{-1}$) *vs.* dry cells mass (g L^{-1}) were obtained from Figure 4-3. The energy conversion was calculated accordingly. The energy conversion, in terms of light, is defined as the ratio of the combustion enthalpy of H_2 to the total energy input into cell cultivation (Uyar *et al.* 2007). Each data point in this figure represents the average value of three experimental repeats with corresponding error bars denoting the standard derivations.

7.4 Discussion

7.4.1 Selection of hydrogels

The characteristics of both hydrogels, alginate and *k*-carrageenan, used in this chapter is summarised in Table 7-3. Based on the requirement of biocompatibility, porosity, transparency, cost, stability, and activity to immobilise non-growing *R. palustris* for H_2 production, the performance of both hydrogels was analysed and compared in this chapter.

Table 7-3: Summary of characteristics of alginate and *k*-carrageenan (Fibler *et al.* 1995)

Gel type	*alginate*	k-*carrageenan*
Pore size (µm)	80~100 (Barbetta *et al.* 2009)	0~20 (Chi *et al.* 2008)
Preparation conditions	mild condition (at room temperature and pH =7)	at melting temperature of 55 °C
Gel mechanism	chemically cross-linked hydrogel	chemically cross-linked hydrogel
Gel solution	3 (w / v) % sodium alginate solution	2.2 (w / v) % *k*-carrageenan solution
Gelling agent	2 (w / v) % calcium chloride (CaCl$_2$) solution	3 (w / v) % potassium chloride (KCl) solution
Cultivation medium	Dulbecco's phosphate buffered saline without calcium chloride and magnesium chloride	defined medium (Gosse *et al.* 2007)

7.4.1.1 Biocompability

Alginate is mainly generated by plants (such as *Laminaria hyperborea, Macrocystis pyrifera,* and *Ascophyllum nodosum*) and bacteria (e.g. *Azotobaeter vinelandii*)

(Smidsrød & Skjåk-Bræk 2000). While, carrageenan is named as a family of gelforming and viscosifying polysaccharides, and it is extracted from some red seaweeds (*Rhodophyta*) (van de Velde et al. 2002). Therefore, both hydrogels are natural extracts, and they are biocompatible with *R. palustris*.

7.4.1.2 Porosity

In general, bacteria are very small in size, 0.2 - 2.0 μm in diameter and 2 - 8 μm in length (Tortora *et al.* 2010). From Table 7-3, alginate has a porous size of 80 – 100 μm (Barbetta *et al.* 2009), and *k*-carrageenon has a porous size of 10 – 20 μm (Chi *et al.* 2008). Therefore, both hydrogels have pore sizes larger than the bacteria size and they can entrap *R. palustris* inside the porous structures through cross-linking bonds. However, the high porosity may cause leakage of whole cells from the open lattice structure.

To test the leakage of whole cells from both cell-immobilised beads, non-growing cells were immobilised in both alginate and *k*-carrageenon and cultivated in media with glycerol and Ar, the liquid sample was extracted on daily basis, and the corresponding optical density was measured and correlated to its dry cell mass. For both cell-immobilised alginate beads and *k*-carrageenan beads, the dry cell mass in the suspension is less than 5 % of that in the immobilised beads during the cultivation. Therefore, both alginate and *k*-carrageenan are capable to immobilise whole cells inside their porous structures.

Apart from pore size and cell leakage, the diffusion rates of substrates and products must be considered to select suitable immobilisation hydrogels. The high porosity of both hydrogels may be advantageous, allowing high diffusion rates of substrates and products. From Table 7-1, comparing the values of average glycerol consumption rate and average H_2 production rate, assuming the enzyme activity is not constrained by other factors, alginate beads have better diffusion rates of substrate and product than that of *k*-carrageenan beads, hence alginate is more suitable to immobilise non-growing *R. palustris*.

7.4.1.3 Transparency

As seen in Chapter 5, the light requirement is vital for H_2 production by *R. palustris*. Thus, immobilisation hydrogels with high transparency are ideal. By observation, both alginate and *k*-carrageenan gels are quite transparent, *i.e.* suitable to immobilise *R. palustris.*

7.4.1.4 Cost

For laboratory use, both sodium alginate (W201502-1KG, £86 per kg) and *k*-carrageenan (C1013-1KG, £237 per kg) are purchased from Sigma Aldrich. The price of alginate is cheaper than that of *k*-carrageenan. And it is predicted that the price of sodium alginate for industrial use may be a lot cheaper. The sodium alginate price at food grade is currently USD7500 – 9000 per tonne (Alibaba 2017).

7.4.1.5 Stability

The gelation of *k*-carrageenan from a disordered to the ordered status is promoted by the addition of the gel-inducing cations including K^+, Rb^+, Cs^+, and NH_4^+, or by lowering the temperature. The strength and the stability of the gel is controlled by the concentration of the gel-inducing cations. Overall *k*-carrageenan gels are hard, strong, brittle, and free / thaw instable (van de Velde et al. 2002). In this chapter, 2.2 (w / v) % *k*-carrageenan aqueous solution and 3 (w / v) % KCl solution were used (Fibler et al. 1995). *k*-carrageenan solution was mixed with the concentrated cell suspension at 55 °C, and the mixture was dripped into the KCl solution. The strong *k*-carrageenan beads formed spontaneously and entrapped the cells in the lattice of cross-linked *k*-carrageenan.

Similarly, the gelation of alginate is formed by the addition of multivalent cations (usually Ca^{2+}) (Smidsrød & Skjåk-Bræk 2000). In this chapter, 3 (w / v) % sodium alginate solution and 2 (w / v) % $CaCl_2$ solution were used (Fibler et al. 1995). Sodium alginate solution was mixed with the concentrated cell suspension at room temperature, and the mixture was dripped into the $CaCl_2$ solution. The droplets

formed alginate beads spontaneously, and the cells were entrapped in the three-dimensional lattice of cross-linked alginate.

Compared to k-carrageenan beads, alginate beads has a much lower chemical stability due to its sensitivity towards chelating compounds (phosphate, citrate, and lactate) or anti-gelling cations (sodium ions (Na^+) and magnesium ions (Mg^{2+})) (Smidsrød & Skjåk-Bræk 2000). Therefore, instead of the defined liquid medium (Gosse et al. 2007), D-PBS without calcium chloride ($CaCl_2$) and magnesium chloride ($MgCl_2$) is chose as the cultivation medium for alginate immobilised beads.

7.4.1.6 Activity

To test the activity of the enzyme nitrogenase, non-growing cells were immobilised in both alginate and k-carrageenon and cultivated in media with glycerol and Ar, the H_2 production performance was analysed and compared to that by the suspended cells.

As seen in Table 7-1, for the same dry cell mass, the average H_2 production rate and energy conversion by the alginate immobilised non-growing cells are ~ 25 % higher than those by the suspended non-growing cells. This implies that the activity of the enzyme in the alginate immobilisation is promoted than that in the suspension. This improvement in activity may be explained by introducing relatively more dry cell mass in the alginate beads.

While, for the same dry cell mass, the average H_2 production rate and energy conversion by the k-carrageenan immobilised non-growing cells are only ~ 7 % of those by the suspended non-growing cells. The dramatic decrease in the enzyme activity in the k-carrageenan immobilisation may be explained by the high melting temperature of k-carrageenan. It is found that the optimal H_2 production cell growth temperature by PNS bacteria varied from 30 °C to 36 °C (Basak & Das 2007). As k-carrageenan has a melting temperature of 55 °C, the concentrated non-growing cell suspension must be mixed with k-carrageenan solution at 55 °C before the immobilisation. This high temperature may decrease the enzyme activity in the k-carrageenan immobilisation.

In summary, based on the requirements in biocompatibility, porosity, transparency, cost, and activity, alginate is the better choice than *k*-carrageenan to immobilise *R. palustris* for H_2 production. As alginate immobilisation matrix has a low chemical stability due to its sensitivity towards the chelating compounds or the anti-gelling cations, D-PBS without $CaCl_2$ and $MgCl_2$ is chose as the cultivation medium instead. However, it is impossible to eliminate all the chelating compounds and the anti-gelling cations in industrial application. Therefore, further investigation of methods to improve the stability of alginate immobilisation is required.

7.4.2 H_2 production by alginate immobilised non-growing cells with different inoculum sizes

To test the H_2 production performance by immobilised non-growing *R. palustris* at various inoculum sizes, non-growing cells were immobilised in alginate at a range of inoculum sizes and cultivated with 10 mM glycerol and Ar as headspace.

From Figure 4-3, the H_2 production rate (mL L^{-1} h^{-1}) increases as the dry cell mass (g L^{-1}) increases. There is a linear relationship between the H_2 production rate and the dry cell mass. A linear regression analysis was carried out at a confidence level of 95 % with intercept at (0, 0). The "least squares" method was employed to fit a line through the experimental data in Figure 4-3. From Table 7-2, the value of R squared was 0.980, very closed to 1, which indicated that the H_2 production rate was very dependent on the immobilised dry cell mass. In addition, the P-value was 3.09 × 10^{-13}, much smaller than 0.05, therefore the H_2 production rate had a strong linear relationship with dry cell mass, which fitted the Leudeking–Piret (LP) model. From the results, $\frac{dP}{dt} = 2.63\,X$. Therefore, the Leudeking–Piret (LP) model can be further used for the alginate immobilised non-growing H_2 production design and optimisation. Compared to the LP model derived from suspended non-growing cells in Chapter 4, the non-growth associated coefficient was improved from 2.52 to 2.63 for alginate immobilisation.

The energy conversion, in terms of light, was calculated as the ratio of the combustion enthalpy of H_2 to the total energy input into cell cultivation (Uyar *et al.*

2007). As the cultivation conditions for all non-growing H_2 production were almost identical with the same light intensities and irradiated area; the energy conversion in this chapter was proportional to the H_2 production rate, ranging from 0.013 ± 0.003 % to 0.113 ± 0.010 %. Since H_2 production rates increased with the cell inoculum sizes, the energy conversion also increased with the cell inoculum sizes.

7.5   Conclusions

In this chapter, two hydrogels alginate and *k*-carrageenan were used to immobilise the non-growing *R. palustris* cells with the same dry cell mass. And the immobilised beads were cultivated in media with 10 mM glycerol and Ar as headspace for H_2 production. Compared to the suspended cells, the H_2 production rate and energy conversion by the alginate immobilised cells are ~ 25 % higher, and those by the *k*-carrageenan immobilised cells are ~ 93 % lower. Based on the requirements in biocompatibility, porosity, transparency, cost, and activity, alginate is the better choice than *k*-carrageenan to immobilise *R. palustris* for H_2 production. As alginate immobilisation matrix has a low chemical stability due to its sensitivity towards the chelating compounds or the anti-gelling cations, D-PBS without $CaCl_2$ and $MgCl_2$ is chosen as the cultivation medium instead. However, it is impossible to eliminate all the chelating compounds and the anti-gelling cations in industrial application. Therefore, further investigation of methods to improve the stability of alginate immobilisation is required.

Then non-growing cells were immobilised in alginate at a range of inoculum sizes and cultivated with 10 mM glycerol and Ar as headspace. The results of H_2 production rates and energy conversion increase as the inoculum size increases. And a linear relationship between the H_2 production rates and the inoculum size is found through the linear regression: $\frac{dP}{dt} = 2.63\,X$. Compared to the LP model derived from suspended non-growing cells in Chapter 4, the non-growth associated coefficient was improved from 2.52 to 2.63 for alginate immobilisation. This again implies that the activity of the enzyme in the alginate immobilisation is promoted than that in the suspension. Therefore, the LP model can be further used for the immobilised non-growing H_2 production design and optimisation. And this preliminary

result revealed the potential of developing an off-the-shelf product of immobilised non-growing *R. palustris* as a biocatalyst for continuous H_2 production.

8 Conclusion and future work

8.1 Conclusion

This dissertation focused on the use of a purple non-sulphur bacterium, *R. palustris,* as a biocatalyst for H_2 production, especially from the waste of biodiesel manufacturing, crude glycerol. The aims were to understand the fundamentals relevant to scaling-up the process and progress development of an off-the-shelf product.

The actual chemical composition of the crude glycerol varies with the type of catalysts and reagents used during the esterification, the conversion and recovery efficiencies of the biodiesel, other impurities in the feedstock, and whether or not the reagents and catalysts are recovered (Yang *et al.* 2012). And the effects of these variation would add additional complexity into understanding the mechanism and optimisation of *R. palustris* for H_2 production. With this in mind, all experimental work in this dissertation was carried out using pure glycerol.

R. palustris, a nitrogen-fixing bacterium, can convert N_2 into NH_3 during cell growth for use in protein synthesis. Both protons and electrons released from organic carbon sources are converted to H_2 by a nitrogenase enzyme (Basak & Das 2007; Ormerod & Ormerod 1961; Lee *et al.* 2011). For growing H_2 production, H_2 is generated as an obligatory but not necessarily advantageous by-product under nitrogen-fixing conditions (Rey *et al.* 2007).

Under nitrogen-depleted conditions, all reductants and energy (*i.e.* ATP) are theoretically directed towards H_2 production without cell growth, *i.e.* converting H^+ from the reductants exclusively to H_2 (McKinlay & Harwood 2010b). For non-growing H_2 production, H_2 is generated as a major product without cell growth. Some research suggests that the non-growing *R. palustris* in nitrogen-depleted conditions act as a biocatalyst for continuous H_2 production (Piskorska et al. 2013; Gosse et al. 2010; Huang et al. 2010a; Melnicki et al. 2008).

The first objective was to determine the ability of *R. palustris* to generate H_2 by non-growing cells in comparison to that by growing cells. In Chapter 3, it was demonstrated that H_2 can be generated by non-growing *R. palustris*, with similar average H_2 production rates and energy conversion to the growing *R. palustris*, but a significant difference in the H_2 yield. H_2 production by non-growing *R. palustris* reached 77.41 ± 4.80 % of the theoretical maximum H_2 yield, about 8-fold as achieved by H_2 production by growing *R. palustris*, 10.45 ± 0.95 % of the theoretical maximum H_2 yield. Cell growth competes electrons and energy with H_2 production. *R. palustris* can absorb energy from light stored as ATP, and from substrate to form an electrochemical gradient. For growing H_2 production, only about 10 % electrons and substrate were used for H_2 production, and the majority was used for cell growth. Whereas, for non-growing H_2 production, when nitrogen source was removed, cell growth was controlled, and most energy and electrons are in theory directed towards H_2 production. Experimentally it was shown that non-growing *R. palustris* was capable of generating H_2 as a biocatalyst for longer than 2000 hours with one refill of 10 mM glycerol in the half way. Therefore, it was found that for small, possibly medium size batch cultivation, H_2 production by growing *R. palustris* were recommended for the ease of operation, while H_2 production by non-growing *R. palustris* would be more economically appealing in scale-up large size continuous cultivation due to the high H_2 yield.

To accomplish the proposed scale-up non-growing H_2 production systems, understanding its product formation kinetics is the key to optimise the H_2 production rate. In Chapter 4, a series of non-growing *R. palustris* with a range of optical densities between 0.2 to 2.0 were prepared and cultivated with 10 mM glycerol and argon to generate H_2. It was found that the H_2 production rate is not growth-associated and depends solely on the dry cell mass. By regression analysis, a strong positive linear relationship between the H_2 production rate ($\frac{dP}{dt}$, mL L^{-1} h^{-1}) and dry cell mass (X, g L^{-1}) was found, which fitted the Leudeking–Piret model, $\frac{dP}{dt} = 2.52\,X$, and is used to aid in the non-growing H_2 production design and optimisation.

Besides the dry cell mass, the enzyme activity, *i.e.* the H_2 production rate, can be improved by cell immobilisation through the protection of the cell stability and the prevention of air inactivation of the enzyme (Francou & Vignais 1984). In addition, cell imobilisation also has advantages in terms of reactor operation, product separation, reactor choice, and reusability of the immobilised biocatalyst (van de Velde *et al.* 2002; Bickerstaff 1997). Therefore, it is appealing to immobilise non-growing *R. palustris* as a biocatalyst, and the immobilised cells can be applied in scale-up continuous H_2 production systems or sold as an off-the-shelf product. In Chapter 7, two hydrogels alginate and *k*-carrageenan were used to immobilise the non-growing *R. palustris* cells with the same dry cell mass. And the immobilised beads were cultivated in media with 10 mM glycerol and Ar as headspace for H_2 production. Compared to the suspended cells, the H_2 production rate and energy conversion by the alginate immobilised cells are ~ 25 % higher, and those by the *k*-carrageenan immobilised cells are ~ 93 % lower. Based on the requirements in biocompatibility, porosity, transparency, cost, and activity, alginate is the better choice than *k*-carrageenan to immobilise *R. palustris* for H_2 production. Then non-growing cells were then immobilised in alginate at a range of inoculum sizes and cultivated with 10 mM glycerol and Ar as headspace. The results of H_2 production rates and energy conversion increase as the inoculum size increases. And a linear relationship between the H_2 production rates and the inoculum size is found through the linear regression: $\frac{dP}{dt} = 2.63\,X$. Compared to the LP model derived from suspended non-growing cells in Chapter 4, the non-growth associated coefficient was improved from 2.52 to 2.63 for alginate immobilisation. This again implies that the activity of the enzyme in the alginate immobilisation is promoted than that in the suspension. And the LP model can be further used for the immobilised non-growing H_2 production design and optimisation.

Apart from growing phase and dry cell mass, light plays a significant role in non-growing H_2 production by *R. palustris,* particular in terms of light intensities and light wavelengths. The most cost-effective of photosynthetic H_2 production system would be directly using natural light (Hallenbeck 2012). The emission spectrum of the incandescent light bulbs (BELL® R80 ES Reflector, London, U.K.) covers the absorbance of *R. palustris*, and it has similar trend as a red sunset. Therefore, this

incandescent light bulb can be used to mimic the real scattering of sunlight during the sunset period to cultivate *R. palustris* for H_2 production.

Excessive or insufficient light intensity may constrain the H_2 production rate (Carvalho *et al.* 2011). In Chapter 5, non-growing *R. palustris* was prepared and acclimated at the highest available light intensity of 228.9 ± 4.5 Wm^{-2}, and then cultivated with 10 mM glycerol and filtered sterile argon at a range of light intensities from 10.6 ± 0.7 to 228.9 ± 4.5 Wm^{-2}. The illumination was provided by incandescent light bulbs, and the light intensity was adjusted and controlled by altering the voltage supplied to the light bulbs. From the results, as the light intensity increased, the photosynthetic performance of *R. palustris*, *i.e.* H_2 production rate also increased to a point before stabling. In the initial light-limiting region, the photonic input was fully utilised by photosynthesis to generate H_2, and the H_2 production rate increased from 0.06 ± 0.01 to 1.28 ± 0.03 $mL\,L^{-1}\,h^{-1}$ as the light intensity increased between 10.6 ± 0.7 to 65.4 ± 1.9 Wm^{-2}. When the light intensity reached above 65.4 ± 1.9 Wm^{-2}, the cells reached the photo-saturation and maintained an average H_2 production rate of 1.36 ± 0.06 $mL\,L^{-1}\,h^{-1}$. As the light intensity increased, the energy conversion increased until it reached to its maximum of 0.152 ± 0.003 % at 65.4 ± 1.9 Wm^{-2}. Energy conversion started to drop with increasing light intensity due to photo-saturation. In addition, non-growing H_2 production had strong dependence on the availability of light with fast response. Energy conversion of H_2 production by non-growing *R. palustris* could be improved through increasing the inoculum size and increasing the illumination surface-to-volume ration of the bioreactor.

To further optimise the energy conversion, investigation of the impact of wavelength on H_2 production by non-growing *R. palustris* is carried out in Chapter 6. Non-growing *R. palustris* was prepared and cultivated to generate H_2 with illumination provided by different light sources including white LEDs, infrared LEDs (with peak at 860 nm), and incandescent light bulb. From the absorbance spectrum of *R. palustris,* the light was absorbed by carotenoids with maxima at 379 nm and 491 nm and bacteriochlorophyll *a* with peaks at 590 nm, 807 nm and 865 nm. At the same light intensity of 10.5 ± 0.5 Wm^{-2}, the H_2 production rate and energy conversion by non-growing cells with incandescent light bulb was the lowest among those three light

sources, which was around 3~4 % of that by infrared and white LEDs. At different light intensities, within the test light intensity ranges, the non-growing H_2 production with infrared LEDs achieved the highest values in maximum H_2 production rate and maximum energy conversion at a relatively low light intensity. Therefore, the infrared region (infrared LEDs) where the bacteriochlorophyll *a* absorption maxima exists was significant for photosynthetic H_2 production, whereas the blue light region (white LEDs) where the carotenoids absorption maxima occurs was not so noteworthy for photosynthetic H_2 production. For photosynthetic H_2 production, it was recommended to place the outdoor bioreactor in the location that it could receive full sunlight during sunrise and sunset period. In addition, infrared LEDs with maxima at 860 nm were suitable as the artificial light source for photosynthetic H_2 production at night.

In summary, this dissertation studies the fundamentals relevant to scaling-up the biohydrogen production process and progress development of an off-the-shelf product of the immobilise biocatalyst. H_2 can be generated by non-growing *R. palustris* at a much higher yield than that by growing cells. For non-growing H_2 production, the H_2 production rate can be optimised by increasing the dry cell mass or immobilising the cells in alginate beads or both. In addition, the energy conversion can be improved through increasing the dry cell mass or the illumination surface-to-volume ration of the bioreactor. And it is recommended to place the outdoor bioreactor in the location that it can receive full sunlight during sunrise and sunset period. In addition, infrared LEDs with maxima at 860 nm are suitable as the artificial light source for photosynthetic H_2 production at night.

8.2 Recommendations for future work

This dissertation mainly focused on the work of H_2 production from glycerol by non-growing *R. palustris*. Only one example of the H_2 production from glycerol by growing *R. palustris* was discussed in Chapter 3 of this dissertation. To understand the H_2 production through photoheterotrophic growth of *R. palustris*, future work is required, especially to investigate the suitable nitrogen source and carbon to nitrogen ration to optimise H_2 production.

The genome sequence has demonstrated that *R. palustris* is metabolically diverse, it can utilise a wide range of carbon source for cell growth and H_2 production. Therefore, *R. palustris* can be used for waste treatment. Apart from crude glycerol in biodiesel manufacturing, utilising wastewater as the carbon source to cultivate *R. palustris* and generate H_2 deserves further study.

Due to the strong restrictions on genetic modification work in the U.K., no genetic engineering work of *R. palustris* was discussed in this project. If the project is carried out in another country, suitable genetic modification work can be carried out to increase the H_2 production performance.

Compared to dark fermentation, photo-fermentation has better H_2 yield, hence discussed in this dissertation. Some researchers suggested that a two-stage fermentation of crude glycerol may improve the H_2 yield, therefore worthy investigating.

The ultimate goal of this project is to scale-up the non-growing H_2 production systems, further work is required to prepare the scale-up process and to build a medium size plant before moving to industrial level.

8.2.1 Nitrogen source and C / N ration

H_2 is mainly generated through photoheterotrophs in PNS bacteria. Nitrogenase is the key enzyme associated mainly with the H_2 production, and its activity is inhibited in the presence of oxygen and ammonia (Koku *et al.* 2002). Ammonia concentration as low as 17 mg / L has been found to rapidly inhibit H_2 production (Lee *et al.* 2011). Ammonium ions also inhibit the H_2 production activity of nitrogenase in PNS bacteria (Gest 1951). Therefore, it is important to supply the nitrogen source for the PNS bacteria in an appropriate form, which does not produce excess ammonia (Sabourin-Provost & Hallenbeck 2009; Chen *et al.* 2007; Ormerod & Ormerod 1961; Koku *et al.* 2002). For example, glutamate appears to be an excellent nitrogen source for H_2 production as it can also be metabolised as a carbon source to store more nitrogen in the biomass (Koku *et al.* 2002). Even so, if the primary carbon source is utilised

completely, whilst glutamate is still present, the nitrogen from the glutamate cannot be fully stored in the proteins of bacteria, it will generate net ammonia by reacting with water, and consequently inhibits the hydrogen production activity of nitrogenase. Therefore, Sasikala *et al.* (1990) and Eroglu *et al.* (2008) recommended using an initial molar ratio of a carbon substrate to glutamate substantially much greater than unity to avoid generating ammonia.

8.2.2   Waste treatment

R. palustris can utilise a wide range of organic carbon sources, including lignin monomers, fatty acids and dicarboxylic acids derived from green plants, animal fats, and seed oils (Larimer *et al.* 2004). Therefore, it is possible for *R. palustris* to utilise organic carbon sources from food waste or industrial wastewater to generate valuable products (Kim *et al.* 2004).

Because *R. palustris* can utilise a wide range of substrates for H_2 production, the feasibility of using wastewater, such as wastewater from dairy plant, sugar refinery, tofu factory, and olive mill *etc.*, as source of nutrients, could be important for the economics of biological H_2 production (Sasikala et al. 1990; Eroglu et al. 2008; Fascetti et al. 1998). Little is known about the metabolism of complex wastes, but studies of hydrogen production from wastewater are abundant in the literature. However, H_2 production rate from wastewater is still low compared to the case when the pure substrate is used. Therefore, utilising wastewater as the carbon source to cultivate PNS bacteria and generate hydrogen deserves further study.

8.2.3   Genetic modification

Genetic modification of the enzymes in photosynthetic bacteria, nitrogenase and hydrogenase, could increase the H_2 production through the following approaches: elimination of uptake hydrogenase, over-expression of hydrogenase or nitrogenase, and increasing the efficiency of hydrogenase or nitrogenase (Kim & Kim 2011). For example, there are two different forms of H_2 evolving hydrogenase in PNS bacteria, [Ni-Fe] hydrogenase where the Ni-Fe atoms act as the active sites, and [Fe-Fe] hydrogenase where the Fe-Fe atoms act as the active sites. The [Ni-Fe] hydrogen

evolving hydrogenase is the most frequently found in PNS bacteria, whereas the [Fe-Fe] hydrogenase is much rarer. Unlike most photosynthetic bacteria, *R. palustris* contains genes encoding hydA, which is able to express the [Fe-Fe] hydrogen evolving hydrogenase (Larimer et al. 2004). Therefore, it has been thought that the hydA could be overexpressed to maximise the hydrogen evolving activity in *R. palustris*, hence increase the hydrogen yield. There are reports of hydrogen evolution attributed to the [Fe-Fe] hydrogenase when similar bacterium *R. rubrum* hydA is overexpressed in that organism, or when overexpressed in another similar PNS bacteria *Rhodobacter sphaeroides* (Kim & Kim 2011). Because of the oxygen sensitivity of hydA, H_2 production is only observed under anaerobic conditions (Hemschemeier & Happe 2005).

From the results in Chapter 4 of this dissertation, it is known that polyhydroxybutyrate (PHB) competes with H_2 production for substrates. To improve the H_2 yield, it is worth to investigate the genetic modification of *R. palustris* to remove the genes encoding PHB accumulation.

8.2.4 Two-stage fermentation

Some researchers have shown that photo-fermentation of glycerol in *R. palustris* can generate about 6 mol H_2 per mol glycerol and achieves 86% of the theoretical maximum H_2 yield owing to some inhibition of *R. palustris* by crude glycerol (Sabourin-Provost & Hallenbeck 2009; Ghosh *et al.* 2012).

In contrast, many microorganisms, other than PNS bacteria, can metabolise the intermediate product of glycerol, pyruvate, to different end products, such as ethanol, butanol, acetone, acetate, butyrate and lactate in dark fermentation (Kivistö *et al.* 2011; Wu, Lu, *et al.* 2012; Jitrwung & Yargeau 2011; Yazdani & Gonzalez 2007; Selembo *et al.* 2009; da Silva *et al.* 2009). In most of these organisms, H_2 is generated as a by-product (Sarma *et al.* 2012). However, some researchers suggest that the H_2 yield in dark fermentation only reaches 33% of its theoretical maxium (Hallenbeck 2009), and incomplete oxidation of the carbon sources results in the production of organic acids as waste products.

Photo-fermentation of glycerol in PNS bacteria is more desirable for H_2 production than dark fermentation with non-PNS microorganisms in where a single-stage-fermentation is to be used. However, because the end products, such as ethanol, butanol, acetone, acetate, butyrate and lactate, produced by non-PNS microorganisms in dark fermentation can be further metabolised by photo-fermentation of PNS bacteria to generate more hydrogen, a two-stage fermentation of crude glycerol, where dark fermentation is followed by photo-fermentation has been considered by some researchers, such as Sabourin-Provost and Hellenbeck, to improve the hydrogen yield from glycerol. By doing so, the maximum hydrogen yield was enhanced to 8 moles hydrogen per mole glycerol (Sabourin-Provost & Hallenbeck 2009).

8.2.5 Scale-up H_2 production systems by non-growing *R. palustris*

8.2.5.1 Process overview
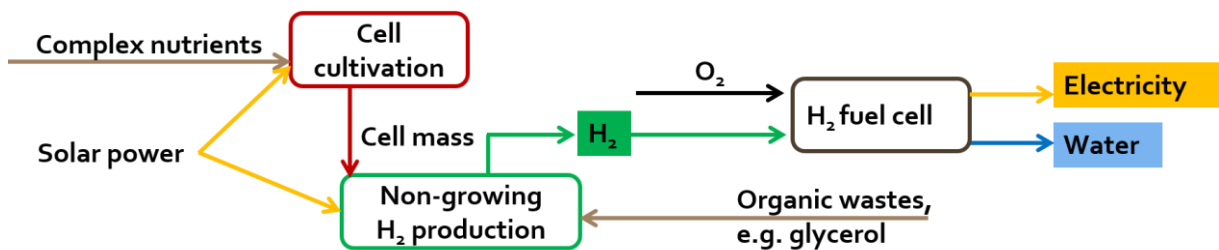
Figure 8-1: Schematic plot of a possible example of industrial bio-hydrogen production plant

A possible example of industrial bio-hydrogen production plant is illustrated in Figure 8-1. Organic wastes, such as crude glycerol from biodiesel manufacturing, are supplied together with the complex nutrients for cell growth of *R. palustris* in suspensions. Then non-growing *R. palustris* is prepared, immobilised as a biocatalyst, and cultivated with organic wastes for continuous H_2 production in the photo-bioreactor designed. H_2 is harvested next, and easily converted to electricity in fuel cells leaving only water as the final product upon its combustion.

Apart from the technical aspects, such as further development in immobilisation and photo-bioreactor design, a life-cycle-analysis and a techno-economic analysis of this method utilising crude glycerol by *R. palustris* must be carried out before constructing the plant.

8.2.5.2 Immobilisation

From the results of Chapter 8 in this dissertation, compared to *k*-carrageenan beads, alginate beads has a much lower chemical stability due to its sensitivity towards chelating compounds (phosphate, citrate, and lactate) or anti-gelling cations (sodium ions (Na^+) and magnesium ions (Mg^{2+})) (Smidsrød & Skjåk-Bræk 2000). Therefore, instead of the defined liquid medium (Gosse et al. 2007), Dulbecco's Phosphate Buffered Saline without calcium chloride ($CaCl_2$) and magnesium chloride ($MgCl_2$) is chose as the cultivation medium for alginate immobilised beads. However, this low chemical stability of alginate immobilisation may be inconvenient in industry. Further research about different immobilisation materials and techniques is required to fit for this purpose.

8.2.5.3 Photo-bioreactor design

From the results in Chapters 5 and 6 in this dissertation, it is known that light is vital for photosynthesis and H_2 production by *R. palustris*. Therefore, the choice of photo-bioreactor type (fixed bed or continuous stirrer tank), the selection of construction material, the actual design must be carefully considered. In addition, researcher shows that mutual shading of cells causes steep gradients of light intensity within the culture, *i.e.* cells away from the culture surface would have rather low light intensities available (Uyar et al. 2007). Increasing the illuminated surface-to-volume ratio to the bioreactor could increase the number of cells exposed to light for H_2 production on the light incident surface, *i.e.* enhance the energy conversion (Hallenbeck 2012; Tsygankov et al. 1994; Adessi et al. 2012; Eroglu et al. 2008; Carvalho et al. 2006; Fibler & Kohring 1995; McKinlay & Harwood 2010b; Ratchford & Fallowfield 1992; Akkerman et al. 2002).

By pursuing the recommended future work, a pilot plant of industrial bio-hydrogen production could be constructed. *R. palustris* could be applied in waste treatment during cell growth. And the cells at the suitable dry cell mass could be harvested and immobilised as biocatalyst for non-growing H_2 production from wastewater. Depends on the contents in the wastewater, two-stage fermentation could be applied to improve the H_2 yield. Genetic modification work could be carried out prior cell

immobilisation to enhance the H_2 production rate. For long-term usage, the enzyme activity could be boosted by adding suitable nitrogen sources at the right carbon to nitrogen ratio. The H_2 harvested could be converted to electricity in fuel cells leaving only water as the final product upon its combustion.

9 References

Abbadi, A. & van Bekkum, H., 1996. Selective chemo-catalytic routes for the preparation of β-hydroxypyruvic acid. *Applied Catalysis A: General*, 148(1), pp.113–122. Available at: http://www.sciencedirect.com/science/article/pii/S0926860X96002293.

Adessi, A. et al., 2012. Sustained outdoor H2 production with Rhodopseudomonas palustris cultures in a 50L tubular photobioreactor. *International Journal of Hydrogen Energy*, 37(10), pp.8840–8849. Available at: http://linkinghub.elsevier.com/retrieve/pii/S0360319912001772 [Accessed November 21, 2012].

Akkerman, I. et al., 2002. Photobiological hydrogen production : photochemical effciency and bioreactor design. *International Journal of Hydrogen Energy*, 27, pp.1195–1208. Available at: http://www.sciencedirect.com/science/article/pii/S036031990200071X.

Alibaba, 2017. alibaba sodium alginate price. *Lianyungang Hantian International Trade China*. Available at: https://www.alibaba.com/product-detail/Sodium-Alginate-pharmaceutical-and-textile-grade_1256962694.html?s=p.

ATCC, 2012. ATCC Medium: 112 Van Niel's Yeast Agar. *ATCC*. Available at: http://www.ncbi.nlm.nih.gov/pubmed/15003161.

ATCC, 2013. Bacterial Culture Guide: tips and techniques for culturing bacteria and bacteriophages. *ATCC*, p.18. Available at: https://www.atcc.org/~/media/PDFs/Culture Guides/Previews/ATCC_Bacterial_Culture_Guide_Preview.ashx.

Ayoub, M. & Abdullah, A.Z., 2012. Critical review on the current scenario and significance of crude glycerol resulting from biodiesel industry towards more sustainable renewable energy industry. *Renewable and Sustainable Energy*

Reviews, 16(5), pp.2671–2686. Available at: http://www.sciencedirect.com/science/article/pii/S1364032112000664.

Barbetta, A., Barigelli, E. & Dentini, M., 2009. Porous Alginate Hydrogels : Synthetic Methods for Tailoring the Porous Texture Porous Alginate Hydrogels : Synthetic Methods for Tailoring the Porous Texture. *Biomacromolecules*, 10(January 2017), pp.2328–2337. Available at: http://pubs.acs.org/doi/pdf/10.1021/bm900517q.

Barrault, J.M., Clacens, Y. & Pouilloux, J., 2004. Selective oligometization of glycerol over mesoporous catalysts. *Top. Catal.*, 27(February), pp.137–142. Available at: https://link.springer.com/article/10.1023/B:TOCA.0000013548.16699.1c.

Basak, N. & Das, D., 2009. Photofermentative hydrogen production using purple non-sulfur bacteria Rhodobacter sphaeroides O.U.001 in an annular photobioreactor: A case study. *Biomass and Bioenergy*, 33(6–7), pp.911–919. Available at: http://linkinghub.elsevier.com/retrieve/pii/S0961953409000348 [Accessed November 21, 2012].

Basak, N. & Das, D., 2007. The prospect of purple non-sulfur (PNS) photosynthetic bacteria for hydrogen production : the present state of the art. *World Journal of Microbiology and Biotechnology*, 23(1), pp.31–42. Available at: https://link.springer.com/article/10.1007/s11274-006-9190-9.

Bickerstaff, G.F., 1997. Immobilization of Enzymes and cells. *Methods in Biotechnology*, 1(May), pp.1–11. Available at: http://www.ncbi.nlm.nih.gov/pubmed/23934795.

Blankenship, R.E., Olson, J.M. & Miller, M., 2004. Anoxygenic Photosynthetic Bacteria. In *Advances in Photosynthesis*. pp. 399–435. Available at: http://www.springerlink.com/index/10.1007/0-306-47954-0.

Bondioli, P. & Della Bella, L., 2005a. An alternative spectrophotometric method for

the determination of free glycerol in biodiesel. *European Journal of Lipid Science and Technology*, 107(3), pp.153–157. Available at: http://doi.wiley.com/10.1002/ejlt.200401054 [Accessed January 23, 2014].

Bondioli, P. & Della Bella, L., 2005b. An alternative spectrophotometric method for the determination of free glycerol in biodiesel. *European Journal of Lipid Science and Technology*, 107(3), pp.153–157. Available at: http://doi.wiley.com/10.1002/ejlt.200401054 [Accessed October 26, 2012].

BP, 2016. *BP Statistical Review of World Energy June 2016*, Available at: https://www.bp.com/content/dam/bp/pdf/energy-economics/statistical-review-2016/bp-statistical-review-of-world-energy-2016-full-report.pdf.

Bradin, D.S., 1996. US Patent 5578090 Biodiesel fuel. , (May 1986). Available at: https://www.google.ch/patents/US5578090.

Brenner, D.J., Krieg, N.R. & Staley, J.T., 2005a. *Bergey's mannual of Systematic Bacteriology* Second Edi. G. M. Garrity, ed., Springer. Available at: http://www.springer.com/series/4157.

Brenner, D.J., Krieg, N.R. & Staley, J.T., 2005b. *Bergey's manual of Systematic Bacteriology* Second Edi. G. M. Garrity, ed., Springer. Available at: http://www.springer.com/series/4157.

Brentner, L.B., Peccia, J. & Zimmerman, J.B., 2010. Challenges in developing biohydrogen as a sustainable energy source: implications for a research agenda. *Environmental science & technology*, 44(7), pp.2243–54. Available at: http://www.ncbi.nlm.nih.gov/pubmed/20222726.

Bühler, W. et al., 2002. Ionic reactions and pyrolysis of glycerol as competing reaction pathways in near- and supercritical water. *Journal of Supercritical Fluids*, 22(1), pp.37–53. Available at: http://www.sciencedirect.com/science/article/pii/S089684460100105X.

Burch, R.R. et al., 2007. US Patent 7169588 Bioconversion a fermentable carbon source 1,3-propanediol by a single microorganism. Available at: http://www.freepatentsonline.com/7169588.html.

Carlozzi, P. et al., 2006. Growth characteristics of Rhodopseudomonas palustris cultured outdoors, in an underwater tubular photobioreactor, and investigation on photosynthetic efficiency. *Applied microbiology and biotechnology*, 73(4), pp.789–95. Available at: http://www.ncbi.nlm.nih.gov/pubmed/16944131 [Accessed October 26, 2012].

Carlozzi, P. & Sacchi, a, 2001. Biomass production and studies on Rhodopseudomonas palustris grown in an outdoor, temperature controlled, underwater tubular photobioreactor. *Journal of biotechnology*, 88(3), pp.239–49. Available at: http://www.ncbi.nlm.nih.gov/pubmed/11434969.

Carrettin, S. et al., 2003. Oxidation of glycerol using supported Pt, Pd and Au catalysts. *Physical Chemistry Chemical Physics*, 5(6), pp.1329–1336. Available at: http://xlink.rsc.org/?DOI=b212047j.

Carvalho, A.P. et al., 2011. Light requirements in microalgal photobioreactors: An overview of biophotonic aspects. *Applied Microbiology and Biotechnology*, 89(5), pp.1275–1288. Available at: http://www.ncbi.nlm.nih.gov/pubmed/21181149 [Accessed November 20, 2012].

Carvalho, A.P., Meireles, L. a. & Malcata, F.X., 2006. Microalgal reactors: A review of enclosed system designs and performances. *Biotechnology Progress*, 22(6), pp.1490–1506. Available at: https://www.ncbi.nlm.nih.gov/pubmed/17137294.

Cerrate, S. et al., 2006. Evaluation of Glycerine from Biodiesel Production as a Feed Ingredient for Broilers. *International Journal of Poultry Science*, 5(11), pp.1001–1007. Available at: http://scialert.net/abstract/?doi=ijps.2006.1001.1007.

Chaminand, J. et al., 2004. Glycerol hydrogenolysis on heterogeneous catalysts.

Green Chemistry, 6(8), p.359. Available at: http://pubs.rsc.org/en/Content/ArticleLanding/2004/GC/b407378a#!divAbstract.

Che, T.M., 1987. US Patent 4642394 Production of propanediols. Available at: http://www.google.ch/patents/US4642394.

Chen, C. et al., 2007. Enhancing phototrophic hydrogen production of Rhodopseudomonas palustris via statistical experimental design. *International Journal of Hydrogen Energy*, 32(8), pp.940–949. Available at: http://linkinghub.elsevier.com/retrieve/pii/S0360319906004514 [Accessed November 21, 2012].

Chen, C.-Y. et al., 2008. Biohydrogen production using sequential two-stage dark and photo fermentation processes. *International Journal of Hydrogen Energy*, 33(18), pp.4755–4762. Available at: http://linkinghub.elsevier.com/retrieve/pii/S0360319908007581 [Accessed November 21, 2012].

Chi, M.C. et al., 2008. Characterization of Bacillus kaustophilus leucine aminopeptidase immobilized in Ca-alginate/k-carrageenan beads. *Biochemical Engineering Journal*, 39(2), pp.376–382. Available at: http://ac.els-cdn.com/S1369703X07003798/1-s2.0-S1369703X07003798-main.pdf?_tid=ba3f8fd6-0b5b-11e7-b88b-00000aab0f26&acdnat=1489787605_d506f009e3c05c57f63013f95b6a8dcb.

Chiu, C.-W., Goff, M.J. & Suppes, G.J., 2005. Distribution of methanol and catalysts between biodiesel and glycerin phases. *AIChE Journal*, 51(4), pp.1274–1278. Available at: http://doi.wiley.com/10.1002/aic.10385.

Ciriminna, R. et al., 2014. Understanding the glycerol market. *European Journal of Lipid Science and Technology*, (September 2015). Available at: http://onlinelibrary.wiley.com/doi/10.1002/ejlt.201400229/pdf.

Daniel, R., Stuertz, K. & Gottschalk, G., 1995. Biochemical and molecular characterization of the oxidative branch of glycerol utilization by Citrobacter freundii. *Journal of Bacteriology*, 177(15), pp.4392–4401. Available at: https://www.ncbi.nlm.nih.gov/pmc/articles/PMC177189/.

Das, D. & Veziroglu, T., 2008. Advances in biological hydrogen production processes. *International Journal of Hydrogen Energy*, 33(21), pp.6046–6057. Available at: http://linkinghub.elsevier.com/retrieve/pii/S036031990800918X.

Das, D. & Veziroglu, T., 2001. Hydrogen production by biological processes : a survey of literature. *International Journal of Hydrogen Energy*, 26, pp.13–28. Available at: http://www.sciencedirect.com/science/article/pii/S0360319900000586.

Dasari, M. a. et al., 2005. Low-pressure hydrogenolysis of glycerol to propylene glycol. *Applied Catalysis A: General*, 281(1–2), pp.225–231. Available at: http://linkinghub.elsevier.com/retrieve/pii/S0926860X0400941X.

Demirel, S. et al., 2007. Use of renewables for the production of chemicals: Glycerol oxidation over carbon supported gold catalysts. *Applied Catalysis B: Environmental*, 70(1–4), pp.637–643. Available at: http://www.sciencedirect.com/science/article/pii/S0926337306002207.

Dharmadi, Y., Murarka, A. & Gonzales, R., 2006. Anaerobic Fermentation of Glycerol by Escherichia coli: A New Platform for Metabolic Engineering. *Biotechnology and bioengineering*, 94(5), pp.821–829. Available at: https://www.ncbi.nlm.nih.gov/pubmed/16715533.

Dimitratos, N. et al., 2006. Investigation on the behaviour of Pt(0)/carbon and Pt(0),Au(0)/carbon catalysts employed in the oxidation of glycerol with molecular oxygen in water. *Journal of Molecular Catalysis A: Chemical*, 256(1–2), pp.21–28. Available at: http://linkinghub.elsevier.com/retrieve/pii/S1381116906007515.

Dimitratos, N. et al., 2005. Synergetic effect of platinum or palladium on gold catalyst in the selective oxidation of D-sorbitol. *Catalysis Letters*, 99(3–4), pp.181–185. Available at: https://link.springer.com/article/10.1007%2Fs10562-005-2114-8?LI=true.

Dobson, R., Gray, V. & Rumbold, K., 2012. Microbial utilization of crude glycerol for the production of value-added products. *Journal of industrial microbiology & biotechnology*, 39(2), pp.217–26. Available at: http://www.ncbi.nlm.nih.gov/pubmed/21948485 [Accessed November 21, 2012].

Donkin, S.S. et al., 2009. Feeding value of glycerol as a replacement for corn grain in rations fed to lactating dairy cows. *Journal of dairy science*, 92(10), pp.5111–5119. Available at: https://www.ncbi.nlm.nih.gov/pubmed/19762829.

DURAN, 2014. DURAN GL 45 Laboratory glass bottles and accessories. , pp.1–30. Available at: http://www.duran-group.com/uploads/tx_fedownloads/DURAN_Laboratory_glass_bottles_and_accessories_A5_E.pdf.

Eroglu, I. et al., 2008. Hydrogen production by Rhodobacter sphaeroides O.U.001 in a flat plate solar bioreactor. *International Journal of Hydrogen Energy*, 33(2), pp.531–541. Available at: http://linkinghub.elsevier.com/retrieve/pii/S0360319907005447 [Accessed November 21, 2012].

Fascetti, E., D'Addario, E. & Robertiello, A., 1998. Photosynthetic hydrogen evolution with volatile organic acids derived from the fermentation of source selected municipal solid wastes. *International Journal of Hydrogen Energy*, 23(9), pp.753–760. Available at: http://www.sciencedirect.com/science/article/pii/S0360319997001237.

Fibler, J. & Kohring, G.W., 1995. Enhanced hydrogen production from aromatic acids by immobilized cells of Rhodopseudomonas palustris. *Applied Microbiol*

Biotechnol, 44, pp.43–46.

Fibler, J., Kohring, W. & Gitthorn, F., 1995. Enhanced hydrogen production from aromatic acids by immobilized cells of Rhodopseudomonas palustris. , pp.3–6. Available at: https://link.springer.com/article/10.1007/BF00164478.

Francou, N. & Vignais, P.M., 1984. Hydrogen production by Rhodopseudomonas capsulate cells entrapped in carrageenan beads. *Biotechnology letters*, 6(10), pp.639–644.

Garcia, R., Besson, M. & Gallezot, P., 1995. Chemoselective catalytic oxidation of glycerol with air on platinum metals. *Applied Catalysis A: General*, 127(1–2), pp.165–176. Available at: http://www.sciencedirect.com/science/article/pii/0926860X95000488.

Van Gerpen, J., 2005. Biodiesel processing and production. *Fuel Processing Technology*, 86, pp.1097–1107. Available at: http://www.sciencedirect.com/science/article/pii/S0378382004001924.

Gest, H., 1951. Metabolic patterns in photosynthetic bacteria. *Bacteriological reviews*, 15(4), pp.183–210. Available at: http://www.pubmedcentral.nih.gov/articlerender.fcgi?artid=180719&tool=pmcentrez&rendertype=abstract.

Ghosh, D., Sobro, I.F. & Hallenbeck, P.C., 2012. Stoichiometric conversion of biodiesel derived crude glycerol to hydrogen: Response surface methodology study of the effects of light intensity and crude glycerol and glutamate concentration. *Bioresource technology*, 106, pp.154–60. Available at: http://www.ncbi.nlm.nih.gov/pubmed/22206915 [Accessed November 11, 2012].

Glim, J., 1992. Chapter 11-2 Photosynthesis : Photoinhibition. *Physiological Ecology*, 1, pp.19–28. Available at: http://www.bryoecol.mtu.edu/chapters/11-2PhotoInhib.pdf.

Gosse, J., 2008. *Investigation of Cellular Factors in Nongrowing Rhodopseudomonas Palustris Hydrogen Production.* University of Minnesota, Minneapolis, MN 55455, United States. Available at: http://books.google.com/books?hl=en&lr=&id=SfjRIEkhYCMC&oi=fnd&pg=PA1& dq=Investigation+of+cellular+factors+in+non-growing+Rhodopseudomonas+palustris+hydrogen+production&ots=Pk4SdokTN S&sig=knyHuTaOgH7kqwqbSLm-58BzXYU [Accessed November 10, 2014].

Gosse, J.L. et al., 2007. Hydrogen production by photoreactive nanoporous latex coatings of nongrowing Rhodopseudomonas palustris CGA009. *Biotechnology progress,* 23(1), pp.124–30. Available at: http://www.ncbi.nlm.nih.gov/pubmed/17269679.

Gosse, J.L. et al., 2010. Progress toward a biomimetic leaf: 4,000 h of hydrogen production by coating-stabilized nongrowing photosynthetic Rhodopseudomonas palustris. *Biotechnology Progress,* 26(4), pp.907–918. Available at: http://www.ncbi.nlm.nih.gov/pubmed/20730752 [Accessed November 21, 2012].

Gottschalk, 1986. *Bacterial Metabolism* 2nd Editio., New York: Springer New York. Available at: http://www.ncbi.nlm.nih.gov/books/NBK7919/.

Hall, D.O. & Rao, K.K., 1999. *Photosynthesis* Sixth Edit., Available at: http://assets.cambridge.org/97805216/42576/sample/9780521642576wsc00.pdf.

Hallenbeck, P.C., 2009. Fermentative hydrogen production: Principles, progress, and prognosis. *International Journal of Hydrogen Energy,* 34(17), pp.7379–7389. Available at: http://linkinghub.elsevier.com/retrieve/pii/S0360319909000238 [Accessed November 12, 2012].

Hallenbeck, P.C., 2012. Microbial technologies in advanced biofuels production. In P. C. Hallenbeck, ed. *Microbial Technologies in Advanced Biofuels Production.* Boston, MA: Springer US, pp. 1–272. Available at: https://link.springer.com/chapter/10.1007%2F978-1-4614-1208-3_4.

Helmenstine, A.M., 2015. Calvin Cyle. *ThoughtCo.* Available at: https://www.thoughtco.com/what-is-the-calvin-cycle-608205 [Accessed March 21, 2017].

Hemschemeier, a & Happe, T., 2005. The exceptional photofermentative hydrogen metabolism of the green alga Chlamydomonas reinhardtii. *Biochemical Society transactions*, 33(Pt 1), pp.39–41. Available at: http://www.ncbi.nlm.nih.gov/pubmed/15667259.

Hu, X. et al., 2002. *Photosynthetic apparatus of purple bacteria.*, Available at: http://www.ncbi.nlm.nih.gov/pubmed/11997980.

Huang, J.J. et al., 2010a. Production of hydrogen gas from light and the inorganic electron donor thiosulfate by Rhodopseudomonas palustris. *Applied and environmental microbiology*, 76(23), pp.7717–22. Available at: http://www.pubmedcentral.nih.gov/articlerender.fcgi?artid=2988585&tool=pmcen trez&rendertype=abstract [Accessed January 16, 2014].

Huang, J.J. et al., 2010b. Production of hydrogen gas from light and the inorganic electron donor thiosulfate by Rhodopseudomonas palustris. *Applied and environmental microbiology*, 76(23), pp.7717–22. Available at: http://www.pubmedcentral.nih.gov/articlerender.fcgi?artid=2988585&tool=pmcen trez&rendertype=abstract [Accessed October 29, 2012].

Hustede, E., Steinbüchel, A. & Schlegel, H.G., 1993. Relationship between the photoproduction of hydrogen and the accumulation of PHB in non-sulphur purple bacteria. *Applied Microbiology and Biotechnology*, 39(1), pp.87–93. Available at: https://eurekamag.com/pdf.php?pdf=009330257.

Ibrahim, S. et al., 2006. The effects of light intensity, inoculum size, and cell immobilisation on the treatment of sago effluent with Rhodopseudomonas palustris strain B1. *Biotechnology and Bioprocess Engineering*, 11(5), pp.377–381. Available at: https://link.springer.com/article/10.1007/BF02932303.

ICIS, 2016. Asia crude glycerine market in stand-off; some sellers keep offers. *ICIS News*. Available at: http://www.icis.com/resources/news/2016/09/08/10032327/asia-crude-glycerine-market-in-stand-off-some-sellers-keep-offers/.

Jitrwung, R. & Yargeau, V., 2011. Optimization of media composition for the production of biohydrogen from waste glycerol. *International Journal of Hydrogen Energy*, 36(16), pp.9602–9611. Available at: http://linkinghub.elsevier.com/retrieve/pii/S0360319911013048 [Accessed November 21, 2012].

Johnson, D.T. & Taconi, K.A., 2009. The Glycerin Glut : Options for the Value-Added Conversion of Crude Glycerol Resulting from Biodiesel Production. *Environmental progress & sustainable energy*, 26(4). Available at: http://onlinelibrary.wiley.com/doi/10.1002/ep.10225/abstract.

Kerr, B.J. et al., 2007. Nutritional value of crude glycerin for nonruminants. In *Proceedings of the 23rd Annual Carolina Swine Nutrition Conference*. Raleigh, NC, pp. 6–18. Available at: https://www.biofuelscoproducts.umn.edu/sites/biodieselfeeds.cfans.umn.edu/files/2007-kerr-nutritional_value_of_crude_glycerin_for_non-ruminants.pdf.

Keskin, T., Abo-Hashesh, M. & Hallenbeck, P.C., 2011. Photofermentative hydrogen production from wastes. *Bioresource technology*, 102(18), pp.8557–68. Available at: http://www.ncbi.nlm.nih.gov/pubmed/21530244 [Accessed November 10, 2012].

Kesling, H.S., Karas, L.J. & Liotta, F.J., 1994. US Patent 5308365 Diesel fuel. , (February 1990). Available at: http://www.google.com/patents/US5308365.

Kim, D.-H. & Kim, M.-S., 2011. Hydrogenases for biological hydrogen production. *Bioresource technology*, 102(18), pp.8423–31. Available at: http://www.ncbi.nlm.nih.gov/pubmed/21435869 [Accessed November 7, 2012].

Kim, H.J. et al., 2004. Transesterification of vegetable oil to biodiesel using heterogeneous base catalyst. *Catalysis Today*, 93–95, pp.315–320. Available at: http://www.sciencedirect.com/science/article/pii/S0920586104002263.

Kim, M., Baek, J. & Lee, J., 2006. Comparison of H2 accumulation by Rhodobacter sphaeroides KD131 and its uptake hydrogenase and PHB synthase deficient mutant. *International Journal of Hydrogen Energy*, 31(1), pp.121–127. Available at: http://linkinghub.elsevier.com/retrieve/pii/S0360319904004069 [Accessed November 21, 2012].

Kimura, H., 1993. Selective oxidation of glycerol on a platinum-bismuth catalyst by using a fixed bed reactor. *Applied Catalysis A: General*, 105(c), pp.147–158. Available at: http://www.sciencedirect.com/science/article/pii/0926860X9380245L.

Kivistö, A., Santala, V. & Karp, M., 2011. Closing the 1,3-propanediol route enhances hydrogen production from glycerol by Halanaerobium saccharolyticum subsp. saccharolyticum. *International Journal of Hydrogen Energy*, 36(12), pp.7074–7080. Available at: http://linkinghub.elsevier.com/retrieve/pii/S0360319911006008 [Accessed November 14, 2012].

Koku, H. et al., 2002. Aspects of the metabolism of hydrogen production by Rhodobacter sphaeroides. *International Journal of Hydrogen Energy*, 27(11–12), pp.1315–1329. Available at: http://linkinghub.elsevier.com/retrieve/pii/S0360319902001271.

Koku, H. et al., 2003. Kinetics of biological hydrogen production by the photosynthetic bacterium Rhodobacter sphaeroides O . U . 001. *International Journal of Hydrogen Energy*, 28, pp.381–388.

Kothari, R. et al., 2012. Fermentative hydrogen production – An alternative clean energy source. *Renewable and Sustainable Energy Reviews*, 16(4), pp.2337–

2346. Available at: http://linkinghub.elsevier.com/retrieve/pii/S1364032112000032 [Accessed November 21, 2012].

Krajewska, B., 2004. Application of chitin- and chitosan-based materials for enzyme immobilizations: a review. *Enzyme and Microbial Technology*, 35(2–3), pp.126–139. Available at: http://linkinghub.elsevier.com/retrieve/pii/S0141022904001231 [Accessed November 6, 2012].

Kumar, N. et al., 2000. Modeling and simulation of clean fuel production by Enterobacter cloacae IIT-BT 08. *International Journal of Hydrogen Energy*, 25, pp.945–952. Available at: http://www.sciencedirect.com/science/article/pii/S0360319900000173.

Lammers, P.J. et al., 2008. Digestible and metabolizable energy of crude glycerol for growing pigs. *Journal of Animal Science*, 86(3), pp.602–608. Available at: https://www.ncbi.nlm.nih.gov/pubmed/18073284.

Larimer, F.W. et al., 2004. Complete genome sequence of the metabolically versatile photosynthetic bacterium Rhodopseudomonas palustris. *Nature biotechnology*, 22(1), pp.55–61. Available at: http://www.ncbi.nlm.nih.gov/pubmed/14704707 [Accessed November 2, 2012].

Law, J.H. & Slepecky, R. a, 1961. Assay of poly-β-hydroxybutyric acid. *J Bacteriol.*, 82(1), pp.33–36. Available at: https://www.ncbi.nlm.nih.gov/pmc/articles/PMC279110/.

Lee, C.M., Hung, G.J. & Yang, C.F., 2011. Hydrogen production by Rhodopseudomonas palustris WP 3-5 in a serial photobioreactor fed with hydrogen fermentation effluent. *Bioresource technology*, 102(18), pp.8350–6. Available at: http://www.ncbi.nlm.nih.gov/pubmed/21600763 [Accessed November 21, 2012].

Luque, R. et al., 2008. Biofuels: a technological perspective. *Energy & Environmental Science*, 1(5). Available at: http://dx.doi.org/10.1039/b807094f.

Márquez-Alvarez, C., Sastre, E. & Pérez-Pariente, J., 2004. Solid Catalysts for the Synthesis of Fatty Esters of Glycerol, Polyglycerols and Sorbitol from Renewable Resources. *Topics in Catalysis*, 27(1–4), pp.105–117. Available at: http://link.springer.com/10.1023/B:TOCA.0000013545.81809.bd.

McKinlay, J.B. et al., 2014a. Non-growing rhodopseudomonas palustris increases the hydrogen gas yield from acetate by shifting from the glyoxylate shunt to the tricarboxylic acid cycle. *Journal of Biological Chemistry*, 289(4), pp.1960–1970. Available at: https://www.ncbi.nlm.nih.gov/pubmed/24302724.

McKinlay, J.B. et al., 2014b. Non-growing rhodopseudomonas palustris increases the hydrogen gas yield from acetate by shifting from the glyoxylate shunt to the tricarboxylic acid cycle. *Journal of Biological Chemistry*, 289(4), pp.1960–1970. Available at: https://www.ncbi.nlm.nih.gov/pubmed/24302724.

McKinlay, J.B. & Harwood, C.S., 2011. Calvin cycle flux, pathway constraints, and substrate oxidation state together determine the H2 biofuel yield in photoheterotrophic bacteria. *mBio*, 2(2), pp.1–9. Available at: http://mbio.asm.org/content/2/2/e00323-10.full.

McKinlay, J.B. & Harwood, C.S., 2010a. Carbon dioxide fixation as a central redox cofactor recycling mechanism in bacteria. *Proceedings of the National Academy of Sciences of the United States of America*, 107(26), pp.11669–75. Available at: http://www.pubmedcentral.nih.gov/articlerender.fcgi?artid=2900684&tool=pmcentrez&rendertype=abstract [Accessed November 21, 2012].

McKinlay, J.B. & Harwood, C.S., 2010b. Photobiological production of hydrogen gas as a biofuel. *Current opinion in biotechnology*, 21(3), pp.244–51. Available at: http://www.ncbi.nlm.nih.gov/pubmed/20303737 [Accessed November 16, 2012].

Melis, A. & Melnicki, M., 2006. Integrated biological hydrogen production. *International Journal of Hydrogen Energy*, 31(11), pp.1563–1573. Available at: http://linkinghub.elsevier.com/retrieve/pii/S0360319906002308 [Accessed October 29, 2012].

Melnicki, M. et al., 2008. Hydrogen production during stationary phase in purple photosynthetic bacteria. *International Journal of Hydrogen Energy*, 33(22), pp.6525–6534. Available at: http://linkinghub.elsevier.com/retrieve/pii/S0360319908010306 [Accessed November 21, 2012].

Nandi, R. & Sengupta, S., 1998. Microbial production of hydrogen: an overview. *Critical reviews in microbiology*, 24(1), pp.61–84. Available at: http://www.ncbi.nlm.nih.gov/pubmed/9561824.

Nath, K. & Das, D., 2004. Improvement of fermentative hydrogen production: various approaches. *Applied microbiology and biotechnology*, 65(5), pp.520–9. Available at: http://www.ncbi.nlm.nih.gov/pubmed/15378294 [Accessed November 13, 2012].

Oda, Y. et al., 2005. Functional Genomic Analysis of Three Nitrogenase Isozymes in the Photosynthetic Bacterium Rhodopseudomonas palustris ‡. *Journal of Bacteriology*, 187(22), pp.7784–7794. Available at: http://jb.asm.org/content/187/22/7784.abstract.

Oh, J., Dash, S. & Lee, H., 2011. Selective conversion of glycerol to 1,3-propanediol using Pt-sulfated zirconia. *Green Chemistry*, 13(8), p.2004. Available at: http://pubs.rsc.org/en/Content/ArticleLanding/2011/GC/c1gc15263g#!divAbstract.

Omnifit, 2013a. Fitting Systems. , pp.1–16. Available at: http://kinesis.co.uk/wp-content/uploads/downloads/2012/03/Omnifit_Fittings_Brochure.pdf.

Omnifit, 2013b. Solvent Safety Bottle Caps barbed adaptors. *Manual*, pp.1–16.

Available at: http://www.products4engineers.nl/resources/upload/j2gtB9-pdf.pdf.

Ormerod, G. & Ormerod, S., 1961. Light-Dependent Utilization of Organic Compounds Photoproduction of Molecular Hydrogen by Photosynthetic Bacteria ; Relationships with Nitrogen Metabolism. *Archives of biochemistry and biophysics*, 94, pp.449–463. Available at: http://www.sciencedirect.com/science/article/pii/000398616190073X.

Ort, D.R. & Yocum, C.F., 1996. Oxygenic photosynthesis: the light reactions. In *Advances in Photosynthesis*. KLUWER ACADEMIC PUBLISHERS, p. 682. Available at: http://www.cabdirect.org/abstracts/19960711196.html;jsessionid=50035ABC214D95D85F5057239BD37955?gitCommit=4.13.29.

Piskorska, M. et al., 2013. Preservation of H(2) production activity in nanoporous latex coatings of Rhodopseudomonas palustris CGA009 during dry storage at ambient temperatures. *Microbial biotechnology*, 6(5), pp.515–25. Available at: http://www.ncbi.nlm.nih.gov/pubmed/23331993 [Accessed January 29, 2013].

Porta, F. & Prati, L., 2004. Selective oxidation of glycerol to sodium glycerate with gold-on-carbon catalyst: an insight into reaction selectivity. *Journal of Catalysis*, 224(2), pp.397–403. Available at: http://linkinghub.elsevier.com/retrieve/pii/S0021951704001149.

Pott, R.W.M., Howe, C.J. & Dennis, J.S., 2012. Photofermentation of crude glycerol from biodiesel using Rhodopseudomonas palustris: Comparison with organic acids and the identification of inhibitory compounds. *Bioresource technology*, 130, pp.725–730. Available at: http://www.ncbi.nlm.nih.gov/pubmed/23334033 [Accessed February 2, 2013].

Pott, R.W.M., Howe, C.J. & Dennis, J.S., 2014. The purification of crude glycerol derived from biodiesel manufacture and its use as a substrate by Rhodopseudomonas palustris to produce hydrogen. *Bioresource technology*,

161

152, pp.464–70. Available at: http://www.ncbi.nlm.nih.gov/pubmed/24326037 [Accessed January 23, 2014].

Queste, S. et al., 2006. Short chain glycerol 1-monoethers - a new class of green solvo-surfactants. *Green Chemistry*, 8(9), p.822. Available at: http://xlink.rsc.org/?DOI=b603973a.

Ratchford, I. a. J. & Fallowfield, H.J., 1992. Performance of a flat plate, air-lift reactor for the growth of high biomass algal cultures. *Journal of Applied Phycology*, 4(1), pp.1–9. Available at: http://www.springerlink.com/index/10.1007/BF00003954.

Rechtsteiner, G.A. & Ganske, J.A., 1998. Using Natural and Artificial Light Sources to Illustrate Quantum Mechanical Concepts. *Chem. Educator*, 4171(98), pp.7–10. Available at: https://link.springer.com/article/10.1007/s00897980230a.

Rey, F.E., Heiniger, E.K. & Harwood, C.S., 2007. Redirection of metabolism for biological hydrogen production. *Applied and environmental microbiology*, 73(5), pp.1665–71. Available at: http://www.pubmedcentral.nih.gov/articlerender.fcgi?artid=1828789&tool=pmcentrez&rendertype=abstract [Accessed February 3, 2014].

Rupprecht, J. et al., 2006. Perspectives and advances of biological H2 production in microorganisms. *Applied microbiology and biotechnology*, 72(3), pp.442–9. Available at: http://www.ncbi.nlm.nih.gov/pubmed/16896600 [Accessed November 1, 2012].

Sabourin-Provost, G. & Hallenbeck, P.C., 2009. High yield conversion of a crude glycerol fraction from biodiesel production to hydrogen by photofermentation. *Bioresource technology*, 100(14), pp.3513–7. Available at: http://www.ncbi.nlm.nih.gov/pubmed/19339176 [Accessed November 3, 2012].

Sarma, S.J., Brar, S.K., Le Bihan, Y., et al., 2012. Bio-hydrogen production by biodiesel-derived crude glycerol bioconversion: a techno-economic evaluation.

Bioprocess and biosystems engineering. Available at: http://www.ncbi.nlm.nih.gov/pubmed/22644063 [Accessed November 12, 2012].

Sarma, S.J., Brar, S.K., Sydney, E.B., et al., 2012. Microbial hydrogen production by bioconversion of crude glycerol: A review. *International Journal of Hydrogen Energy*, 37(8), pp.6473–6490. Available at: http://linkinghub.elsevier.com/retrieve/pii/S0360319912001000 [Accessed November 11, 2012].

Sasikala, C.H., Ramana, C.H. V & Rao, P.R., 1995. Regulation of simultaneous hydrogen photoproduction during growth by pH and glutamate in Rhodobacter sphaeroides O.U. 001. *International Journal of Hydrogen Energy*, 20(2), pp.123–126. Available at: http://www.sciencedirect.com/science/article/pii/0360319994E0009N.

Sasikala, K. et al., 1990. Photoproduction of hydrogen , nitrogenase and hydrogenase activities of free and immobilized whole cells of Rhodobacter sphaeroides O . U . 001. *FEMS Microbiology Letters*, 72, pp.23–28. Available at: http://www.sciencedirect.com/science/article/pii/037810979090338Q.

Saxena, R.C., Adhikari, D.K. & Goyal, H.B., 2009. Biomass-based energy fuel through biochemical routes: A review. *Renewable and Sustainable Energy Reviews*, 13(1), pp.167–178. Available at: http://linkinghub.elsevier.com/retrieve/pii/S1364032107001256 [Accessed November 3, 2012].

Scheuring, S. et al., 2006. The photosynthetic apparatus of Rhodopseudomonas palustris: structures and organization. *Journal of molecular biology*, 358(1), pp.83–96. Available at: http://www.ncbi.nlm.nih.gov/pubmed/16500674.

Schwartz, E. & Friedrich, B., 2006. *The Prokaryotes* M. Dworkin et al., eds., Springer New York. Available at: http://www.springerlink.com/index/10.1007/0-387-30742-7 [Accessed October 27, 2012].

Seifert, C. et al., 2001. Identification and expression of the genes and purification and characterization of the gene products involved in reactivation of coenzyme B 12 - dependent glycerol dehydratase of Citrobacter freundii. *Proteins*, 2378, pp.2369–2378.

Selembo, P. a. et al., 2009. High hydrogen production from glycerol or glucose by electrohydrogenesis using microbial electrolysis cells. *International Journal of Hydrogen Energy*, 34(13), pp.5373–5381. Available at: http://linkinghub.elsevier.com/retrieve/pii/S0360319909006855 [Accessed November 8, 2012].

Sierra, E. et al., 2008. Characterization of a flat plate photobioreactor for the production of microalgae. *Chemical Engineering Journal*, 138(1–3), pp.136–147. Available at: http://linkinghub.elsevier.com/retrieve/pii/S1385894707004068 [Accessed November 9, 2012].

da Silva, G.P., Mack, M. & Contiero, J., 2009. Glycerol: a promising and abundant carbon source for industrial microbiology. *Biotechnology advances*, 27(1), pp.30–9. Available at: http://www.ncbi.nlm.nih.gov/pubmed/18775486 [Accessed November 2, 2012].

Smidsrød, O. & Skjåk-Bræk, G., 2000. Alginate as immobilization matrix for cells. *Minerva Biotecnologica*, 12(4), pp.223–233. Available at: http://tf5lu9ym5n.scholar.serialssolutions.com/?sid=google&auinit=O&aulast=Smidsrød&atitle=Alginate+as+immobilization+matrix+for+cells&id=doi:10.1016/0167-7799(90)90139-O&title=Trends+in+biotechnology+(Regular+ed.)&volume=8&date=1990&spage=71&issn=0167-77.

Soares, R.R., Simonetti, D. a. & Dumesic, J. a., 2006. Glycerol as a Source for Fuels and Chemicals by Low-Temperature Catalytic Processing. *Angewandte Chemie*, 118(24), pp.4086–4089. Available at: http://doi.wiley.com/10.1002/ange.200600212.

Sonntag, N.O. V., 1982. Glycerolysis of fats and methyl esters — Status, review and critique. *Journal of the American Oil Chemists Society*, 59(10), p.795A–802A. Available at: https://link.springer.com/article/10.1007/BF02634442.

Tabita, F.R., 1995. The Biochemistry and Metabolic Regulation of Carbon Metabolism and Fixation in Purple Bacteria. *Anoxygenic Photosynthetic Bacteria*, 2, pp.885–914. Available at: https://link.springer.com/chapter/10.1007%2F0-306-47954-0_41.

Taylor, B. et al., 2013. Techno-economic assessment of carbon-negative algal biodiesel for transport solutions. *Applied Energy*, 106, pp.262–274. Available at: http://dx.doi.org/10.1016/j.apenergy.2013.01.065.

Teles, J.H., Rieber, N. & Harder, W., 1994. US Patent 5359094 Preparation of glyceryl carbonate. , p.US5359094A. Available at: http://www.google.ch/patents/US5359094.

Thermo-Scientific, 2014. Storing bacterial samples for optimal viability. , pp.8–10. Available at: http://www.thermoscientific.com/content/tfs/en/about-us/general-landing-page/storing-bacterial-samples-for-optimal-viability.html.

Thiel, T., 1999a. Maintenance of Bacterial Strains. *Science in the Real World: Microbes in Action*, p.3. Available at: http://www.umsl.edu/~microbes/pdf/maintenanceofbacteria.pdf.

Thiel, T., 1999b. Streaking microbial cultures on agar plates. *Science in the Real World: Microbes in Action*. Available at: http://scholar.google.com/scholar?hl=en&btnG=Search&q=intitle:Streaking+Microbial+Cultures+on+Agar+Plates#0%5Cnhttp://scholar.google.com/scholar?hl=en&btnG=Search&q=intitle:?Streaking+microbial+cultures+on+agar+plates?#0.

Tian, X. et al., 2010. Characteristics of a biofilm photobioreactor as applied to photo-hydrogen production. *Bioresource technology*, 101(3), pp.977–83. Available at:

http://www.ncbi.nlm.nih.gov/pubmed/19818607 [Accessed November 19, 2012].

Tian, X. et al., 2009. Photo-hydrogen production rate of a PVA-boric acid gel granule containing immobilized photosynthetic bacteria cells. *International Journal of Hydrogen Energy*, 34(11), pp.4708–4717. Available at: http://linkinghub.elsevier.com/retrieve/pii/S0360319909004807 [Accessed October 9, 2014].

Tortora, G.J., Funke, B.R. & Case, C.L., 2010. *Microbiology An Introduction*, Available at: https://www.slideshare.net/NeilMoreno2/microbiology-an-introduction-12th-edition-pdf-free-by-tortora.

Tsygankov, A.A. et al., 1994. Photobioreactor with Photosynthetic Bacteria Immobilized on Porous Glass for Hydrogen Photoproduction. *Journal of Fermentation and Bioengineering*, 77(5), pp.575–578. Available at: http://www.sciencedirect.com/science/article/pii/0922338X94901341.

Uyar, B. et al., 2007. Effect of light intensity, wavelength and illumination protocol on hydrogen production in photobioreactors. *International Journal of Hydrogen Energy*, 32(18), pp.4670–4677. Available at: http://linkinghub.elsevier.com/retrieve/pii/S0360319907003746 [Accessed October 31, 2012].

van de Velde, F. et al., 2002. Carrageenan: A Food-Grade and Biocompatible Support for Immobilisation Techniques. *Advanced Synthesis & Catalysis*, 344(8), pp.815–835. Available at: http://doi.wiley.com/10.1002/1615-4169(200209)344:8%3C815::AID-ADSC815%3E3.0.CO;2-H.

Watanabe, M. et al., 2007. Acrolein synthesis from glycerol in hot-compressed water. *Bioresource Technology*, 98(6), pp.1285–1290. Available at: http://www.sciencedirect.com/science/article/pii/S096085240600201X.

Welander, P. V. et al., 2009. Hopanoids Play a Role in Membrane Integrity and pH

Homeostasis in Rhodopseudomonas palustris TIE-1. *Journal of Bacteriology*, 191(19), pp.6145–6156. Available at: http://jb.asm.org/cgi/doi/10.1128/JB.00460-09.

Whittenbury, R. & McLee, A.G., 1967. Rhodopseudomonas palustris and Rh. viridis--photosynthetic budding bacteria. *Archiv für Mikrobiologie*, 59(1), pp.324–34. Available at: http://www.ncbi.nlm.nih.gov/pubmed/5602470.

Wu, S.C., Lu, P.F., et al., 2012. Bio-hydrogen production enhancement by co-cultivating Rhodopseudomonas palustris WP3-5 and Anabaena sp. CH3. *International Journal of Hydrogen Energy*, 37(3), pp.2231–2238. Available at: http://linkinghub.elsevier.com/retrieve/pii/S0360319911024335 [Accessed November 21, 2012].

Wu, S.C., Liou, S.Z. & Lee, C.M., 2012. Correlation between bio-hydrogen production and polyhydroxybutyrate (PHB) synthesis by Rhodopseudomonas palustris WP3-5. *Bioresource technology*, 113, pp.44–50. Available at: http://www.ncbi.nlm.nih.gov/pubmed/22342035 [Accessed October 29, 2014].

Xu, D. et al., 2009. Catalytic gasification of glycine and glycerol in supercritical water. *International Journal of Hydrogen Energy*, 34(13), pp.5357–5364. Available at: http://linkinghub.elsevier.com/retrieve/pii/S0360319908011166 [Accessed November 21, 2012].

Yang, F., Hanna, M. a & Sun, R., 2012. Value-added uses for crude glycerol--a byproduct of biodiesel production. *Biotechnology for biofuels*, 5(1), p.13. Available at: http://www.pubmedcentral.nih.gov/articlerender.fcgi?artid=3313861&tool=pmcentrez&rendertype=abstract [Accessed November 11, 2012].

Yazdani, S.S. & Gonzalez, R., 2007. Anaerobic fermentation of glycerol: a path to economic viability for the biofuels industry. *Current opinion in biotechnology*, 18(3), pp.213–9. Available at: http://www.ncbi.nlm.nih.gov/pubmed/17532205

[Accessed November 12, 2012].

Zhou, C.-H. (Clayton) et al., 2008. Chemoselective catalytic conversion of glycerol as a biorenewable source to valuable commodity chemicals. *Chem. Soc. Rev.*, 37(3), pp.527–549. Available at: http://xlink.rsc.org/?DOI=B707343G.